hydrology

MDPI

Article

Flow Topology in the Confluence of an Open Channel with Lateral Drainage Pipe

Mohammad Nazari-Sharabian [1], Moses Karakouzian [1,*] and Donald Hayes [2]

[1] Department of Civil and Environmental Engineering and Construction, University of Nevada, Las Vegas, NV 89154, USA; nazarish@unlv.nevada.edu
[2] U.S. Army Engineer Research and Development Center, Vicksburg, MS 39180, USA; donald.hayes@unlv.edu
* Correspondence: mkar@unlv.nevada.edu

Received: 5 July 2020; Accepted: 12 August 2020; Published: 15 August 2020

Abstract: The purpose of this paper is to develop design guidelines for flood control channel height in the vicinity of the confluence of a submerged drainage pipe and a flood control channel. The water exchange in the confluence of an open channel with a lateral drainage pipe produces unique hydraulic characteristics, ultimately affecting the water surface elevation in the channel. An accurate prediction of the water surface elevation is essential in the successful design of a high-velocity channel. By performing several experiments, and utilizing a numerical model (FLOW-3D), this study investigated the impact of submerged lateral drainage pipe discharges into rectangular open channels on flow topology in the confluence hydrodynamics zone (CHZ). The experiments were conducted in different flume and junction configurations and flow conditions. Moreover, the simulations were performed on actual size channels with different channel, pipe, and junction configurations and flow conditions. The flow topology in the CHZ was found to be highly influenced by the junction angle, as well as the momentum ratios of the channel flow and the pipe flow. The findings of this study were used to develop conservative design curves for channel confluences with lateral drainage pipe inlets. The curves can be used to estimate water surface elevation rise in different channel and pipe configurations with different flow conditions to determine the channel wall heights required to contain flows in the vicinity of laterals.

Keywords: flood control channel; open channel; channel and pipe confluence; flow topology; FLOW-3D

1. Introduction

Confluences of open channels and lateral drainage pipes are important elements in the hydraulic networks of man-made canals [1]. They are necessarily encountered at the end of urban sewage or agricultural subsurface drainage networks, where they release water [2]. Flow through lateral drainage pipes to open channels impacts channel capacity and disrupts the natural flow of water by creating turbulence in the vicinity of the inlet pipe, as well as influencing flow characteristics in the confluence hydrodynamics zone (CHZ) (Figure 1). Even though these confluences represent a critical component of drainage system geometry, they have received surprisingly little attention from researchers and engineers. This is mainly due to the relatively large number of parameters involved, along with the complex flow features occurring in the CHZ [3]. As a result, no comprehensive data set has been compiled that describes the 3D flow field within the CHZ [4].

Figure 1. The confluence of an open channel with a lateral drainage pipe.

The complexity of an open channel confluence stems from flow mixing, secondary circulation, post-confluence flow separation, contraction, and backwater effects. These effects, in turn, result in a large number of parameters required to adequately describe flow patterns and turbulent flow structures, due to flow merging [5]. In a CHZ, the flow topology is governed by parameters such as confluence geometry (angle, channel widths, bed discordance presence, and cross-sectional shape) and momentum ratio, as well as the ratio between the incoming flows, etc. [6].

Studying the combination of flows in open channel confluences with lateral drainage pipes has a direct application in drainage system open channel network design. One important parameter in such design is estimating the rise in flow depth, due to the lateral flow effect, and in a CHZ this effect can be significant [7]. An understanding of these flow conditions is necessary for the hydraulic design of the channel walls (height and length) that are required to contain these flows in the vicinity of laterals [8]. In this regard, the present study seeks to answer the following questions:

- What would be the impact of submerged lateral drainage pipe discharges into rectangular open channels on the flow topology (including maximum water height) in a CHZ for different channel widths, flow rates, Froude numbers, confluence angles, inlet pipe diameters, and lateral flows to the main channel flow ratios?
- Under what circumstances would the maximum increase in water surface elevation be confined to the desired values (e.g., 10%, or 20%)?

The first and only study to date on the hydraulic behavior of a pipe outlet into an open channel, allowing the combination of free-surface and pressurized flows, was conducted by Nedelec and Gay in 2008 [9]. This limited experimental study explored the hydraulic properties of subsurface drainage outlets into an open-air stream. This experimental study had several limitations, one of which was that the flow in channels during floods is super-critical, while the study was confined to sub-critical flow. Another limitation was that the angle of the inlet pipe was 90° with respect to the flume, while some flood control agencies recommend smaller pipe entry angles. Additionally, the results of the small-sized flume experiments could not be extrapolated to actual flood control channel dimensions.

Recognizing the knowledge gap, this study addresses the limitations identified in the literature review, utilizing experimental and numerical studies, and contributes to a better knowledge of flow topology in the CHZ of an open channel and a pipe. Additionally, this study can provide a benchmark experimental dataset for the validation of future numerical models. The experimental studies were performed for sub-critical and super-critical flow conditions with different junction angles. Results from these experiments were used to validate the numerical model (FLOW-3D) simulations. Finally, the validated numerical model was implemented to simulate actual flood control channel dimensions, in order to propose recommendations for the design of channels with lateral pipe inlets.

These recommendations are based on conservative design curves, developed on the basis of the momentum principle, according to the relationship between the relative rise in channel water height, lateral discharge to channel flow ratio, and confluence angle. Figure 2 shows the flow chart of this study.

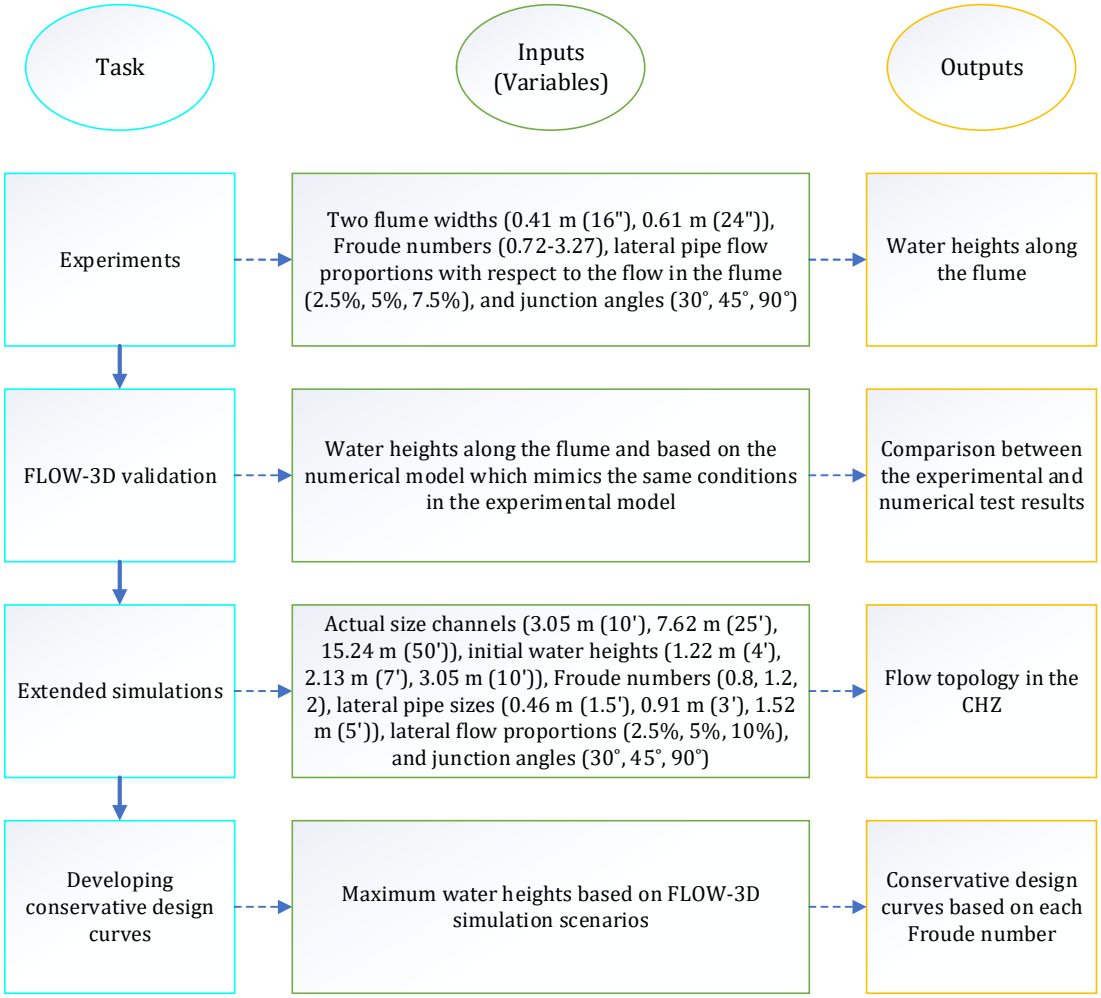

Figure 2. The flow chart of this study.

2. Materials and Methods

2.1. Experiments

The flume in the Fluid Dynamics Laboratory of the University of Nevada, Las Vegas (UNLV) is 14.63 m (48′) long and 0.81 m (32″) wide, with a height of 0.61 m (24″). In order to obtain super-critical flows in the flume, considering the availability of pumps at UNLV, the flume had to be narrowed to get reasonable flow velocities, water depths, and desired Froude numbers. Therefore, to provide the desired flow conditions, as well as to evaluate the effect of channel width on the main channel flow disturbances, at first, the flume was narrowed to 0.61 m (24″) (wide channel) and then to 0.41 m (16″) (narrow channel). A 5.1-cm (2″) diameter inlet pipe was installed through the flume wall 7.62 m (25′) downstream of the flume entrance to provide lateral flow to the channel. Flow through the inlet was provided through a separate variable-speed pump fed by water from the flume sump (Figure 3).

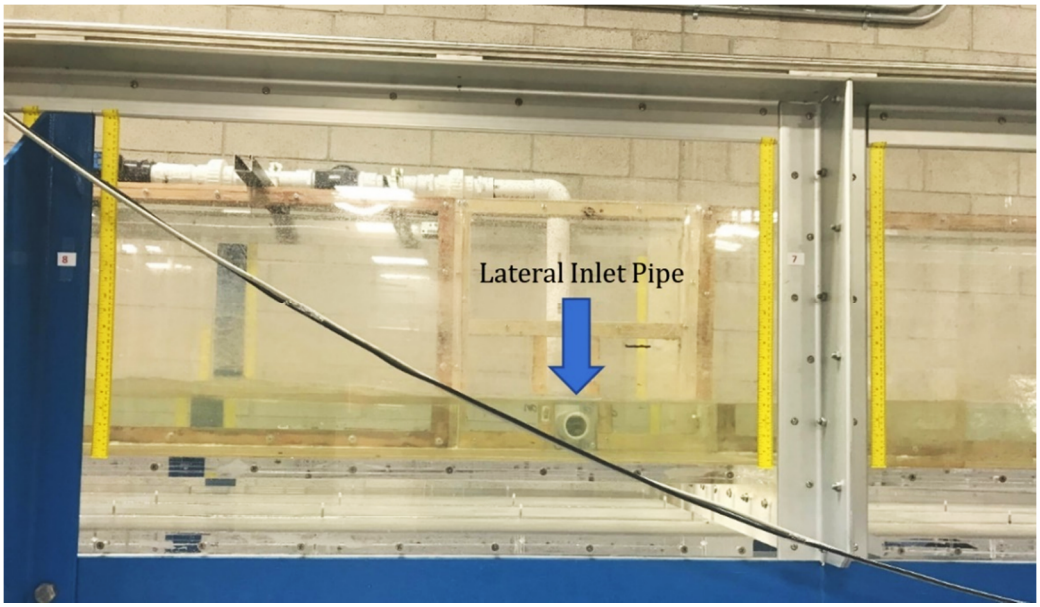

Figure 3. The 2″ diameter inlet pipe installed on the flume wall.

Moreover, three inlet connections at 30, 45, and 90° were constructed to feed lateral flow to the channel at desired angles. Figures 4 and 5 show the wide channel and narrow channel configurations, respectively.

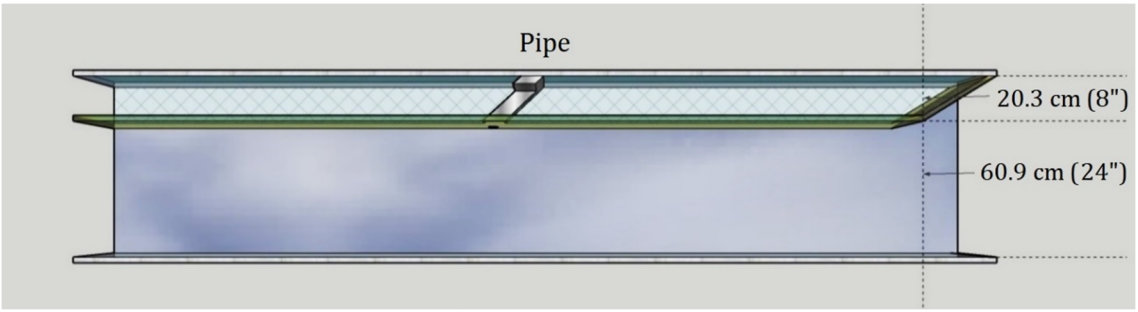

Figure 4. Wide channel configuration (top view).

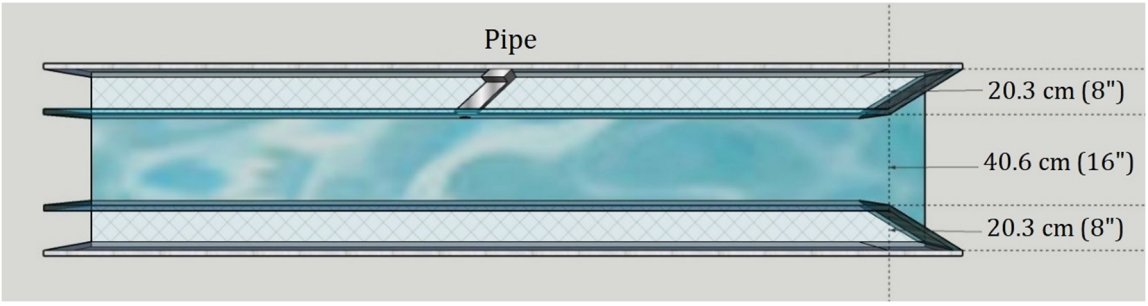

Figure 5. Narrow channel configuration (top view).

After setting up the flume, the experiments were conducted in both wide and narrow channel configurations; 30°, 45°, and 90° junction angles; with lateral flow to main channel flow ratios of 2.5% and 5% for the wide channel, and 2.5%, 5%, and 7.5% for the narrow channel; and different Froude

numbers, from 0.72 (sub-critical) to 3.27 (super-critical). Figure 6 shows how lateral flows were fed to the main channel through the pipe. Table 1 summarizes the experimental scenarios.

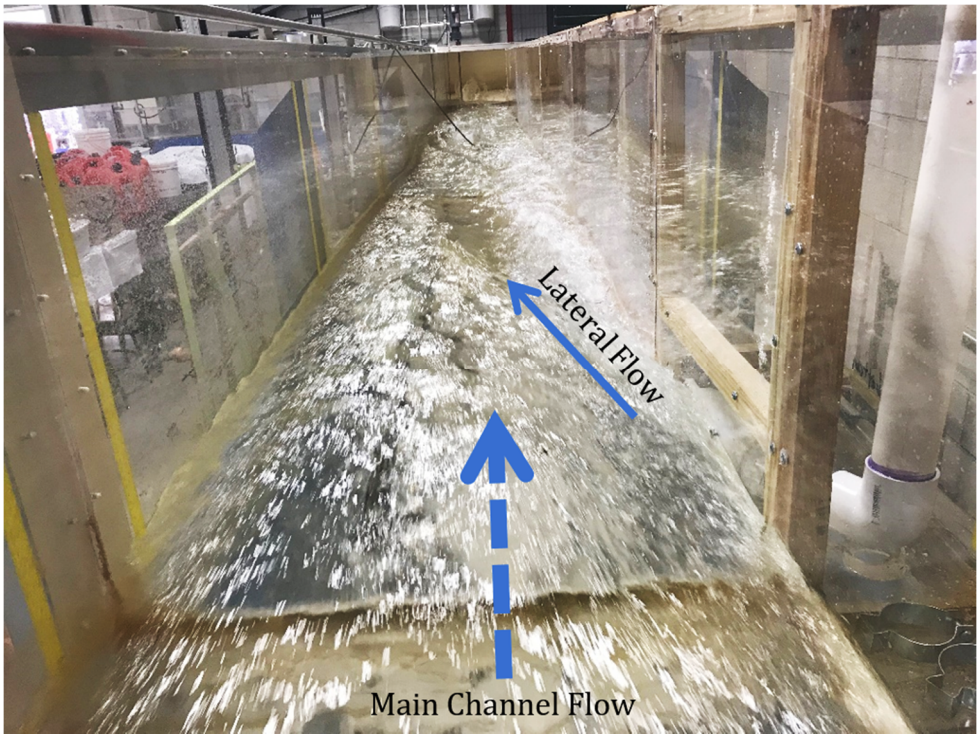

Figure 6. Lateral flow to the main channel (back view).

Table 1. Experimental scenarios.

Flume Width (m)	Flume Slope (%)	Flow Rate (m^3/s)	Fr (-)	Junction Angle (degree)	Lateral Flow Proportion (%)
0.41 (16″)	0.00	0.13	0.72	30, 45, 90	2.5, 5.0, 7.5
	0.42	0.12	0.95	30, 45, 90	2.5, 5.0, 7.5
	0.68	0.14	1.45	30, 45, 90	2.5, 5.0, 7.5
	0.97	0.14	1.74	30, 45, 90	2.5, 5.0, 7.5
	1.68	0.14	2.01	30, 45, 90	2.5, 5.0, 7.5
	2.15	0.13	2.32	30, 45, 90	2.5, 5.0, 7.5
	2.60	0.13	2.80	30, 45, 90	2.5, 5.0, 7.5
	3.51	0.13	3.27	30, 45, 90	2.5, 5.0, 7.5
0.61 (24″)	0.00	0.18	0.80	30, 45, 90	2.5, 5.0
	0.44	0.18	1.0	30, 45, 90	2.5, 5.0
	0.56	0.18	1.2	30, 45, 90	2.5, 5.0
	0.89	0.18	1.6	30, 45, 90	2.5, 5.0
	1.67	0.18	2.0	30, 45, 90	2.5, 5.0
	2.22	0.18	2.4	30, 45, 90	2.5, 5.0
	3.33	0.18	3.1	30, 45, 90	2.5, 5.0
Total number of tests: 120					

Measurement Equipment

In this study, the ultrasonic GREYLINE AVFM 5.0 sensor was mounted on the invert of the flume to measure the flow rate, flow velocity, and water surface elevation in the flume. The sensor mounts on the bottom of a channel with a stainless-steel mounting bracket and a single screw into the bottom of the channel. This device uses a submerged ultrasonic sensor to measure the velocity, flow rate,

and water surface elevation. The sensor is completely sealed with no orifices or ports, and resists fouling, corrosion, and abrasion. The AVFM 5.0 can measure forward flow velocity up to 6 m/s (20 ft/s) and reverse flow up to 1.5 m/s (5 ft/s). The submerged velocity/level sensor measures flow in partially full and surcharged pipes and channels with pressure up to 68.95 kPa (10 psi) [10].

2.2. Numerical Modeling

Conventional 1D numerical modeling treats the junctions by means of internal boundary conditions for the shallow water equations by applying mass continuity combined with a simplified momentum or energy conservation at the junctions [1,4,8,11–14]. It is readily apparent that such boundary conditions and simplified mathematical models are incapable of fully describing the highly turbulent 3D flow features present at a CHZ. The difficulty of adequately describing this flow with simplified mathematical models leads to the necessity of using a 3D computational fluid dynamics (CFD) code to visualize and understand the flow conditions in a CHZ. Numerical modeling is a less time-consuming and expensive way to obtain the various flow parameters needed for engineering design. Once a 3D model is validated, numerical experiments can be designed and conducted for the systematic examination of the standalone effects of different primary controls upon the flow structure development. A 3D CFD model solves the full 3D form of the Navier–Stokes equations, with (Reynolds-averaging (RANS)) or without temporal averaging (direct numerical simulation (DNS)); hence, it is capable of adequately reproducing the evolving primary and secondary flow patterns and turbulent flow structures.

Computer-based simulations are now the dominant tool for understanding and visualizing turbulent flow structures [15]. However, controlled flow visualization experiments are still necessary to direct, develop, and validate the numerical simulations now dominant in the field [16]. Considering the large number of scenarios and limitations in setting up different laboratory experiments, a numerical model (FLOW-3D) was used in this study to simulate the flow topology for different channel configurations, lateral inlet pipe sizes and angles, main channel flow, and lateral flow conditions. FLOW-3D is a general-purpose computational fluid dynamics (CFD) software. It employs specially developed numerical techniques to solve motion equations for fluids to obtain transient, three-dimensional solutions to multi-scale, multi-physics flow problems. An array of physical and numerical options allows users to apply FLOW-3D to a wide variety of fluid flow phenomena [17].

In this study, the simulations were performed on: Three different channel widths of 3.05 (10′), 7.62 (25′), 15.24 m (50′); with three initial water heights in the channel of 1.22 (4′), 2.13 (7′), 3.05 m (10′); three junction angles of 30, 45, 90°; and three inlet pipe diameters of 0.46 (1.5′), 0.91 (3′), 1.52 m (5′); with lateral flow to main channel flow ratios of 2.5%, 5.0%, 10% (based on the flow rates in the 3.05 m (10′) channel); and, three Froude numbers of 0.8, 1.2, 2.0. In all scenarios, the channel bed slope was 0.05%. Table 2 summarizes the simulation scenarios. It should be noted that the lateral flow proportions in the 7.62 (25′) and 15.24 m (50′) channels were based on the 3.05 m (10′) channel, since 2.5%, 5.0%, and 10% of the flow rate in the 7.62 (25′) and 15.24 m (50′) channels would result in very high and uncommon velocities in the lateral inlet pipe. According to the Hydrologic Criteria and Drainage Design Manual (HCDDM) of the Clark County Regional Flood Control District (CCRFCD), the maximum flow velocity in a lateral drainage pipe into a flood control channel should not exceed 10.67 m/s (35 ft/s) [18]. For this reason, the lateral pipe flow proportions in all scenarios in this study were based on the 3.05 m (10′) channel. However, pipe flow velocities up to 15.24 m/s (50 ft/s) were considered, regarding the fact that higher flow velocities may occur under critical conditions.

Table 2. Simulation scenarios.

Width (m)	Initial Water Height (m)	Fr (-)	Inlet Pipe Diameter (m)	Junction Angle (Degree)	Lateral Flow Proportion (%)
3.05 (10′)	1.22 (4′)	0.8, 1.2, 2.0	0.46 (1.5′), 0.91 (3′)	30, 45, 90	2.5, 5, 10
	2.13 (7′)	0.8, 1.2, 2.0	0.46 (1.5′), 0.91 (3′), 1.52 (5′)	30, 45, 90	2.5, 5, 10
	3.05 (10′)	0.8, 1.2, 2.0	0.46 (1.5′), 0.91 (3′), 1.52 (5′)	30, 45, 90	2.5, 5, 10
7.62 (25′)	1.22 (4′)	0.8, 1.2, 2.0	0.46 (1.5′), 0.91 (3′)	30, 45, 90	2.5, 5, 10
	2.13 (7′)	0.8, 1.2, 2.0	0.46 (1.5′), 0.91 (3′), 1.52 (5′)	30, 45, 90	2.5, 5, 10
	3.05 (10′)	0.8, 1.2, 2.0	0.46 (1.5′), 0.91 (3′), 1.52 (5′)	30, 45, 90	2.5, 5, 10
15.24 (50′)	1.22 (4′)	0.8, 1.2, 2.0	0.46 (1.5′), 0.91 (3′)	30, 45, 90	2.5, 5, 10
	2.13 (7′)	0.8, 1.2, 2.0	0.46 (1.5′), 0.91 (3′), 1.52 (5′)	30, 45, 90	2.5, 5, 10
	3.05 (10′)	0.8, 1.2, 2.0	0.46 (1.5′), 0.91 (3′), 1.52 (5′)	30, 45, 90	2.5, 5, 10
Total number of simulations: 648					

2.2.1. Governing Equations

The governing equations on fluid flow are mass continuity and momentum equations. The general mass continuity equation is:

$$V_F \frac{\partial \rho}{\partial t} + \frac{\partial}{\partial x}(\rho u A_x) + R\frac{\partial}{\partial y}\left(\rho v A_y\right) + \frac{\partial}{\partial z}(\rho w A_z) + \xi \frac{\rho u A_x}{x} = R_{DIF} + R_{SOR} \quad (1)$$

where V_F is the fractional volume open to flow, ρ is the fluid density, R_{DIF} is a turbulent diffusion term, and R_{SOR} is a mass source. The velocity components (u, v, w) are in the coordinate directions (x, y, z) or $(r,\ R_{SOR}, z)$. A_x is the fractional area open to flow in the x-direction, while A_y and A_z are similar area fractions for flow in the y and z directions, respectively. The coefficient R depends on the choice of the coordinate system. When Cartesian coordinates are used, R is set to unity and ξ is set to zero. The first term on the right side of Equation (1), is a turbulent diffusion term:

$$R_{DIF} = \frac{\partial}{\partial x}\left(v_p A_x \frac{\partial]\rho}{\partial x}\right) + R\frac{\partial}{\partial y}\left(v_\rho A_y R\frac{\partial \rho}{\partial y}\right) + \frac{\partial}{\partial z}\left(v_\rho A_z \frac{\partial \rho}{\partial z}\right) + \xi \frac{v_\rho A_x}{x}\frac{\partial \rho}{\partial x} \quad (2)$$

where the coefficient v_ρ is equal to $S_c \frac{\mu}{\rho}$, in which μ is the coefficient of momentum diffusion (i.e., the viscosity); and S_c is a constant, whose reciprocal is usually referred to as the turbulent Schmidt number. This type of mass diffusion only makes sense for turbulent mixing processes in fluids having a non-uniform density. The last term, R_{SOR}, on the right side of Equation (1) is a density source term that can be used, for example, to model mass injection through porous obstacle surfaces. Compressible flow problems require the solution of the full density transport equation, as stated in Equation (1). For incompressible fluids, ρ is a constant, and Equation (1) reduces to the incompressibility condition:

$$\frac{\partial}{\partial x}(u A_x) + R\frac{\partial}{\partial y}\left(v A_y\right) + \frac{\partial}{\partial z}(w A_z) + \xi \frac{u A_x}{x} = \frac{R_{SOR}}{\rho} \quad (3)$$

For problems in which the propagation of acoustic pressure waves is important, but the fluid may otherwise be treated as incompressible, the density time derivative is approximated by:

$$\frac{\partial \rho}{\partial t} \approx \frac{1}{c^2}\frac{\partial p}{\partial t}$$

where c^2 is the square of the sound speed, and p is the pressure. This approximation is valid in the range $\left|\frac{\delta\rho}{\rho}\right| < 0.1$. With this approximation, the modified continuity equation then becomes:

$$\frac{V_F}{\rho c^2}\frac{\partial p}{\partial t} + \frac{\partial u A_x}{\partial x} + R\frac{\partial v A_y}{\partial y} + \frac{\partial w A_z}{\partial z} + \xi\frac{u A_x}{x} = \frac{R_{SOR}}{\rho} \tag{4}$$

2.2.2. Momentum Equations

The equations of motion for the fluid velocity components (u, v, w) in the three coordinate directions are Navier–Stokes equations with some additional terms:

$$\begin{aligned}
&\tfrac{\partial u}{\partial t} + \tfrac{1}{V_F}\Big\{uA_x\tfrac{\partial u}{\partial x} + vA_yR\tfrac{\partial u}{\partial y} + wA_z\tfrac{\partial u}{\partial z}\Big\} - \xi\tfrac{A_y v^2}{xV_F} \\
&\qquad = -\tfrac{1}{\rho}\tfrac{\partial p}{\partial x} + G_x + f_x - b_x - \tfrac{R_{SOR}}{\rho V_F}(u - u_w - \delta u_s) \\
&\tfrac{\partial v}{\partial t} + \tfrac{1}{V_F}\Big\{uA_x\tfrac{\partial v}{\partial x} + vA_yR\tfrac{\partial v}{\partial y} + wA_z\tfrac{\partial v}{\partial z}\Big\} + \xi\tfrac{A_y uv}{xV_F} \\
&\qquad = -\tfrac{1}{\rho}\Big(R\tfrac{\partial p}{\partial y}\Big) + G_y + f_y - b_y - \tfrac{R_{SOR}}{\rho V_F}(v - v_w - \delta v_s) \\
&\tfrac{\partial w}{\partial t} + \tfrac{1}{V_F}\Big\{uA_x\tfrac{\partial w}{\partial x} + vA_yR\tfrac{\partial w}{\partial y} + wA_z\tfrac{\partial w}{\partial z}\Big\} \\
&\qquad = -\tfrac{1}{\rho}\tfrac{\partial p}{\partial z} + G_z + f_z - b_z - \tfrac{R_{SOR}}{\rho V_F}(w - w_w - \delta w_s)
\end{aligned} \tag{5}$$

In these equations, (G_x, G_y, G_z) are body accelerations, (f_x, f_y, f_z) are viscous accelerations, (b_x, b_y, b_z) are flow losses in porous media or across porous baffle plates, and the final terms account for the injection of mass at a source represented by a geometry component. The term $\mathrm{U}_w = (u_w, v_w, w_w)$ in Equation (5) is the velocity of the source component, which will generally be non-zero for a mass source in a general moving objects model. The term $\mathrm{U}_s = (u_s, v_s, w_s)$ is the velocity of the fluid at the surface of the source, relative to the source itself. It is computed in each control volume as:

$$\mathrm{U}_s = \frac{dQ}{\rho Q dA}n \tag{6}$$

where dQ is the mass flow rate, ρQ is the fluid source density, dA is the area of the source surface in the cell, and n is the outward normal to the surface. When $\delta = 0.0$, in Equation (5), the source is of the stagnation pressure type, whereas if $\delta = 1.0$, the source is of the static pressure type. For a variable dynamic viscosity μ, the viscous accelerations are:

$$\begin{aligned}
\rho V_F f_x &= wsx - \Big\{\tfrac{\partial}{\partial x}(A_x\tau_{xx}) + R\tfrac{\partial}{\partial y}\Big(A_y\tau_{xy}\Big) + \tfrac{\partial}{\partial z}(A_z\tau_{xz}) + \tfrac{\xi}{x}\Big(A_x\tau_{xx} - A_y\tau_{yy}\Big)\Big\} \\
\rho V_F f_y &= wsy - \Big\{\tfrac{\partial}{\partial x}\Big(A_x\tau_{xy}\Big) + R\tfrac{\partial}{\partial y}\Big(A_y\tau_{yy}\Big) + \tfrac{\partial}{\partial z}\Big(A_z\tau_{yz}\Big) + \tfrac{\xi}{x}\Big(A_x + A_y\Big)\tau_{xy}\Big\} \\
\rho V_F f_z &= wsz - \Big\{\tfrac{\partial}{\partial x}(A_x\tau_{xz}) + R\tfrac{\partial}{\partial y}\Big(A_y\tau_{yz}\Big) + \tfrac{\partial}{\partial z}(A_z\tau_{zz}) + \tfrac{\xi}{x}(A_x\tau_{xz})\Big\}
\end{aligned} \tag{7}$$

where

$$\tau_{xx} = -2\mu\left\{\frac{\partial u}{\partial x} - \frac{1}{3}\left(\frac{\partial u}{\partial x} + R\frac{\partial v}{\partial y} + \frac{\partial w}{\partial z} + \frac{\xi u}{x}\right)\right\} \tag{8}$$

$$\tau_{yy} = -2\mu\left\{R\frac{\partial v}{\partial y} + \xi\frac{u}{x} - \frac{1}{3}\left(\frac{\partial u}{\partial x} + R\frac{\partial v}{\partial y} + \frac{\partial w}{\partial z} + \frac{\xi u}{x}\right)\right\} \tag{9}$$

$$\tau_{zz} = -2\mu\left\{\frac{\partial w}{\partial z} - \frac{1}{3}\left(\frac{\partial u}{\partial x} + R\frac{\partial v}{\partial y} + \frac{\partial w}{\partial z} + \frac{\xi u}{x}\right)\right\} \tag{10}$$

$$\tau_{xy} = -\mu\left\{\frac{\partial v}{\partial x} + R\frac{\partial u}{\partial y} - \frac{\xi v}{x}\right\} \tag{11}$$

$$\tau_{xz} = -\mu\left\{\frac{\partial u}{\partial z} + \frac{\partial w}{\partial x}\right\} \tag{12}$$

$$\tau_{yz} = -\mu\left\{\frac{\partial v}{\partial z} + R\frac{\partial w}{\partial y}\right\} \tag{13}$$

In the above expressions, the terms *wsx*, *wsy*, and *wsz* are wall shear stresses. If these terms are omitted, there is no wall shear stress because the remaining terms contain the fractional flow areas (A_x, A_y, A_z), which vanish at the walls. The wall stresses are modeled by assuming a zero tangential velocity on the portion of any area closed to flow. Mesh and moving obstacle boundaries are an exception because they can be assigned non-zero tangential velocities. In this case, the allowed boundary motion corresponds to a rigid body translation of the boundary parallel to its surface. For turbulent flows, a law-of-the-wall velocity profile is assumed near the wall, which modifies the wall shear stress magnitude.

2.2.3. Fluid Interfaces and Free-Surfaces

Fluid configurations are defined in terms of a volume of fluid (VOF) function, $F\ (x, y, z, t)$. This function represents the volume of fluid #1 per unit volume and satisfies the equation:

$$\frac{\partial F}{\partial t} + \frac{1}{V_F}\left[\frac{\partial}{\partial x}(FA_x u) + R\frac{\partial}{\partial y}\left(FA_y v\right) + \frac{\partial}{\partial z}(FA_z w) + \xi\frac{FA_x u}{x}\right] = F_{DIF} + F_{SOR} \tag{14}$$

where

$$F_{DIF} = \frac{1}{V_F}\left\{\frac{\partial}{\partial x}\left(v_F A_x \frac{\partial F}{\partial x}\right) + R\frac{\partial}{\partial x}\left(v_F A_y R\frac{\partial F}{\partial y}\right) + \frac{\partial}{\partial z}\left(v_F A_z \frac{\partial F}{\partial z}\right) + \xi\frac{v_F A_x F}{x}\right\} \tag{15}$$

The diffusion coefficient is defined as $v_F = c_F\frac{\mu}{\rho}$, where c_F is a constant whose reciprocal is sometimes referred to as a turbulent Schmidt number. This diffusion term only makes sense for the turbulent mixing of two fluids whose distributions are defined by the F function. The term F_{SOR} corresponds to the density source R_{SOR} in Equation (1); F_{SOR} is the time change rate of the fluid #1 volume fraction, associated with the mass source for fluid #1. The interpretation of F depends on the type of problem being solved. Incompressible problems must involve either a single fluid with a free-surface or two fluids and no free-surfaces. For a single fluid, F represents the volume fraction occupied by the fluid. Thus, fluid exists where $F = 1$, and void regions correspond to locations where $F = 0$. "Voids" are regions without fluid mass that have a uniform pressure assigned to them. Physically, they represent regions filled with a vapor or gas, whose density is insignificant with respect to the fluid density. Two-fluid problems may be composed of either two incompressible fluids, or one incompressible and one compressible fluid. F represents the volume fraction of the incompressible fluid component in either case, which is referred to as fluid #1. The complementary region, with the volume fraction $1 - F$, represents fluid #2, and may have either a constant density, or its density may be computed from the compressible fluid equation-of-state. More details regarding FLOW-3D governing equations can be found in the FLOW-3D user's manual [17].

3. Results and Discussion

3.1. Flume Test Results

3.1.1. Water Height Measurements

Changes in flow proportions and junction angles resulted in measurable changes in the flow pattern. Figures 7–9 provide examples of water height measurements in the wide channel configuration, with and without lateral flow in a 90° junction, which were used to calculate the maximum water height ratios in the flume. Other flume test results are available in Appendix A.

According to Figure 7, since the flow rates used for all scenarios were almost similar, in cases where the flow velocity was higher, the water height was lower. For instance, the water height for the Fr = 0.8 scenario was the highest, while for the Fr = 3.1, it was the lowest. Higher fluctuations were observed at the upstream of the flume in higher Froude numbers. This was due to the angled plate that was installed at the entrance of the flume (see Figure 4) to narrow the channel, which caused the formation of waves. However, the impacts diminished further downstream of the flume.

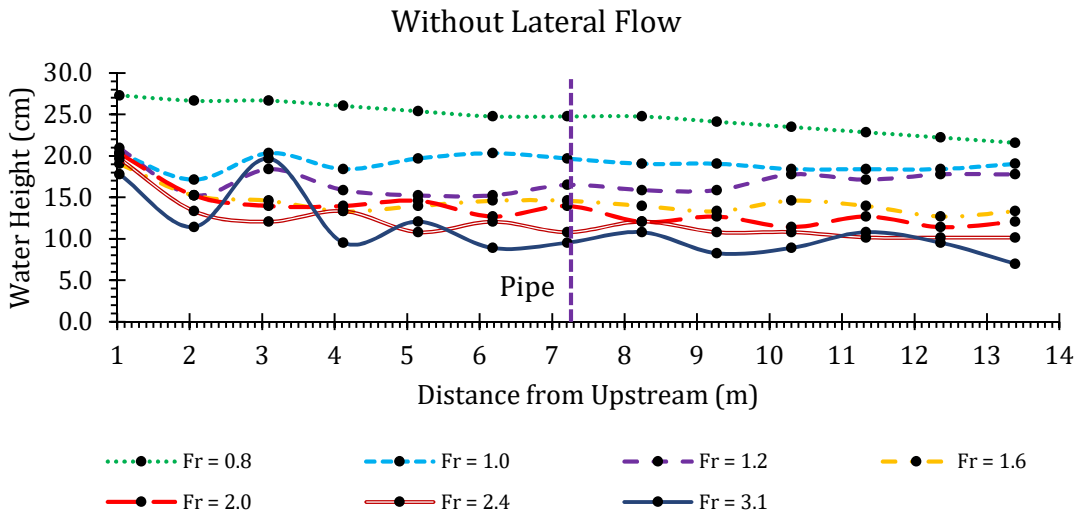

Figure 7. Water heights in the wide channel, without lateral flow.

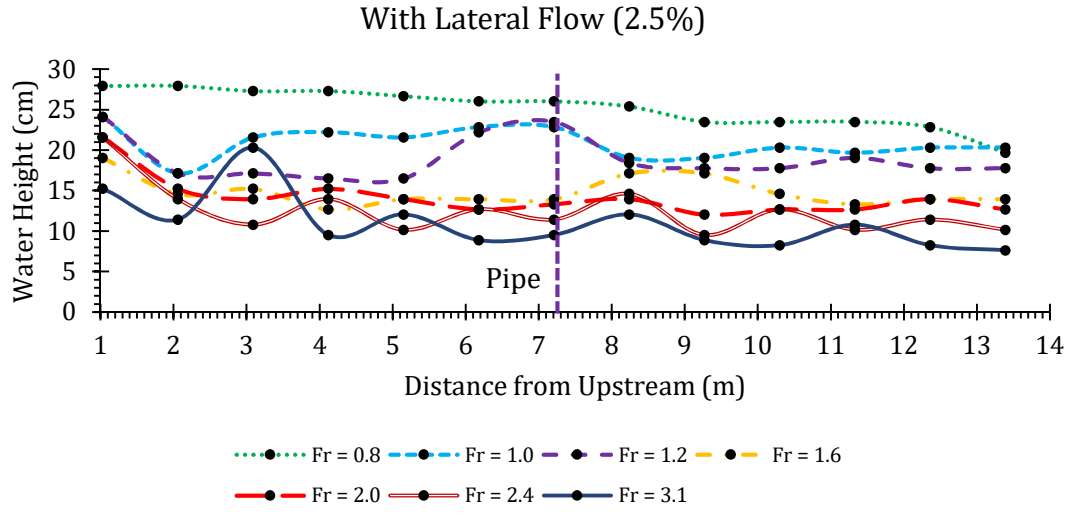

Figure 8. Water heights in the wide channel, with 2.5% lateral flow.

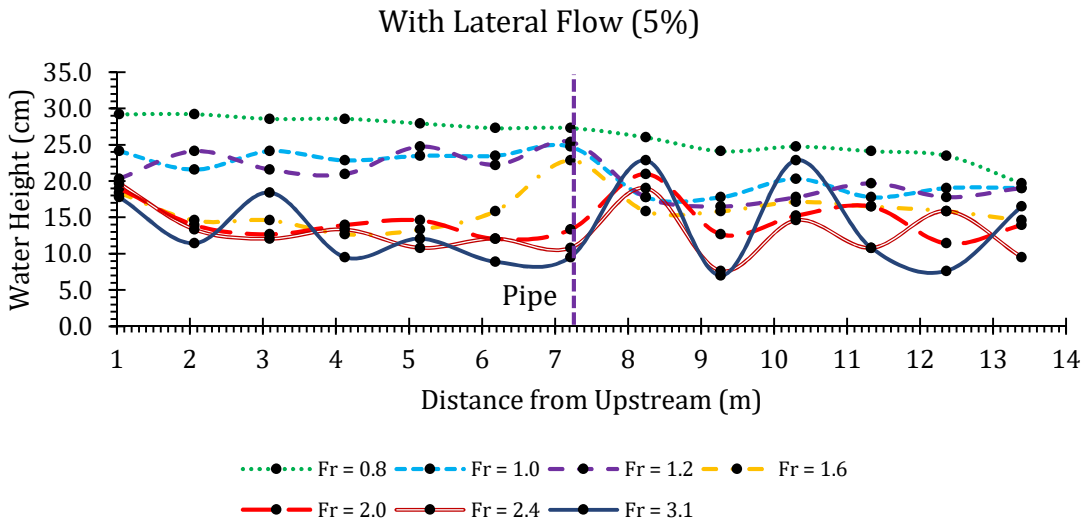

Figure 9. Water heights in the wide channel, with 5.0% lateral flow.

Figure 8 shows that as the lateral flow entered the channel, water heights in all scenarios were impacted either upstream or downstream of the pipe. The results showed that for Fr = 0.8, 1.0, and 1.2, the maximum water height occurred upstream of the pipe, while for Fr = 1.6, 2.0, 2.4, and 3.1, the maximum water height occurred downstream of the pipe. This was because the flow momentum was higher in the higher Froude numbers, which pushed the jet of water through the pipe further downstream. High peaks in the flume's entrance should be neglected as the highest water heights, since their formation was due to the angled wall installed upstream of the flume, which created local waves.

Furthermore, comparing Figures 8 and 9, as the lateral flow proportion increased, water height peaks increased as well. According to Figure 9, the water height peak for Fr = 0.8, 1.0, 1.2, and 1.6 occurred upstream of the pipe, while for Fr = 2.0, 2.4, and 3.1, it occurred downstream of the pipe. Compared with the 2.5% lateral flow, more water height peaks were observed upstream of the pipe.

3.1.2. Water Height Ratios

Experimental test results were used to calculate the maximum water height ratios in the channel, by dividing the maximum water height in the channel with lateral flow, by the water height in the channel without lateral flow. In Figures 10–15, the maximum water height ratios for both wide and narrow channels are presented. Moreover, Tables 3–8 present maximum water height ratios, along with the flow rate and velocity in the flume and the pipe for each scenario. In the wide channel, the flow rate in the flume was maintained at the maximum value that could be achieved in the lab, but different flow rates were used in the narrow channel. For both channel configurations, to achieve certain flow velocities, and consequently, certain Froude numbers in the flume, the flume angle was adjusted.

90° Junction

Table 3. Experimental results for the 90° junction in the wide channel.

Fr (-)	Q Flume (m^3/s)	V Flume (m/s)	θ Junc. (Deg.)	2.5% Lateral Flow			5% Lateral Flow		
				q Pipe (m^3/s)	v Pipe (m/s)	H/H_0	q Pipe (m^3/s)	v Pipe (m/s)	H/H_0
0.8	0.18	1.37	90	0.0045	2.23	1.05	0.0091	4.45	1.1
1	0.18	1.55	90	0.0045	2.23	1.16	0.0091	4.45	1.26
1.2	0.18	1.65	90	0.0045	2.23	1.46	0.0091	4.45	1.63
1.6	0.18	1.86	90	0.0045	2.23	1.29	0.0091	4.45	1.57
2	0.18	2.10	90	0.0045	2.23	1.22	0.0091	4.45	1.74

Table 4. Experimental results for the 90° junction in the narrow channel.

Fr (-)	Q Flume (m^3/s)	V Flume (m/s)	θ Junc. (deg.)	2.5% Lateral Flow			5% Lateral Flow			7.5% Lateral Flow		
				q Pipe (m^3/s)	v Pipe (m/s)	H/H_0	q Pipe (m^3/s)	v Pipe (m/s)	H/H_0	q Pipe (m^3/s)	v Pipe (m/s)	H/H_0
0.72	0.1322	1.16	90	0.0034	1.65	1.14	0.0065	3.26	1.17	0.0099	4.91	1.20
0.95	0.1158	1.34	90	0.0028	1.43	1.30	0.0057	2.87	1.40	0.0088	4.30	1.48
1.45	0.1368	1.89	90	0.0034	1.68	1.12	0.0068	3.38	1.58	0.0102	5.06	1.73
1.74	0.1385	2.13	90	0.0034	1.71	1.13	0.0068	3.41	1.29	0.0105	5.12	1.71
2.01	0.1399	2.35	90	0.0034	1.74	1.16	0.0071	3.44	1.32	0.0105	5.18	1.26
2.32	0.1294	2.53	90	0.0031	1.58	1.24	0.0065	3.20	1.29	0.0096	4.79	1.53
2.8	0.1322	2.87	90	0.0034	1.65	1.20	0.0065	3.26	1.60	0.0099	4.91	1.87
3.27	0.1280	3.17	90	0.0031	1.58	1.29	0.0065	3.17	1.86	0.0096	4.75	2.50

According to Figure 10, the maximum water height ratios in the 5% lateral flow were higher than in the 2.5%. Moreover, in the 2.5% case, the maximum ratio occurred for Fr = 1.2, and for higher Froude numbers, the water height peak decreased. This was because the water jet through the pipe could reach the outer wall of the flume, and the water height peak was created by the combined effects of splashing, along with the incoming flow from the flume upstream. As the Froude number increased, the jet was deflected and could not reach the outer wall of the flume to create flow splashing. For Froude numbers smaller than 1.2, the water height in the channel was higher, compared with other Froude numbers, and the water height around the pipe was less impacted by the lateral flow through the submerged pipe. This resulted in lower maximum water height ratios in the channel.

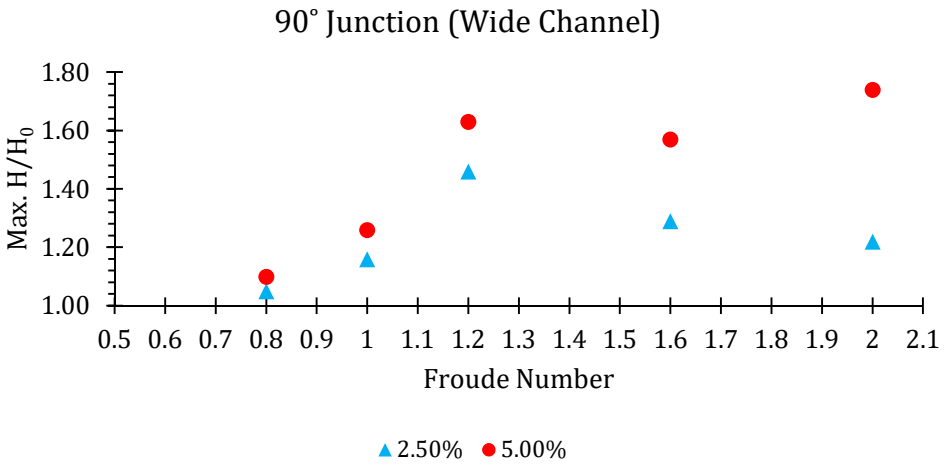

Figure 10. Maximum water height ratios in a 90° junction (wide channel).

Similarly, for the 5% lateral flow, in Fr = 1.2, the maximum water height ratio increased compared with the smaller Froude numbers. However, the maximum ratio occurred for Fr = 2. This can be justified by the fact that as the water height for similar flow rates is lower for higher Froude numbers, and as the 5% lateral flow jet is strong enough to create a blockage in the water path, this blockage could cause a hydraulic jump that increases the water height in the confluence.

In the narrow channel (Figure 11), similar to the wide channel (Figure 10), as the lateral flow proportion increased, maximum water height ratios increased in the flume as well. In the 2.5% lateral flow case, the maximum water height ratio occurred for Fr = 0.95, but for 5% and 7.5% lateral flow proportions, the maximum occurred for Fr = 1.45.

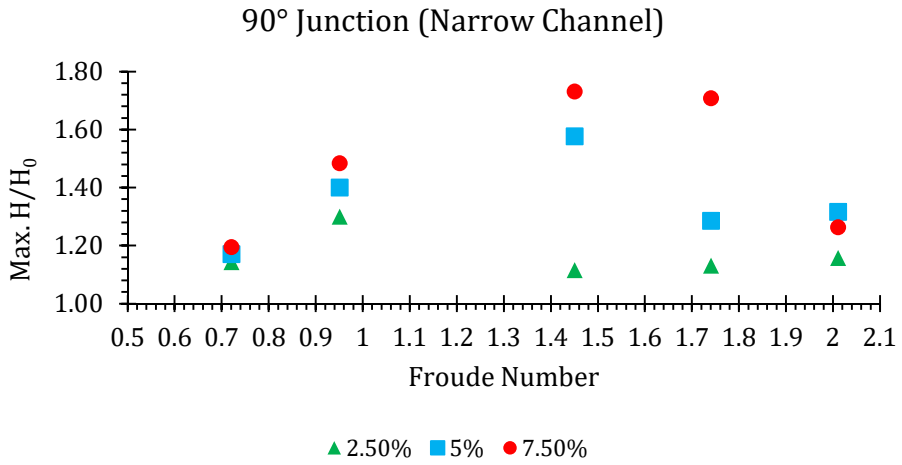

Figure 11. Maximum water height ratios in a 90° junction (narrow channel).

45° Junction

Table 5. Experimental results for the 45° junction in the wide channel.

Fr (-)	Q Flume (m^3/s)	V Flume (m/s)	θ Junc. (Deg.)	2.5% Lateral Flow			5% Lateral Flow		
				q Pipe (m^3/s)	v Pipe (m/s)	H/H_0	q Pipe (m^3/s)	v Pipe (m/s)	H/H_0
0.8	0.18	1.37	45	0.0045	2.23	1.03	0.0975	4.45	1.06
1	0.18	1.55	45	0.0045	2.23	1.14	0.0975	4.45	1.14
1.2	0.18	1.65	45	0.0045	2.23	1.16	0.0975	4.45	1.2
1.6	0.18	1.86	45	0.0045	2.23	1.19	0.0975	4.45	1.3
2	0.18	2.10	45	0.0045	2.23	1.22	0.0975	4.45	1.28

Table 6. Experimental results for the 45° junction in the narrow channel.

Fr (-)	Q Flume (m^3/s)	V Flume (m/s)	θ Junc. (Deg.)	2.5% Lateral Flow			5% Lateral Flow			7.5% Lateral Flow		
				q Pipe (m^3/s)	v Pipe (m/s)	H/H_0	q Pipe (m^3/s)	v Pipe (m/s)	H/H_0	q Pipe (m^3/s)	v Pipe (m/s)	H/H_0
0.72	0.1322	1.16	45	0.0034	1.65	1.12	0.0065	3.26	1.13	0.0099	4.91	1.13
0.95	0.1158	1.34	45	0.0028	1.43	1.16	0.0057	2.87	1.16	0.0088	4.30	1.15
1.45	0.1368	1.89	45	0.0034	1.68	1.04	0.0068	3.38	1.16	0.0102	5.06	1.08
1.74	0.1385	2.13	45	0.0034	1.71	1.19	0.0068	3.41	1.13	0.0105	5.12	1.17
2.01	0.1399	2.35	45	0.0034	1.74	1.11	0.0071	3.44	1.16	0.0105	5.18	1.21
2.32	0.1294	2.53	45	0.0031	1.58	1.12	0.0065	3.20	1.12	0.0096	4.79	1.24
2.8	0.1322	2.87	45	0.0034	1.65	1.40	0.0065	3.26	1.33	0.0099	4.91	1.53
3.27	0.1280	3.17	45	0.0031	1.58	1.36	0.0065	3.17	1.29	0.0096	4.75	1.36

In the 45° junction, the results show that similar to the 90° junction, higher lateral flows correspond to higher maximum water height ratios in the flume. According to Figure 12, in the wide channel, for the 2.5% lateral flow, the maximum water height ratio occurred for Fr = 2, while for the 5% lateral flow, the maximum occurred for Fr = 1.6.

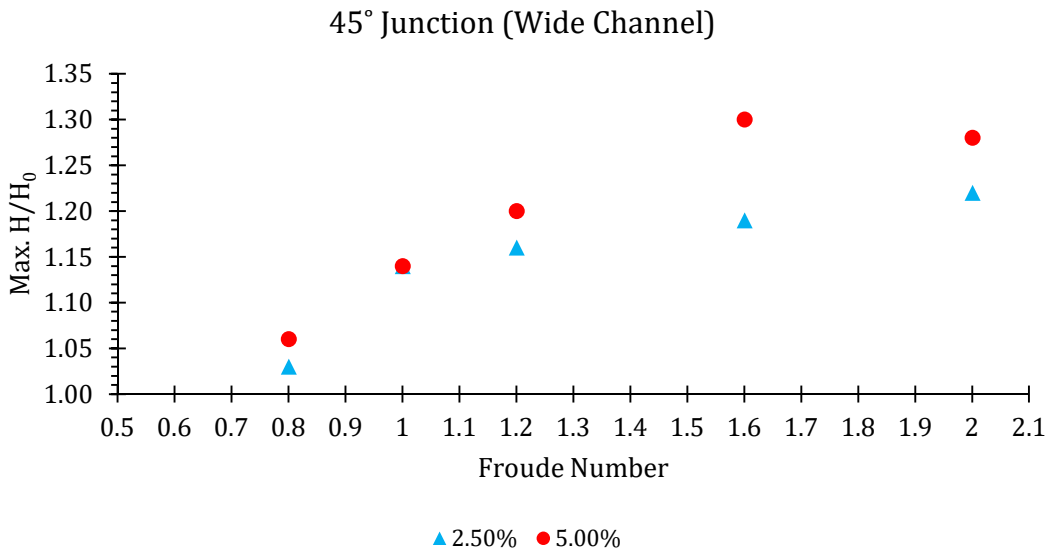

Figure 12. Maximum water height ratios in a 45° junction (wide channel).

In the narrow channel, and for the 45° junction (Figure 13), when the water was sub-critical in the channel, the maximum water height ratios were almost the same for all scenarios. For super-critical flow conditions, the maximum values did not show a distinct pattern. However, the maximum water height ratios for 2.5%, 5%, and 7.5% lateral flow proportions occurred at Fr = 1.74, 2.01, and 2.01, respectively.

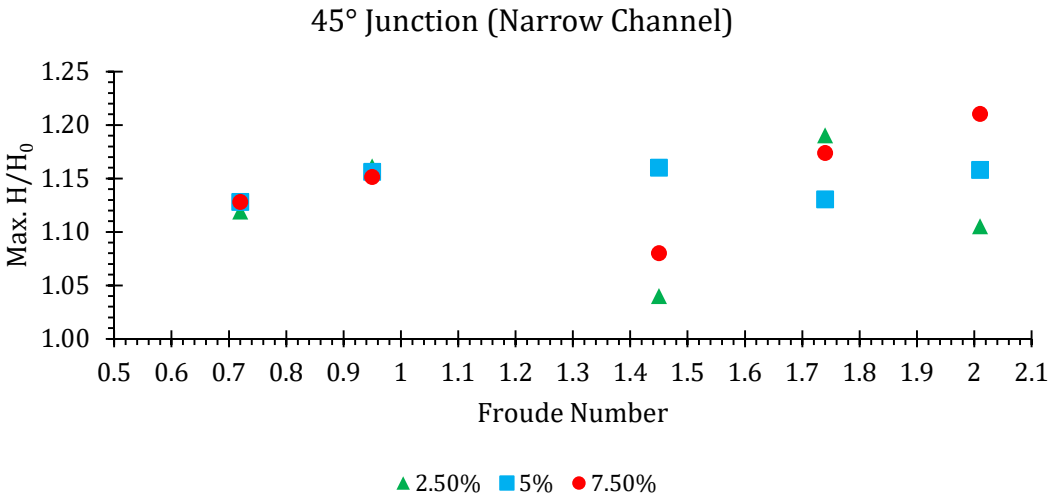

Figure 13. Maximum water height ratios in a 45° junction (narrow channel).

30° Junction

Table 7. Experimental results for the 30° junction in the wide channel.

Fr (-)	Q Flume (m^3/s)	V Flume (m/s)	θ Junc. (Deg.)	2.5% Lateral Flow			5% Lateral Flow		
				q Pipe (m^3/s)	v Pipe (m/s)	H/H_0	q Pipe (m^3/s)	v Pipe (m/s)	H/H_0
0.8	0.18	1.37	30	0.0045	2.23	1.03	0.009	4.45	1.03
1	0.18	1.55	30	0.0045	2.23	1.10	0.009	4.45	1.10
1.2	0.18	1.65	30	0.0045	2.23	1.12	0.009	4.45	1.12
1.6	0.18	1.86	30	0.0045	2.23	1.10	0.009	4.45	1.10
2	0.18	2.10	30	0.0045	2.23	1.11	0.009	4.45	1.11

Table 8. Experimental results for the 30° junction in the narrow channel.

Fr (-)	Q Flume (m^3/s)	V Flume (m/s)	θ Junc. (Deg.)	2.5% Lateral Flow			5% Lateral Flow			7.5% Lateral Flow		
				q Pipe (m^3/s)	v Pipe (m/s)	H/H_0	q Pipe (m^3/s)	v Pipe (m/s)	H/H_0	q Pipe (m^3/s)	v Pipe (m/s)	H/H_0
0.72	0.1322	1.16	30	0.0034	1.65	1.13	0.0065	3.26	1.13	0.0099	4.91	1.13
0.95	0.1158	1.34	30	0.0028	1.43	1.13	0.0057	2.87	1.18	0.0088	4.30	1.18
1.45	0.1368	1.89	30	0.0034	1.68	1.12	0.0068	3.38	1.17	0.0102	5.06	1.08
1.74	0.1385	2.13	30	0.0034	1.71	1.19	0.0068	3.41	1.19	0.0105	5.12	1.24
2.01	0.1399	2.35	30	0.0034	1.74	1.16	0.0071	3.44	1.21	0.0105	5.18	1.21
2.32	0.1294	2.53	30	0.0031	1.58	1.29	0.0065	3.20	1.29	0.0096	4.79	1.29
2.8	0.1322	2.87	30	0.0034	1.65	1.40	0.0065	3.26	1.33	0.0099	4.91	1.40
3.27	0.1280	3.17	30	0.0031	1.58	1.20	0.0065	3.17	1.29	0.0096	4.75	1.27

In the 30° junction, and the wide channel (Figure 14), for both 2.5% and 5% lateral flow proportions, the maximum water height ratio occurred for Fr = 1.2. In the narrow channel (Figure 15), the maximum water height ratios for 2.5%, 5%, and 7.5% lateral flow proportions occurred at Fr = 1.74, 2.01, and 1.74, respectively.

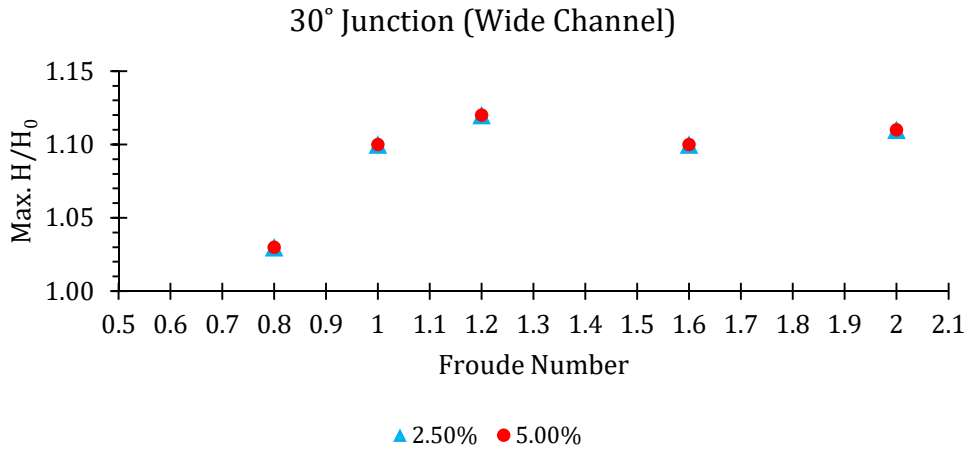

Figure 14. Maximum water height ratios in a 30° junction (wide channel).

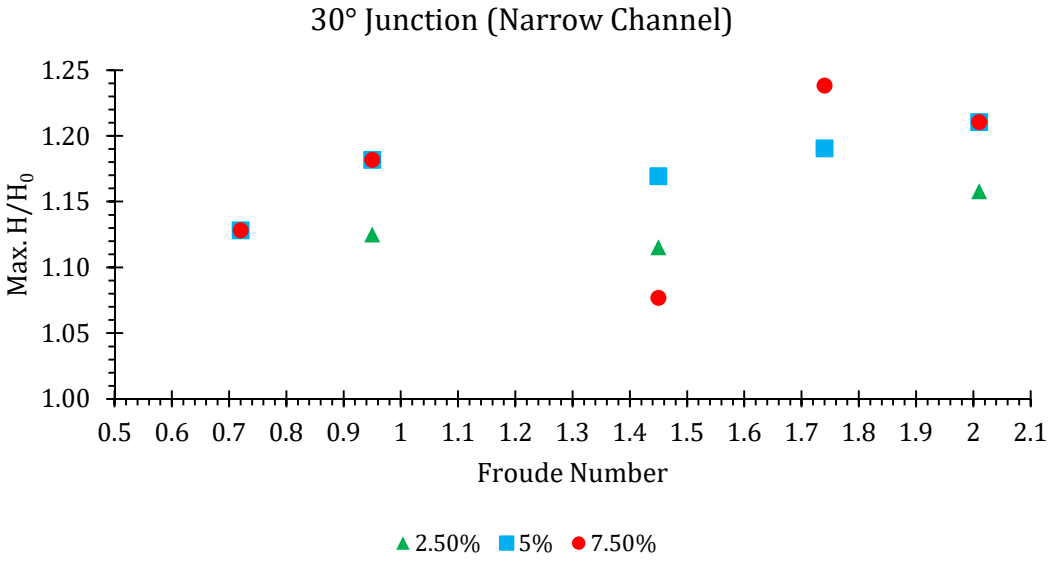

Figure 15. Maximum water height ratios in a 30° junction (narrow channel).

Based on the results for the 90°, 45°, and 30° junctions, both in the wide and narrow channel configurations, it can be concluded that, as the lateral pipe angle and lateral flow proportion increase, the maximum water height ratios in the channel also increase.

3.2. Numerical Model Setup

3.2.1. Geometry

Geometry is constructed in FLOW-3D by assembling solid geometric objects to define the flow region for a simulation. The flow geometry is then embedded in the computational grid by the preprocessor using a technique called FAVOR^{TM}, an acronym for fractional area/volume obstacle representation. This method computes open area fractions on the cell faces, along with the open volume fraction, and reconstructs the geometry based on these parameters. This approach offers a simple and accurate way to represent complex surfaces in the domain without requiring a body-fitted grid.

Figure 16 shows a 3D view of the channel and its components, modeled in FLOW-3D. A roughness height (absolute roughness) of 0.001 m was assigned to all components, as the absolute roughness of ordinary concrete.

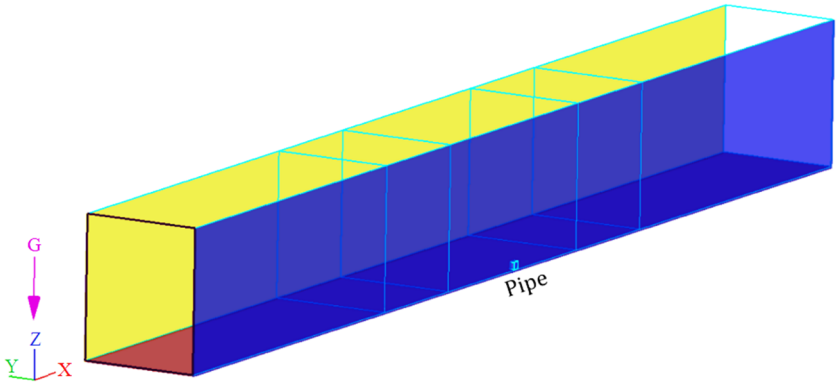

Figure 16. 3D view of the channel components and mesh planes.

3.2.2. Meshing

FLOW-3D uses a structured mesh that may be defined in either a cartesian or cylindrical coordinate system. It is possible to define multiple mesh blocks (multi-block gridding) to create more efficient meshes when modeling complex flow domains. In this study, finer grids were used near the confluence, and coarser grids were used further away from the junction, where the influence of the confluence diminishes (Figure 17). This kind of grid design has the potential to capture the near confluence flow behavior efficiently, while reducing computation cost. Table 9 presents the grid size for each mesh block.

Table 9. Grid sizes in each mesh block in the channel.

Mesh Block	Grid Size (cm)
1	2
2	1.5
3	1
4 (Pipe)	0.7

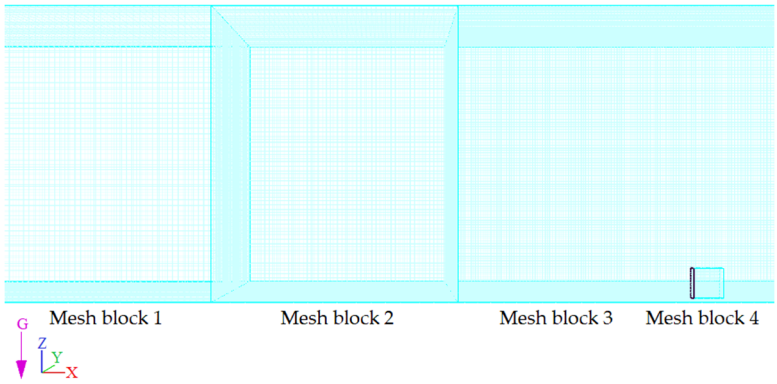

Figure 17. Meshing the channel, using four different grid sizes.

3.2.3. Favor

FAVOR^{TM} is a very powerful method for incorporating geometry effects into the governing equations, but like all discrete methods, it is affected by the resolution of the computational grid. This is because the preprocessor generates area fractions for each cell face in the grid by determining which corners of the face are inside of a defined geometry. If all four corners of a cell face are inside the geometry, then the entire face is defined to be within the geometry. Similarly, if all corners lie outside, then the entire face is assumed to be outside the geometry. When some face corners are inside a geometry and some are outside, the intersection of the geometry with face edges is computed. Area fractions are then computed from these intersection points, assuming straight-line connections between the intersection points within the face. The straight-line assumption introduces a small error in the fractional area when the geometry boundary is curved inside the cell. The approximation is consistent with the other assumptions in the equation development, and improves as the grid resolution is refined [17].

Figure 18 shows a 3D view of the favored channel. According to the figure, all components are properly captured in the mesh space. Moreover, Figure 19 shows how the pipe was modeled as a hole in a pipe complement attached to the inner wall of the flume, along with its favored view for 45° and 30° junctions.

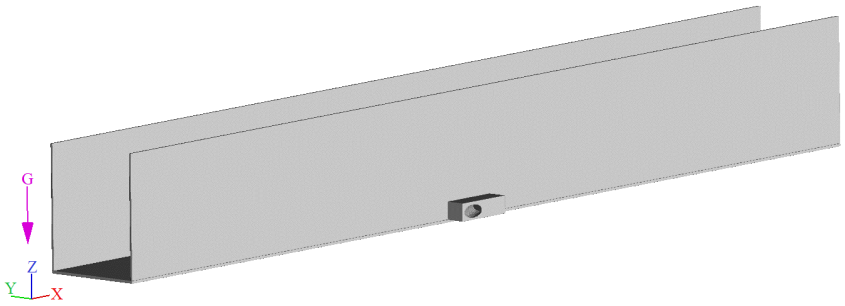

Figure 18. 3D favored view of the channel.

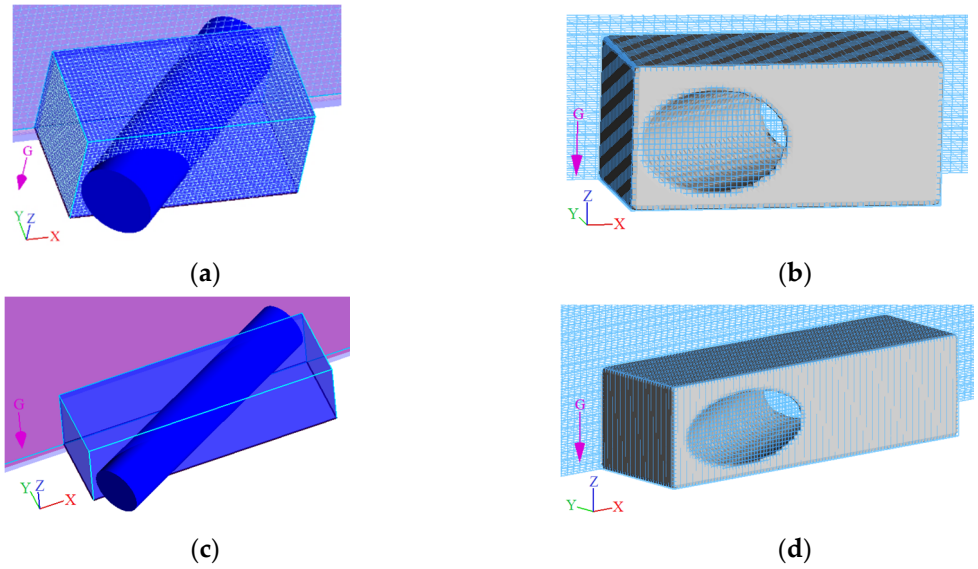

Figure 19. (**a**,**c**): Pipe defined as a hole that passes through the channel wall and the pipe complement; (**b**,**d**): Favored view of the lateral inlet pipe.

3.2.4. Boundary Conditions

The equations governing the motion of fluid flow can be categorized as initial-boundary value problems, meaning that the solution must be known at the initial time and boundaries to be found. This paradox is managed by assuming the solution at the boundaries (setting the boundary conditions) and initial time (initial conditions), and using these assumed values to solve the governing PDE inside of the domain. This implies that the solution to the problem is fundamentally defined by what is assumed at the boundaries. Therefore, it is quite important that the solution assumed at the boundary is a good approximation at this location.

Figure 20 shows the boundary conditions on each mesh block face for the entire channel volume. The boundary conditions on the inner and outer walls, as well as and the channel bottom, were "wall". The boundary condition at the top of each mesh block was "symmetry". At the channel entrance, between the mesh blocks, and at the end of the channel, the boundary conditions were "volume flow rate", "grid overlay", and "outflow", respectively.

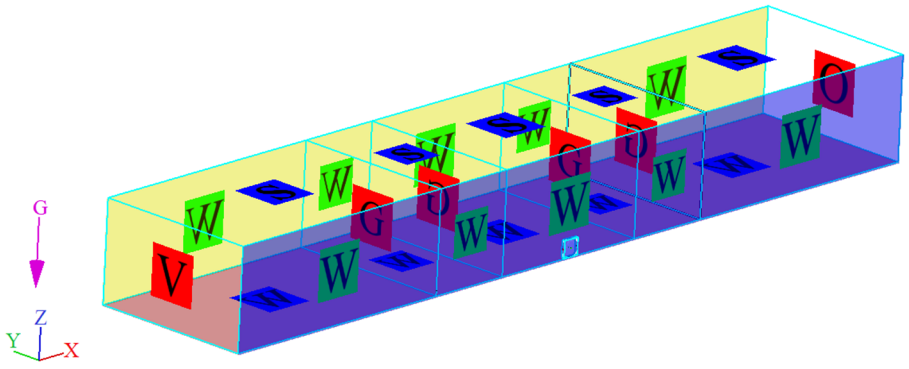

Figure 20. Boundary conditions in the simulated channel.

The wall boundary condition applies the no-slip condition at the boundary, as well as a zero-velocity condition normal to the boundary. The symmetry boundary condition applies a zero-gradient condition at the boundary, as well as a zero-velocity condition normal to the boundary. The volume flow rate boundary condition applies the specified flow rate at the boundary. The grid overlay boundary

condition applies the solution from the restart source simulation, as a boundary condition in a restart simulation. Finally, the outflow boundary condition uses a Sommerfeld radiation condition to dynamically estimate the conditions at the boundary.

3.2.5. Initial Conditions

Initial conditions define the starting conditions in a simulation. As mentioned in the mesh boundary conditions, the initial state of the solution for transient fluid flow problems must be known in order to find a solution. Further, in a manner similar to what is done with boundary conditions, the initial conditions are assumed, approximating the true state at time t = 0. The accuracy of the initial conditions is somewhat less important than that of the boundary conditions because their effect is reduced as time progresses. Because of this effect, it is common to define the initial fluid geometry with reasonable accuracy, but to assume that the pressure and velocity fields are uniform. This typically produces good results within a relatively short time, where the solution is affected by physical initial conditions.

In this study, the initial conditions were: An empty channel at time zero; a certain water height and velocity upstream of the channel, depending on the desired Froude number; and a certain flow rate through the pipe, depending on the desired flow proportion relative to the flow rate in the channel.

3.2.6. Other Considerations in Setting up the Model

In setting up the model in FLOW-3D, the reference pressure was set to 1 atm; the reference temperature was 20 °C; the fluid used was water at 20 °C; and the finish time for most of the simulations was 20 s unless longer simulation times were required for the flow in the channel to reach steady-state conditions. Moreover, the renormalized group (RNG) model was used as the turbulence model.

3.2.7. Convergence and Validation

Fluid flow problems are highly nonlinear. Only through imposing restrictive conditions can the governing Navier–Stokes equations be solved analytically. As a result, CFD solutions must be calculated iteratively. By their nature, iterative solution methods require a convergence criterion that is used to decide when the iterations can be terminated. In FLOW-3D, all relaxation and convergence criteria are selected by the program itself. Further, all selections are adjusted dynamically by the program to follow the development of the solution. One such case would be the use of a very large convergence criteria and no over-relaxation, as a way to reach steady-state conditions with less CPU time. Figures 21 and 22 show that by the end of the simulation time (for one of the simulated scenarios, as an example), the solution converged and the time-step size was within the stability limits, respectively.

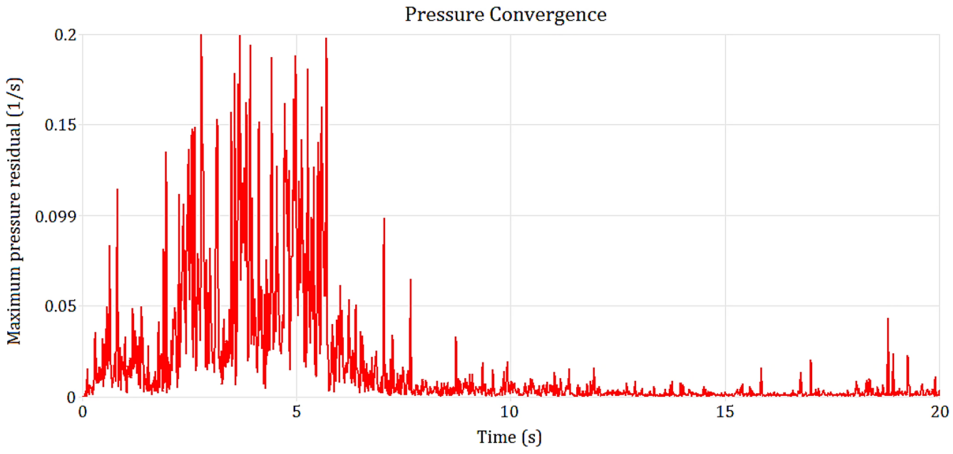

Figure 21. The convergence of the numerical modeling solution.

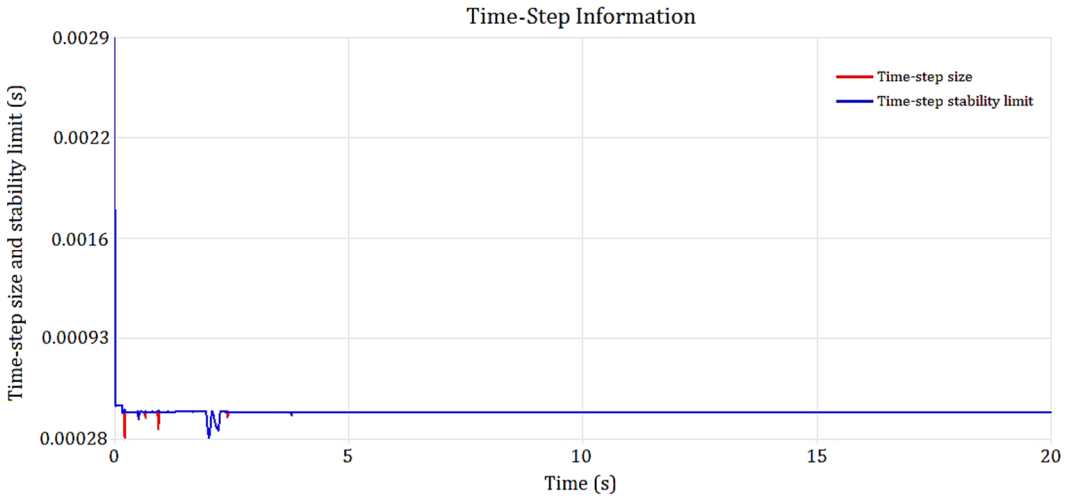

Figure 22. Time-step information of the simulation.

Using CFD allows researchers to understand flow behavior and quantify important flow parameters, given that the CFD solver has been properly validated using observations. Once validated, the 3D numerical model can be used to investigate the flow characteristics at the junction.

The results of three experiments with different Froude numbers (0.8, 2.0, 3.1) were used to validate the FLOW-3D model. These three cases were selected to cover both the sub-critical and super-critical conditions in the flume. The flume wall was made of plexiglass sheets attached at certain lengths (1.03 m), making a total of 13 columns. The simulation and experimental results of water heights at each column are presented in Figures 23–25.

Using the Nash–Sutcliffe efficiency function (NS) (Equation (16)), the goodness of fit between the observed and simulated values were evaluated and are presented in Table 10. In Equation (16), "H" is a variable, such as the flow surface elevation; "m" and "s" stand for measured and simulated; the bar indicates the average; and "i" is the ith measured or simulated value. The NS function has a range of $-\infty$ to 1. NS = 1 corresponds to a perfect match of simulated values to the observed data. The values between 0 and 1 indicate that the simulated and observed values are in close agreement, whereas values less than 0 show that the model has no predictive power [19,20].

Good agreement was found between predicted water surface levels and the experimental measurements across the stream, throughout the flume, as shown in Figures 23–25. The high NS values obtained indicated that the model was able to simulate flow profiles in an open channel with lateral flow, with high accuracy. The small differences between simulation and experimental results can be attributed to errors in reading water heights in the lab, due to flow turbulence and flume waves.

$$NS = 1 - \frac{\sum_i |H_m - H_s|_i^2}{\sum_i |H_{m,i} - \overline{H}_m|_i^2} \quad (16)$$

Table 10. FLOW-3D validation results.

Froude Number	Nash–Sutcliffe Efficiency
0.8	0.87
2.0	0.83
3.1	0.85

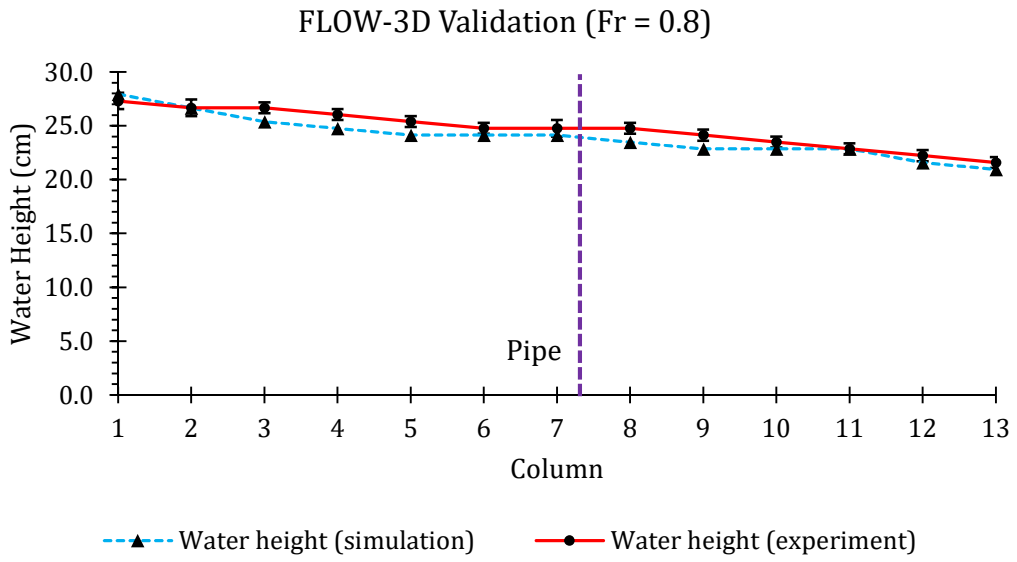

Figure 23. Water heights in the flume and based on FLOW-3D results, for Fr = 0.8.

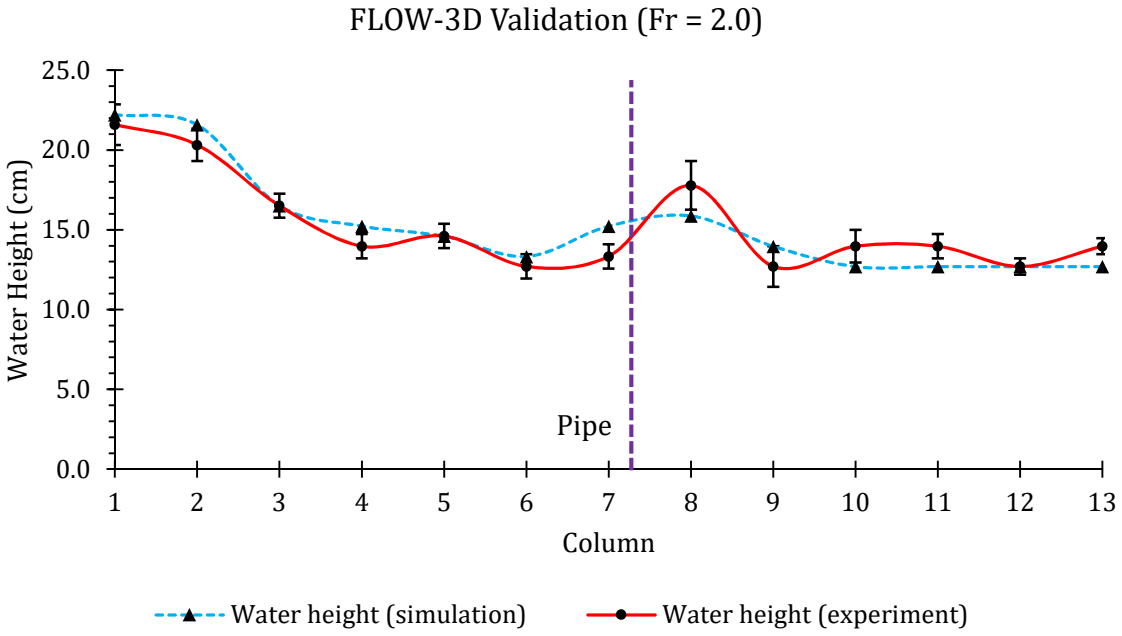

Figure 24. Water heights in the flume and based on FLOW-3D results, for Fr = 2.0.

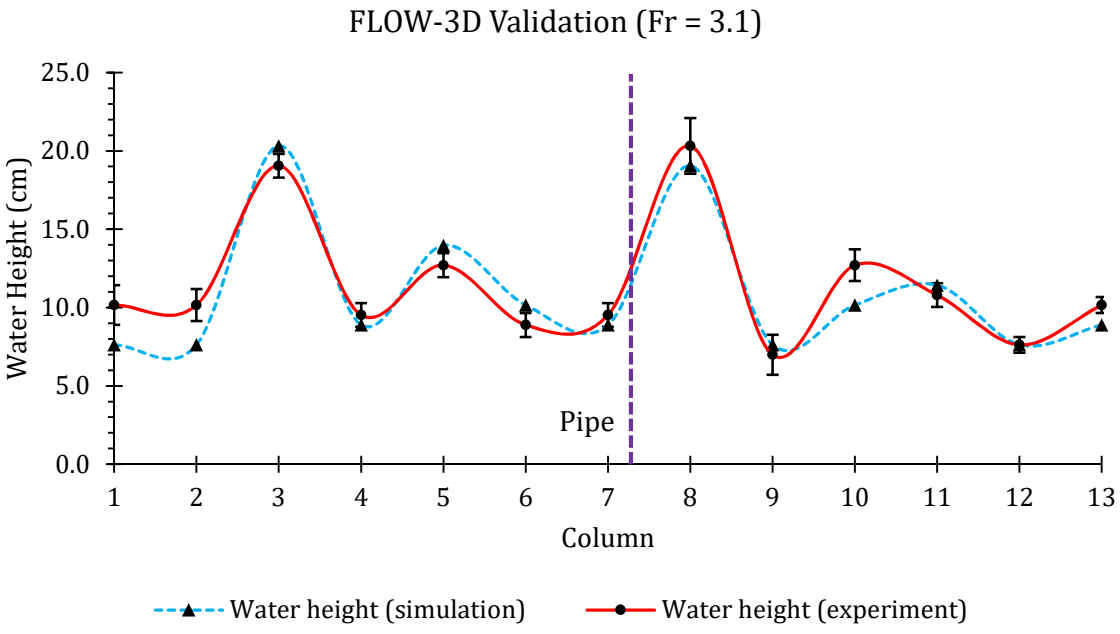

Figure 25. Water heights in the flume and based on FLOW-3D results, for Fr = 3.1.

3.3. Simulation Results

Surface Water Elevations and Conservative Design Curves

The incoming tributary flow caused a rise of water surface elevation, and for sub-critical flow conditions, resulted in a back-water effect towards the upstream (Figure 26). Additionally, larger junction angles allowed the tributary flow to penetrate further into the confluence, which in some cases resulted in flow splashing on the outer wall of the channel (Figure 27). After the mixing between the tributary and mainstream, the confluence cross-sectional flow field gradually recovered to that of a normal open channel, at the downstream of the confluence.

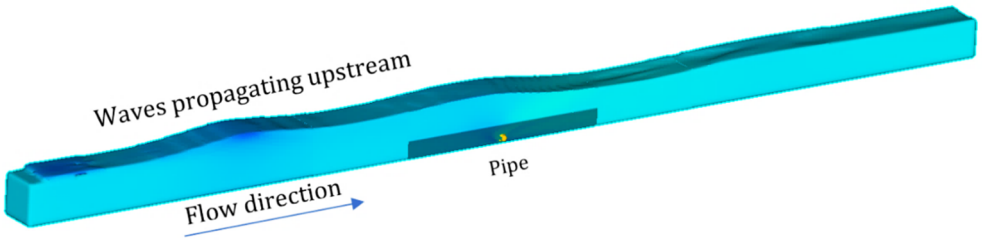

Figure 26. Back-water effect in a channel with sub-critical flow.

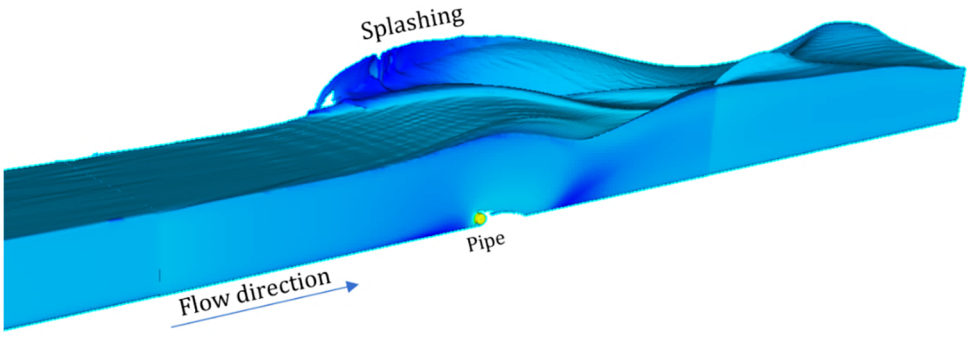

Figure 27. Splashing on the outer wall of a channel with super-critical flow and 90° junction angle.

Among the 648 scenarios simulated, in 42 cases, as a result of the interaction between channel flow and lateral flow through the pipe, waves were formed in the channel, and in other cases the impact was local. Waves were not observed in 15.24 m (50′)-wide channels, since the channel flow momentum could overcome the pipe flow momentum, and the jet could not reach the outer wall. Among 42 cases that showed the formation of waves in 3.05 (10′) and 7.62 m (25′) channels, 30 cases occurred in 3.05 m (10′)-channels and 12 cases in 7.62 m (25′)-channels. Moreover, in 27 of the 42 cases, the flow was sub-critical, and in the other 15, it was super-critical. These findings indicate that narrower channel and pipe confluences, with lower Froude numbers, are more prone to the formation of waves in the channels.

The simulation results and conservative design curves for the three channel widths, and based on the Froude numbers of the flow in the channels, are presented in Figures 28–33. Detailed FLOW-3D results are available in Appendix B. In the following figures, W is the channel width; H_0 is the initial water height in the channel without lateral flow; H is the maximum water height in the channel with lateral flow; Q is the flow rate in the channel; V is the flow velocity in the channel; q is the flow rate in the pipe; v is the flow velocity in the pipe; and θ is the junction angle. As the two flows merged in the confluence, the flow rate and velocity in the channel and pipe were the two factors impacting the maximum water height in the channel. Accordingly, the momentum ratios of the channel and the pipe ($\frac{QV + qv(\cos\theta)}{qv(\sin\theta)}$), could be related to the H/H_0, as shown in Figure 28, Figure 30, and Figure 32.

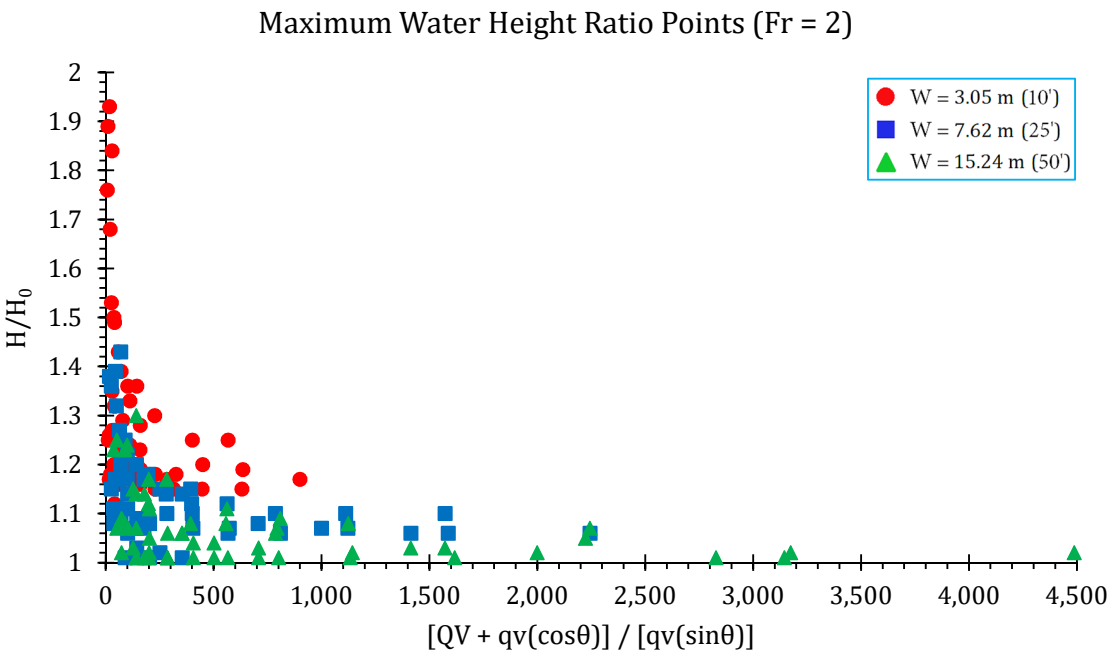

Figure 28. Simulation results for Fr = 2 in the channel.

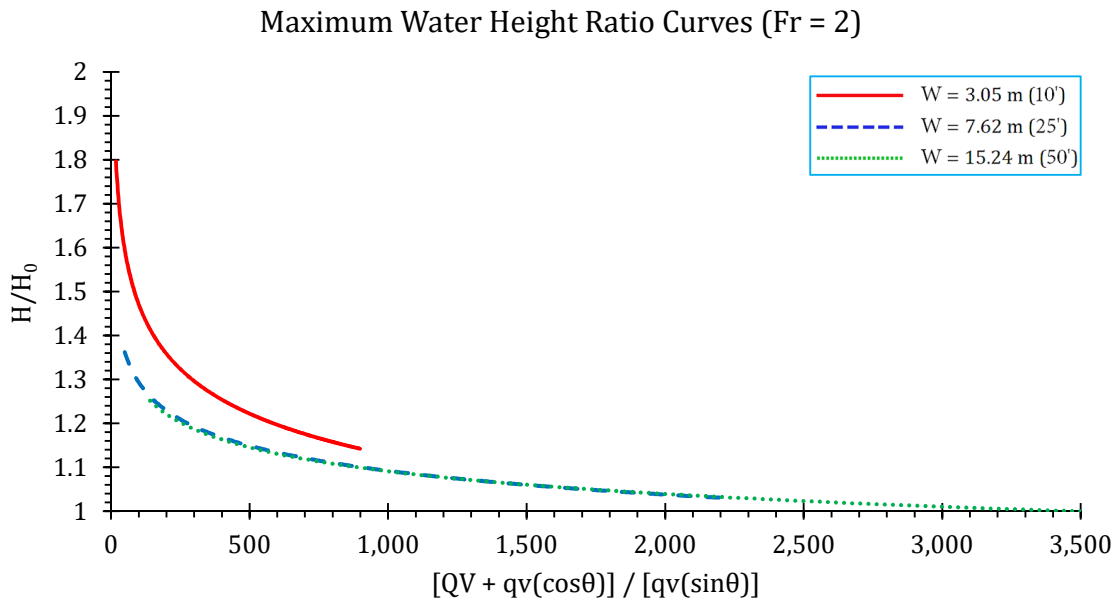

Figure 29. Conservative design curves for Fr = 2 in the channel.

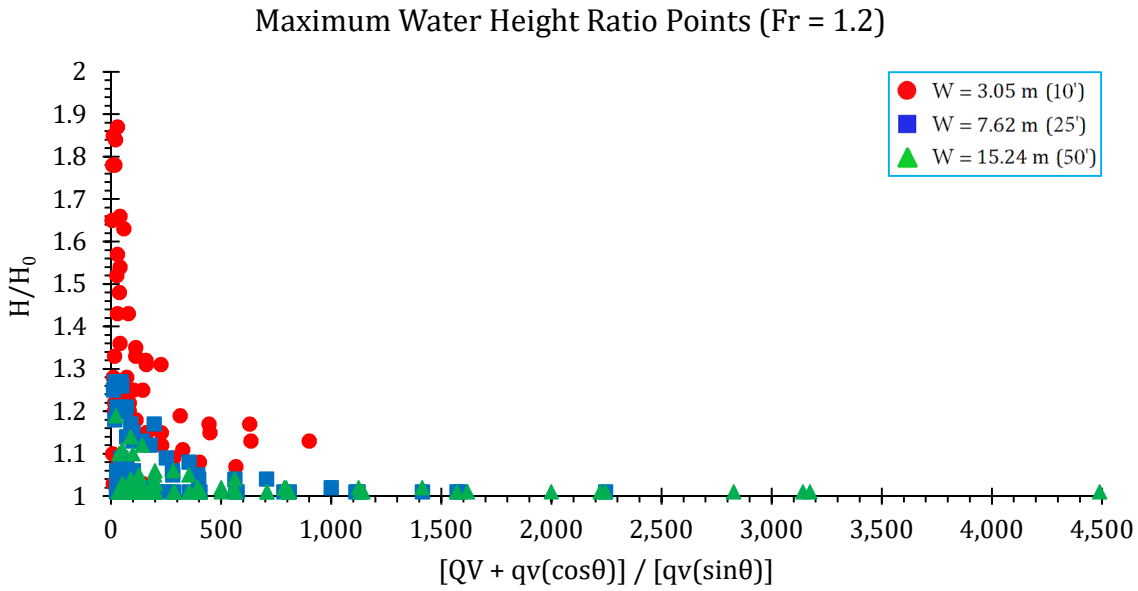

Figure 30. Simulation results for Fr = 1.2 in the channel.

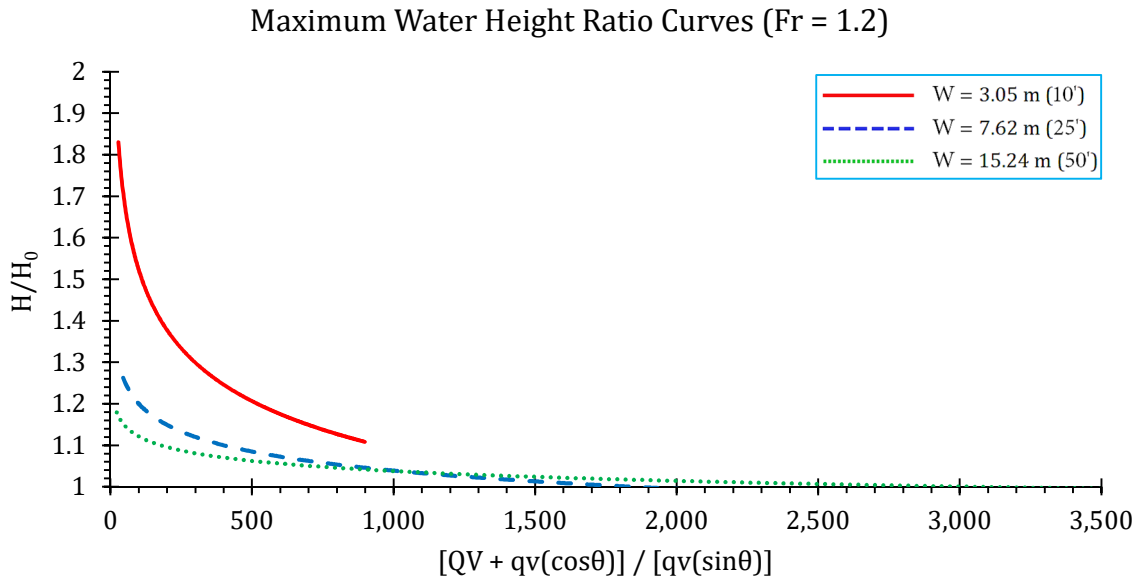

Figure 31. Conservative design curves for Fr = 1.2 in the channel.

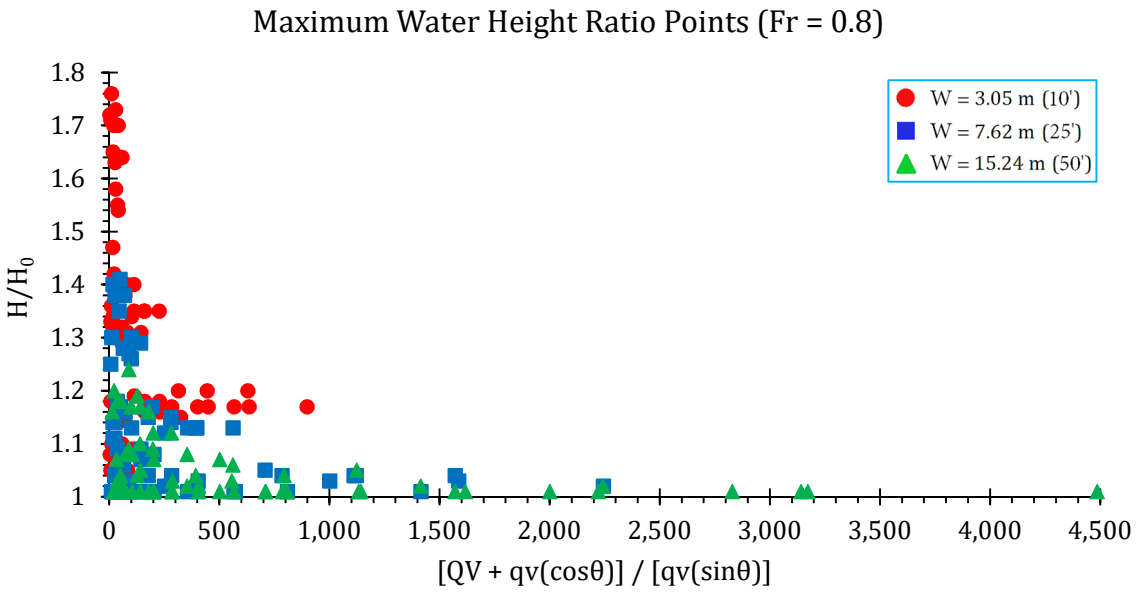

Figure 32. Simulation results for Fr = 0.8 in the channel.

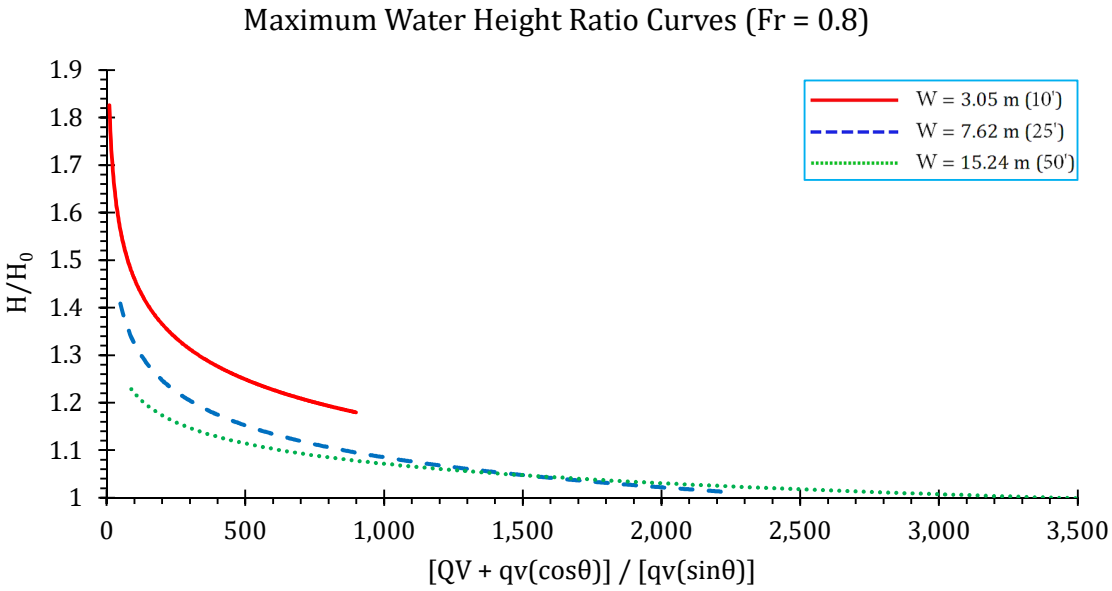

Figure 33. Conservative design curves for Fr = 0.8 in the channel.

In all three charts, in Figure 28, Figure 30, and Figure 32, the results show that the highest H/H_0 values were observed for W = 3.05 m (10′), and as the channel width increased to 7.62 (25′), and then to 15.24 m (50′), the points, representing the maximum water height ratios in the channel (H/H_0), accumulated at the lower parts of the charts. The results indicate that $\frac{QV + qv(\cos\theta)}{qv(\sin\theta)}$ values of 500 and 1000 could be considered as critical numbers. Among almost all scenarios, in cases where the value of $\frac{QV + qv(\cos\theta)}{qv(\sin\theta)}$ was greater than 500, the maximum increase in water height was 20%. Similarly, in cases where $\frac{QV + qv(\cos\theta)}{qv(\sin\theta)}$ was greater than 1000, the maximum increase in water height was 10%. Additionally, in cases where the $\frac{QV + qv(\cos\theta)}{qv(\sin\theta)}$ values were greater than 500, impacts on the channel flow were local, while wave impacts were observed in channels in smaller $\frac{QV + qv(\cos\theta)}{qv(\sin\theta)}$ ranges.

The following design guidelines are conservative. The guidelines provide conservative designs for extreme flow conditions in the channel and the pipe. Accordingly, the designer needs to first establish the expected extreme flow conditions in the channel and the pipe. Then, using the guidelines with the expected extreme flow conditions in the channel and the pipe as functional design criteria, the design will accommodate these extreme flow conditions. The uncertainty resides in the estimation of the expected extreme flow conditions in the channel and the pipe and not in the design guidelines.

Moreover, it should be mentioned that the presence of impurities such as sediments in water will impact the unit weight (density) of the water and the roughness of the materials impacts the momentum of the water. The design guidelines are based on the relative momentums of the flows in the channel and the pipe. Since the momentum is a function of the unit weight (density), the guidelines include the effect of the presence of impurities in water and the roughness of the materials.

4. Conclusions and Recommendations

This study utilized a hybrid experimental–numerical approach to investigate the flow topology in the confluence of rectangular open channels with submerged lateral drainage pipe discharges to develop design guidelines for flood control channel height. The scenarios covered a range of channel widths, flow rates, Froude numbers, junction angles, inlet pipe diameters, and lateral flows to main channel flow ratios. Clear water at 20 °C with no impurities was used both in the experiments and numerical modeling.

The experimental results showed that as the junction angle and the lateral flow proportions increased, the maximum water height ratios in the channel also increased. Moreover, the numerical modeling results showed that as the ratio of channel flow momentum to pipe flow momentum ($\frac{QV + qv(\cos\theta)}{qv(\sin\theta)}$) increased, H/H_0 in the channel decreased. Additionally, narrower channel and pipe confluences, with lower Froude numbers, were found to be more prone to the formation of waves in the channel.

The results indicated that the momentum ratios of 500 and 1000 could be considered as critical numbers. Among almost all scenarios, in the cases where the value of $\frac{QV + qv(\cos\theta)}{qv(\sin\theta)}$ was greater than 500, the maximum increase in channel water height was 20%. Similarly, in cases where $\frac{QV + qv(\cos\theta)}{qv(\sin\theta)}$ was greater than 1000, the maximum water height increase in the channel was 10%. Additionally, in cases where the $\frac{QV + qv(\cos\theta)}{qv(\sin\theta)}$ values were greater than 500, the impacts on water height changes in the channel were local (at the pipe), while channel wave impacts were observed in low momentum ratios. Furthermore, for the channel's sub-critical and super-critical conditions, the waves propagated upstream and downstream of the channel, respectively.

Based on the findings of this study, if junctions are to be constructed at angles larger than 30°, it is recommended that the momentum ratio between the channel and the pipe flow ($\frac{QV + qv(\cos\theta)}{qv(\sin\theta)}$) be greater than 500, to limit the impacts of the lateral drainage pipe flow to the main channel flow around the pipe (local); it is also recommended to limit the maximum increase in the water height to 20%.

The design guidelines presented in this study are conservative, and they provide conservative designs for extreme flow conditions in the channel and the pipe. The designer has to first establish the expected extreme flow conditions in the channel and the pipe. Then, using the guidelines with the expected extreme flow conditions in the channel and the pipe, the design will accommodate these extreme flow conditions. The uncertainty resides in the estimation of the expected extreme flow conditions in the channel and the pipe and not in the design guidelines.

For future extension of this research, it is recommended to study: (1) The impact of flow through submerged lateral pipes into other channel and pipe confluence configurations (e.g., trapezoidal and triangular channels), different pipe sizes, and junction angles; (2) Froude numbers and lateral flow proportions outside the range covered in this study; (3) water with debris and impurities, under different environmental conditions (e.g., in the presence of wind); (4) the penetration length of the jet through the pipe into the channel, and its impact on the flow characteristics and flow topology in the channel.

Author Contributions: Conceptualization, M.N.-S., M.K., and D.H.; methodology, M.N.-S., M.K., and D.H.; software, M.N.-S.; validation, M.N.-S.; resources, M.N.-S. and M.K.; writing—original draft preparation, M.N.-S.; writing—review and editing, M.K. and D.H.; supervision, M.K. and D.H.; funding acquisition, M.K. All authors have read and agreed to the published version of the manuscript.

Funding: This research was funded by the Clark County Regional Flood Control District (CCRFCD), and the publication fees for this article were supported by the UNLV University Libraries Open Article Fund.

Conflicts of Interest: The authors declare no conflict of interest.

Appendix A

In this section, the results of all experimental tests conducted in the flume are presented in Figures A1–A45.

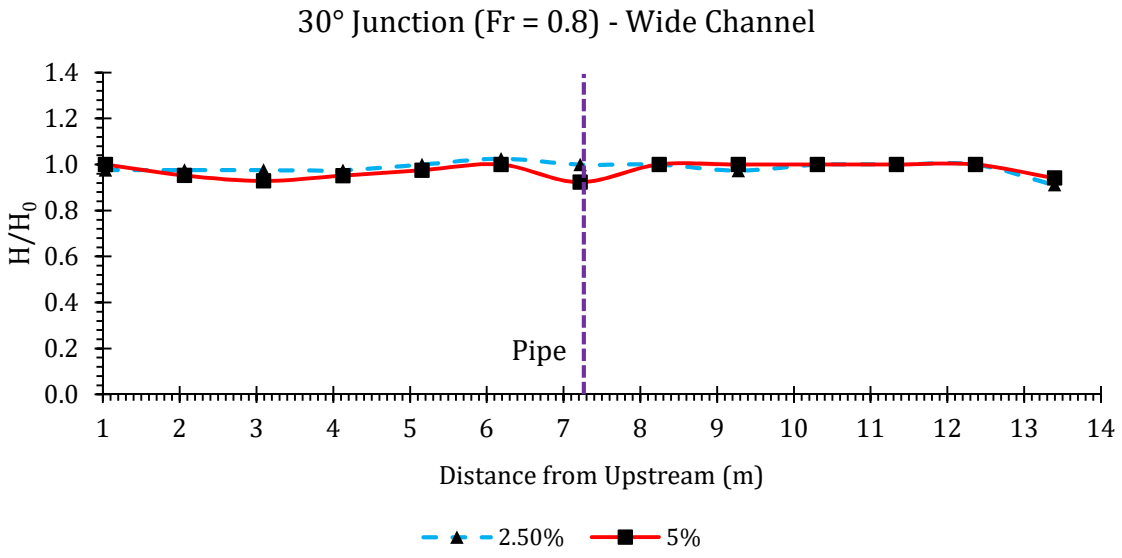

Figure A1. Water height ratios in a 30° junction for Fr = 0.8 in the wide channel.

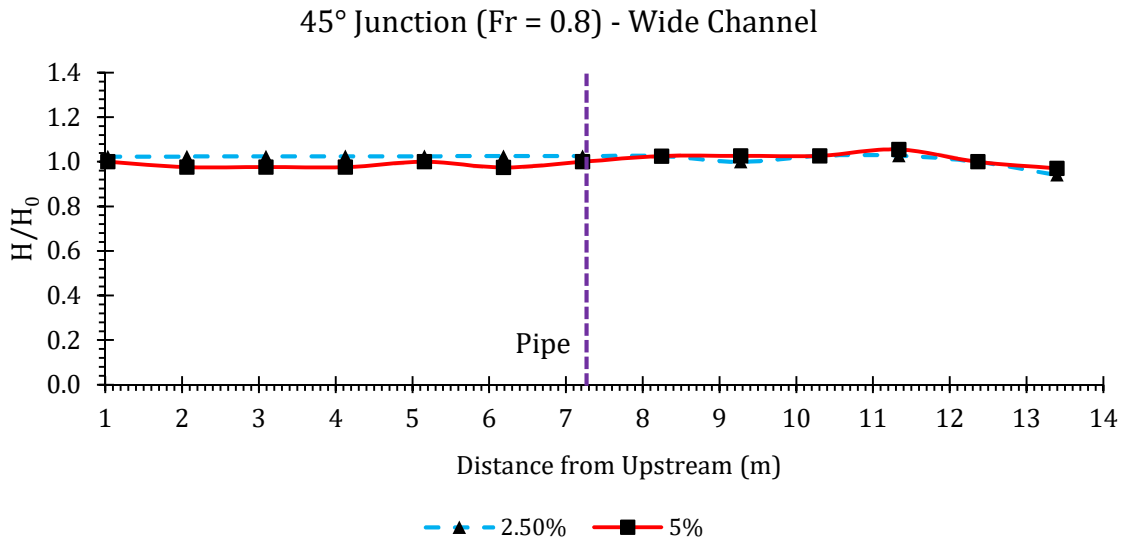

Figure A2. Water height ratios in a 45° junction for Fr = 0.8 in the wide channel.

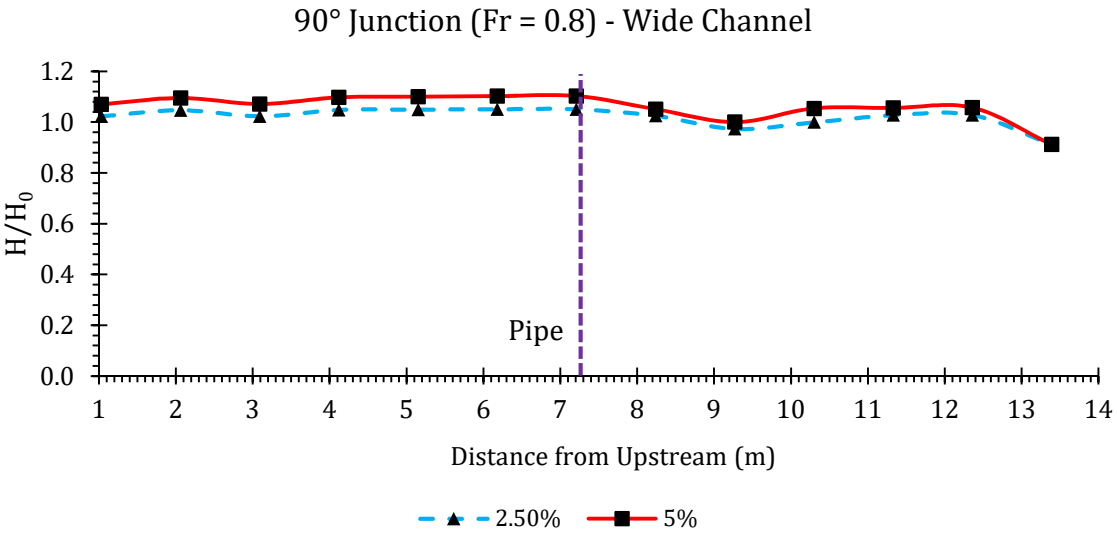

Figure A3. Water height ratios in a 90° junction for Fr = 0.8 in the wide channel.

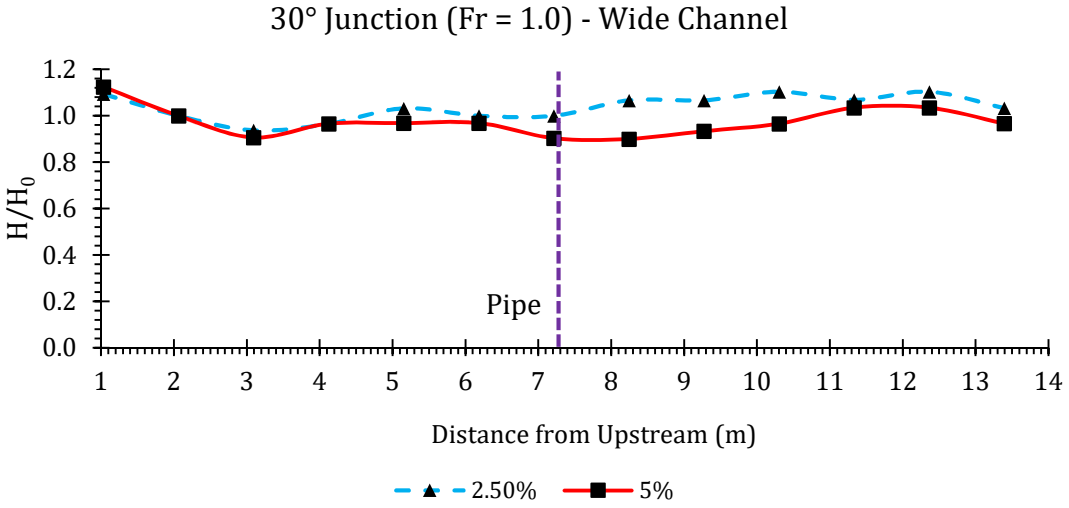

Figure A4. Water height ratios in a 30° junction for Fr = 1.0 in the wide channel.

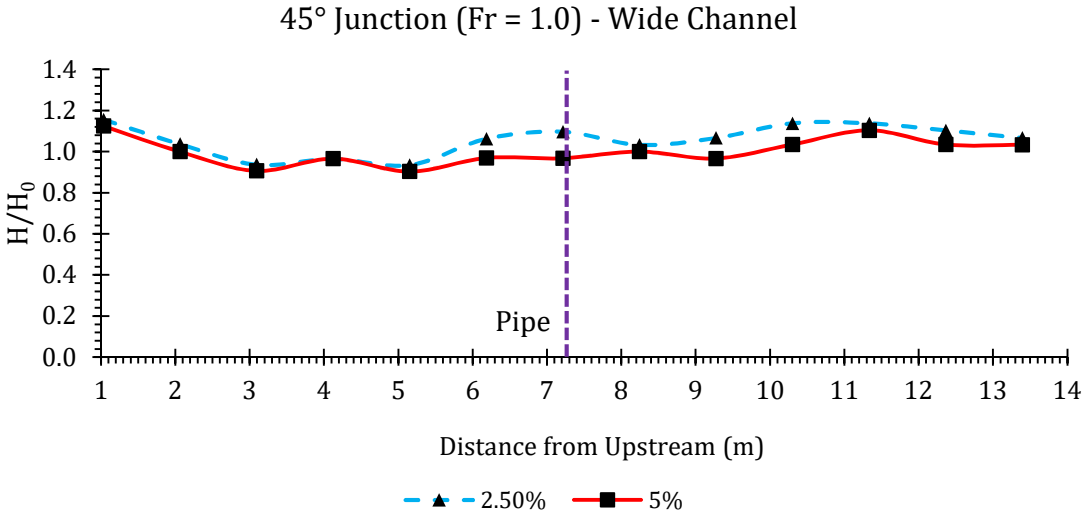

Figure A5. Water height ratios in a 45° junction for Fr = 1.0 in the wide channel.

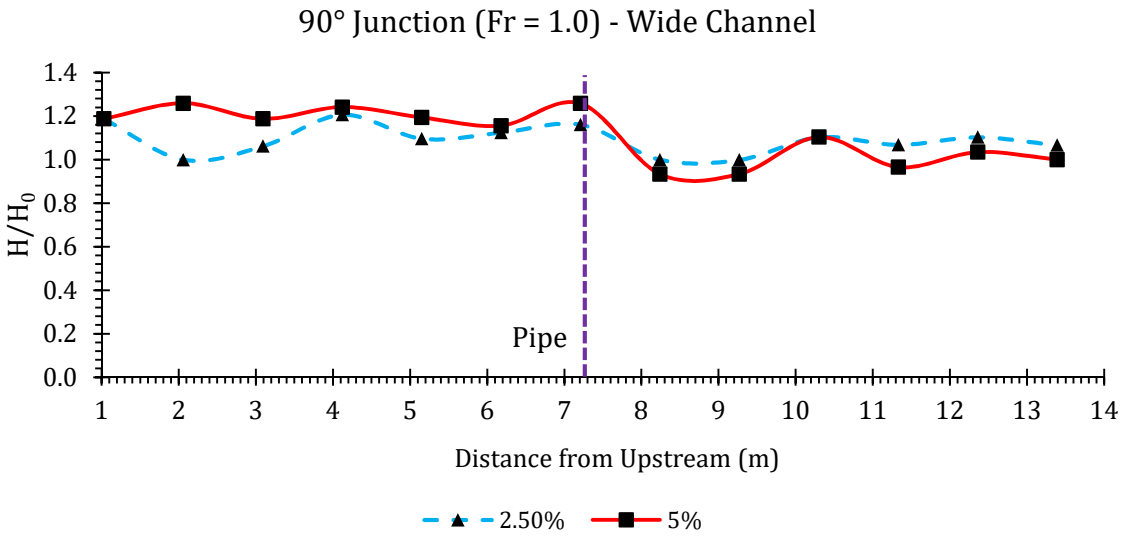

Figure A6. Water height ratios in a 90° junction for Fr = 1.0 in the wide channel.

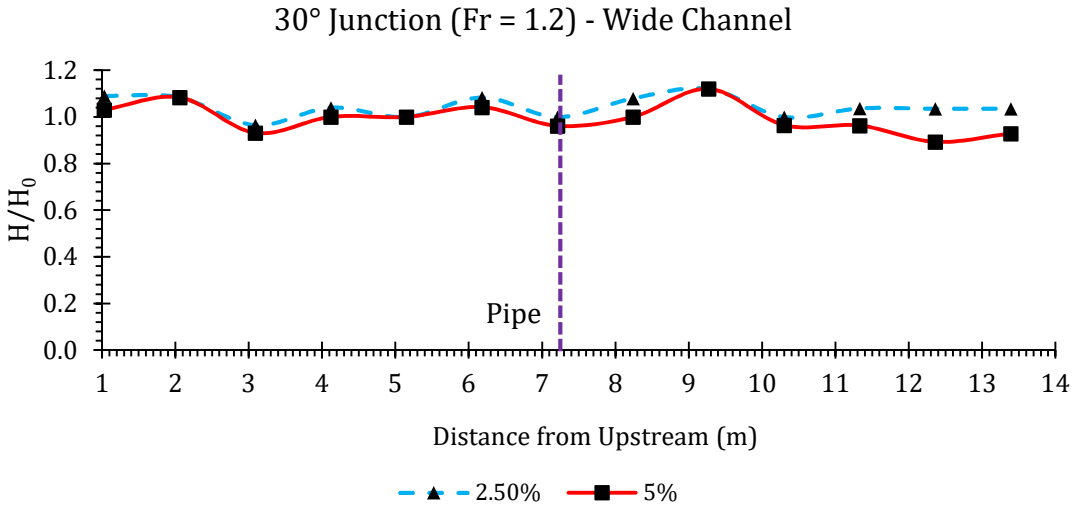

Figure A7. Water height ratios in a 30° junction for Fr = 1.2 in the wide channel.

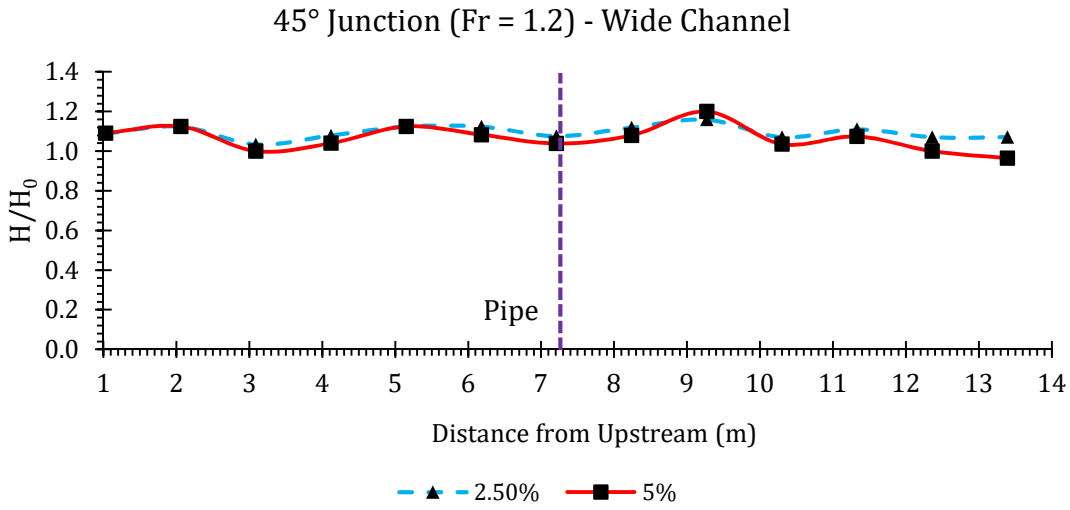

Figure A8. Water height ratios in a 45° junction for Fr = 1.2 in the wide channel.

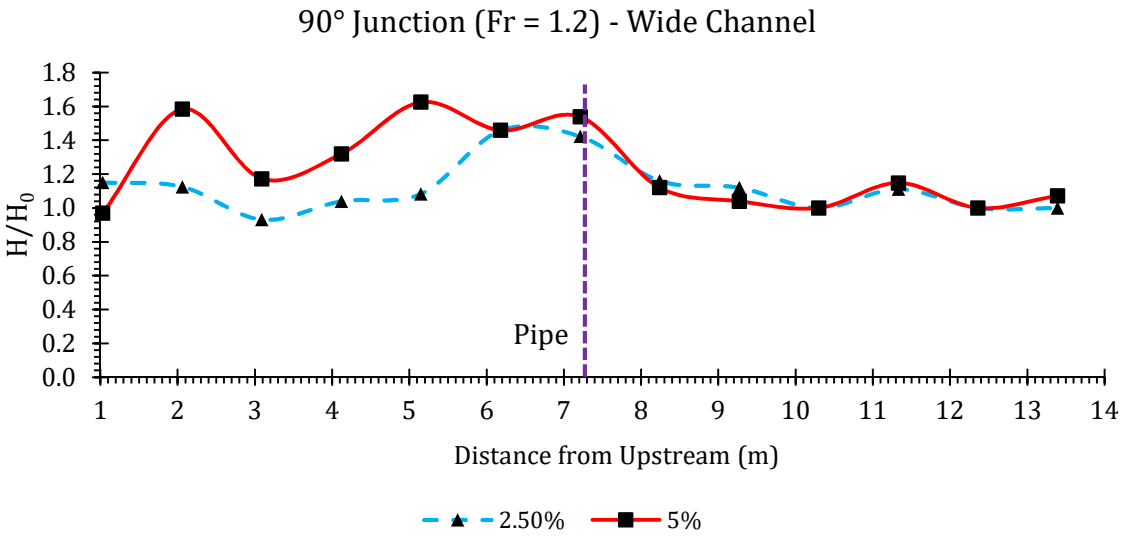

Figure A9. Water height ratios in a 90° junction for Fr = 1.2 in the wide channel.

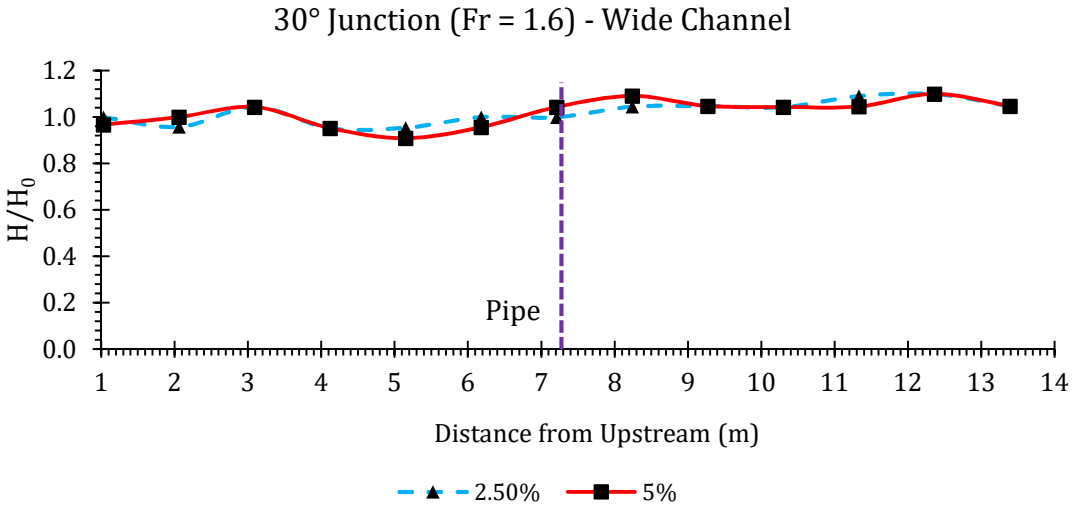

Figure A10. Water height ratios in a 30° junction for Fr = 1.6 in the wide channel.

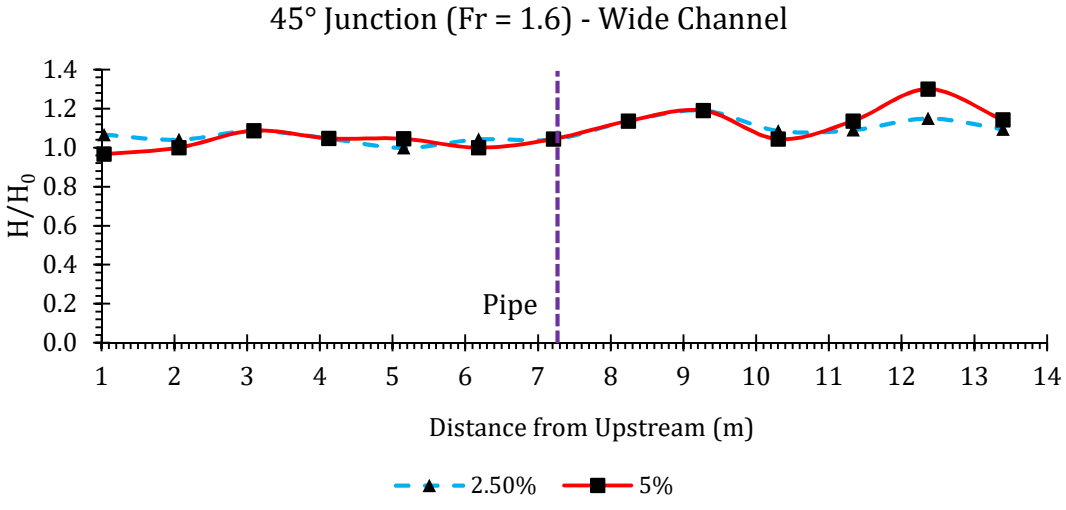

Figure A11. Water height ratios in a 45° junction for Fr = 1.6 in the wide channel.

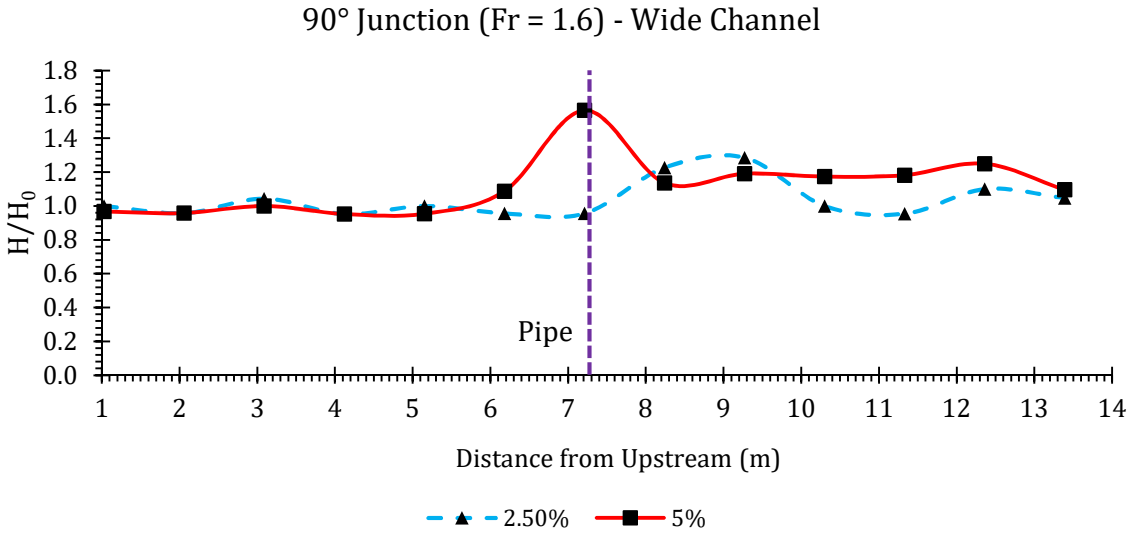

Figure A12. Water height ratios in a 90° junction for Fr = 1.6 in the wide channel.

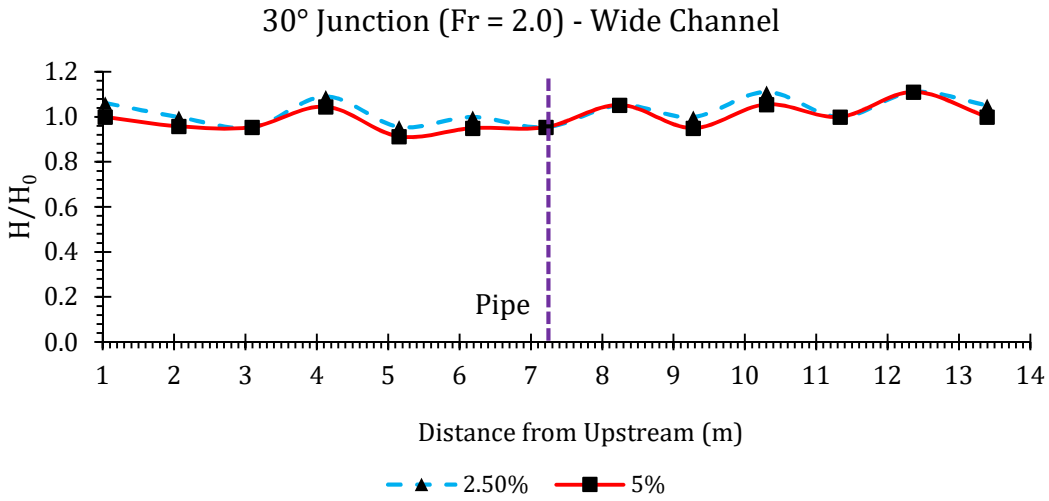

Figure A13. Water height ratios in a 30° junction for Fr = 2.0 in the wide channel.

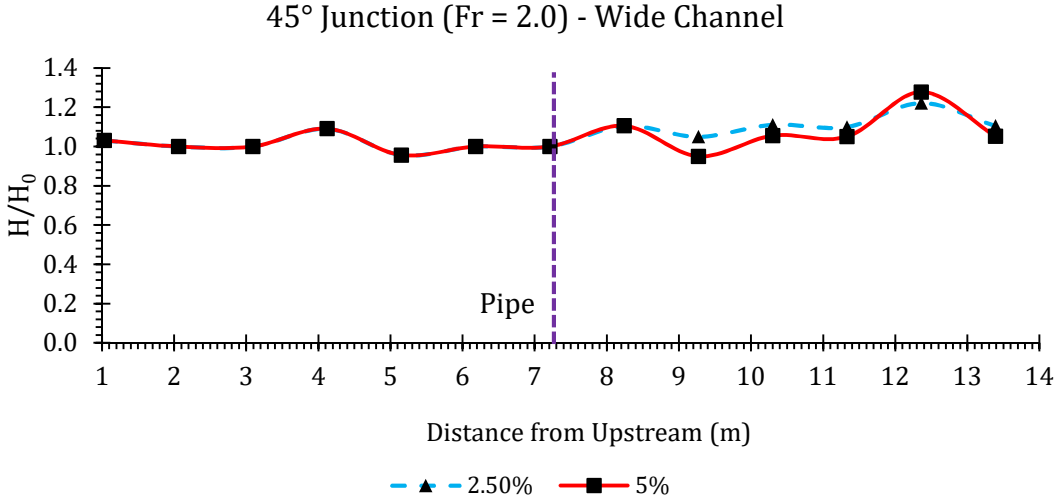

Figure A14. Water height ratios in a 45° junction for Fr = 2.0 in the wide channel.

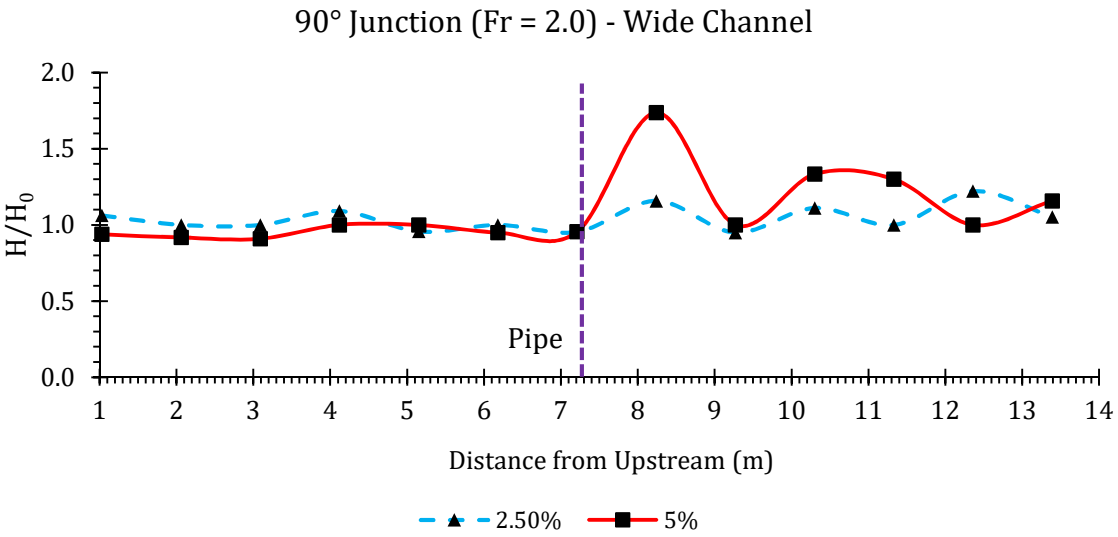

Figure A15. Water height ratios in a 90° junction for Fr = 2.0 in the wide channel.

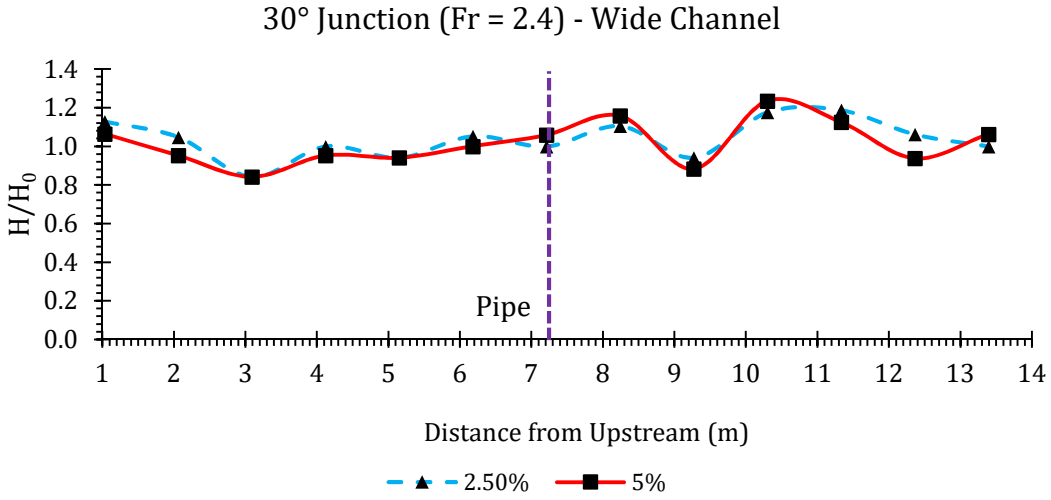

Figure A16. Water height ratios in a 30° junction for Fr = 2.4 in the wide channel.

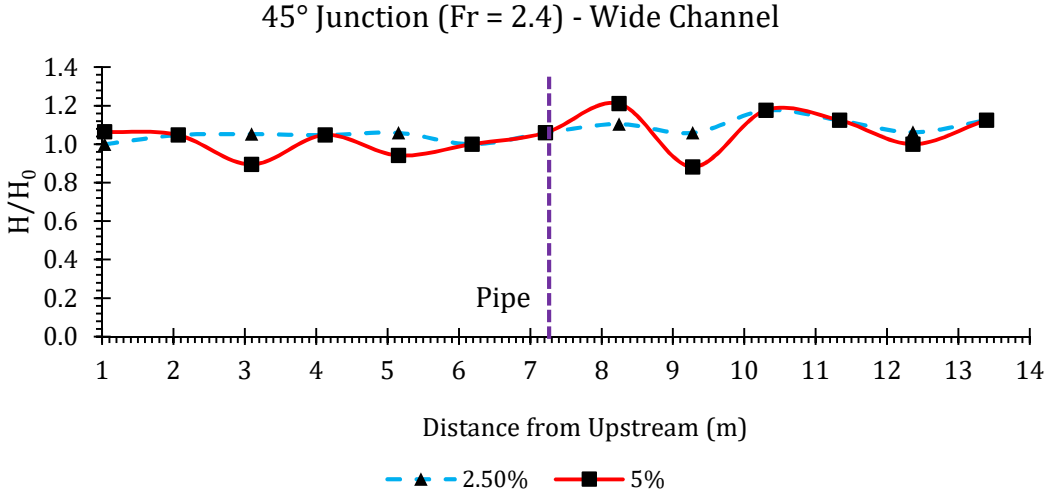

Figure A17. Water height ratios in a 45° junction for Fr = 2.4 in the wide channel.

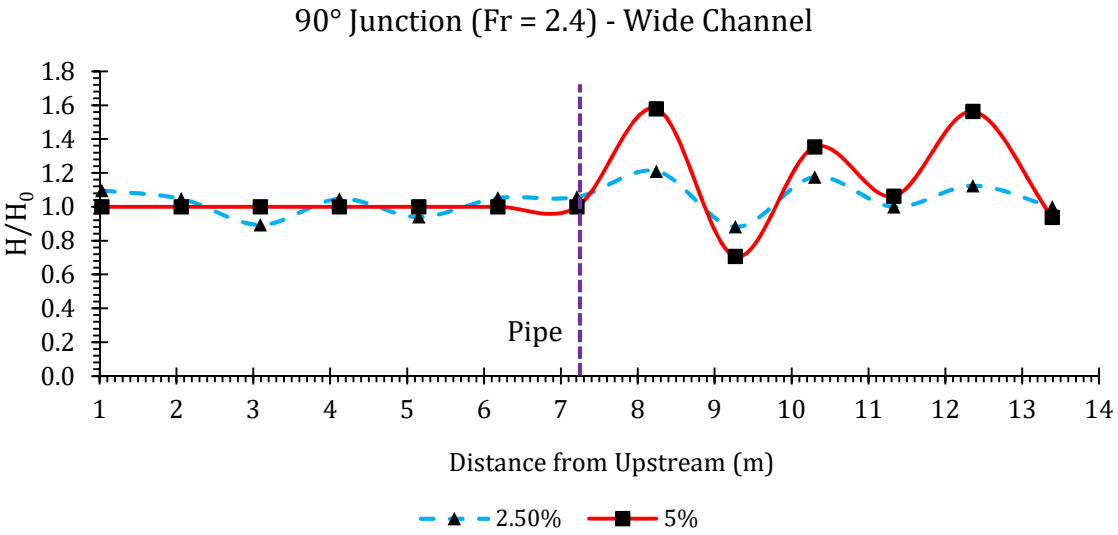

Figure A18. Water height ratios in a 90° junction for Fr = 2.4 in the wide channel.

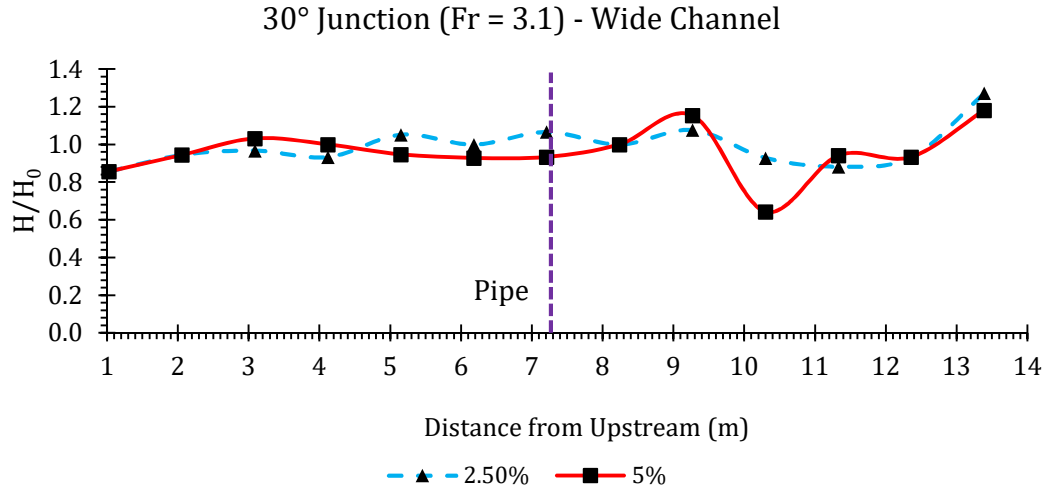

Figure A19. Water height ratios in a 30° junction for Fr = 3.1 in the wide channel.

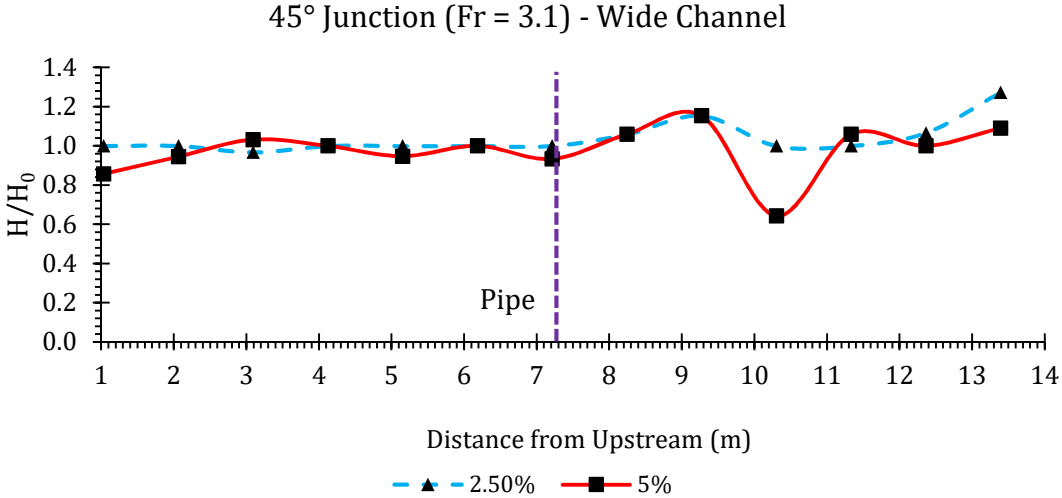

Figure A20. Water height ratios in a 45° junction for Fr = 3.1 in the wide channel.

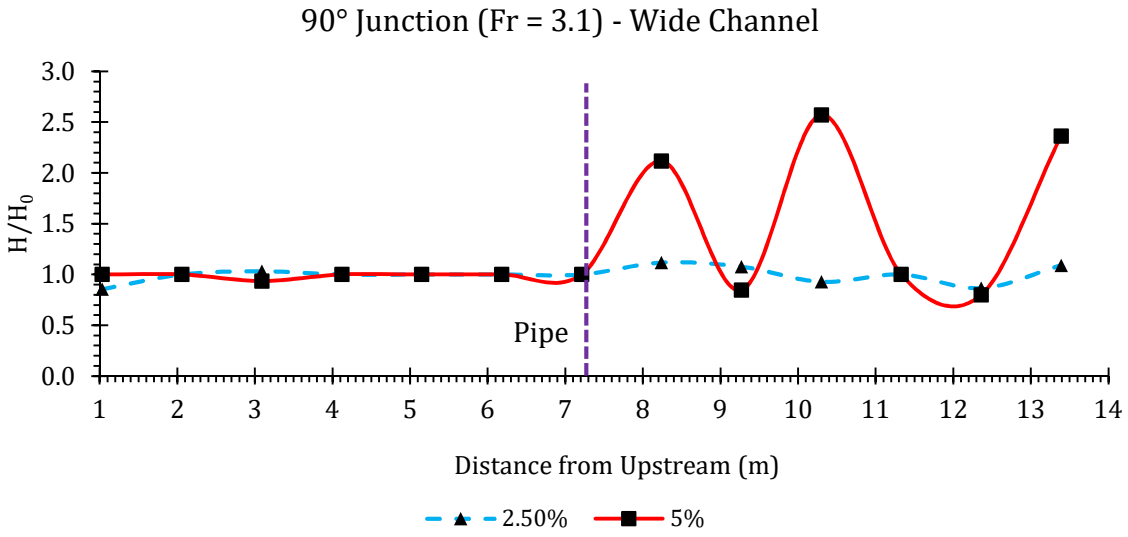

Figure A21. Water height ratios in a 90° junction for Fr = 3.1 in the wide channel.

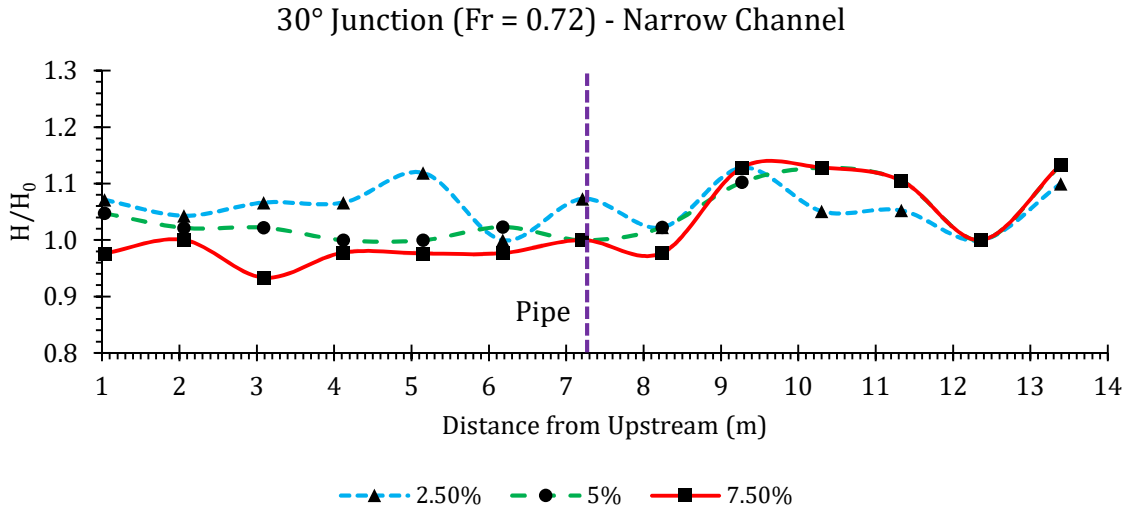

Figure A22. Water height ratios in a 30° junction for Fr = 0.72 in the narrow channel.

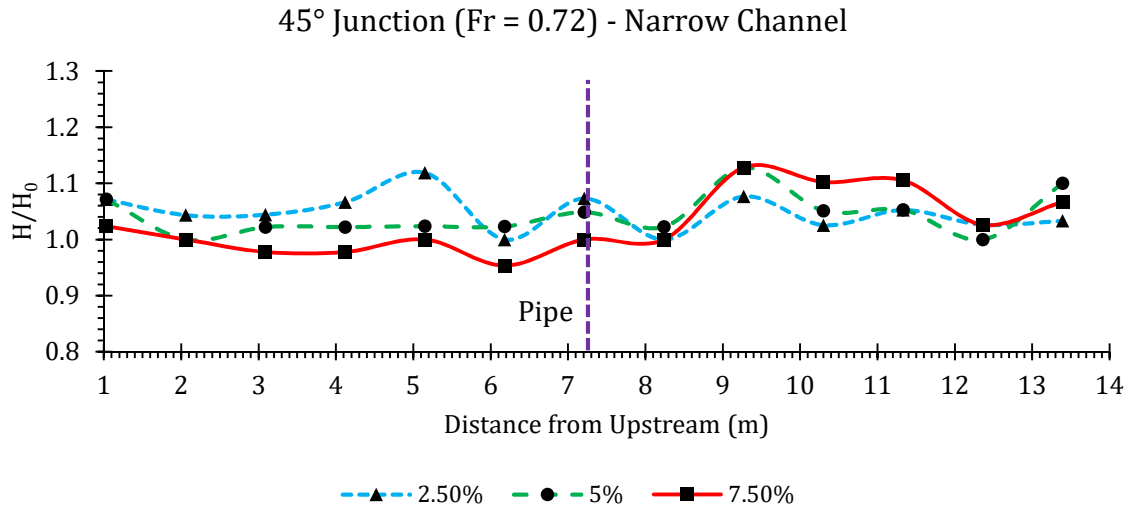

Figure A23. Water height ratios in a 45° junction for Fr = 0.72 in the narrow channel.

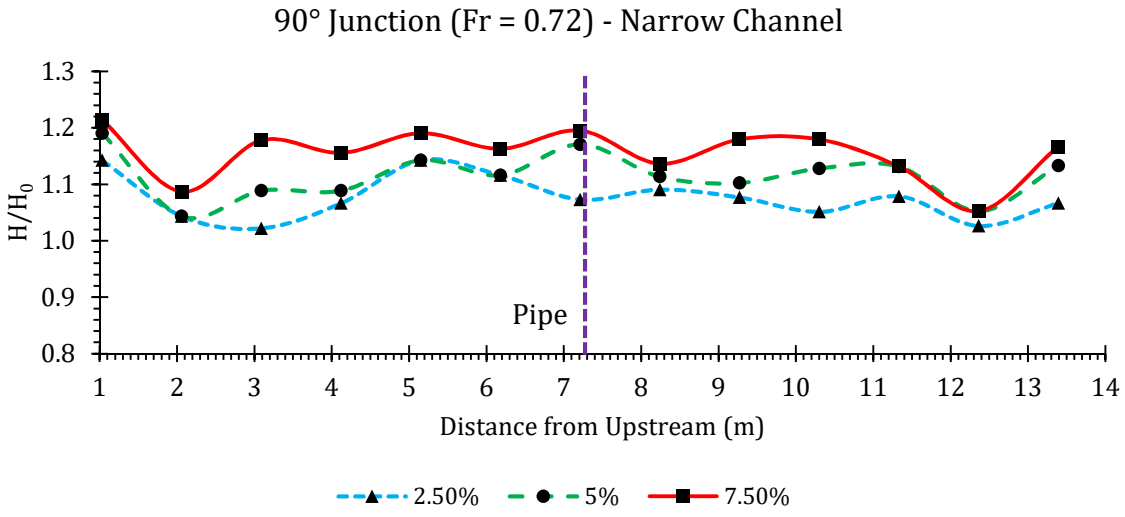

Figure A24. Water height ratios in a 90° junction for Fr = 0.72 in the narrow channel.

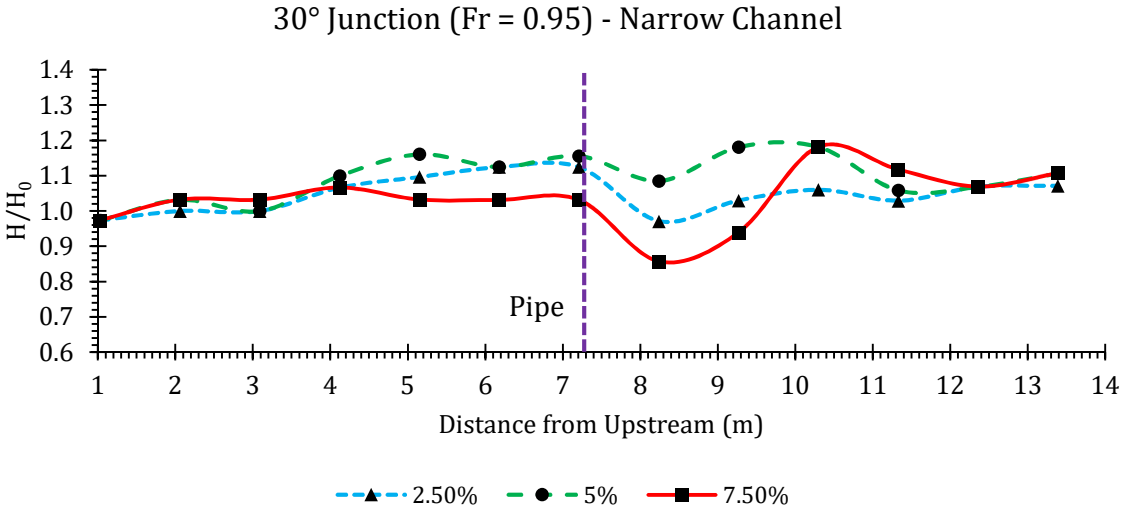

Figure A25. Water height ratios in a 30° junction for Fr = 0.95 in the narrow channel.

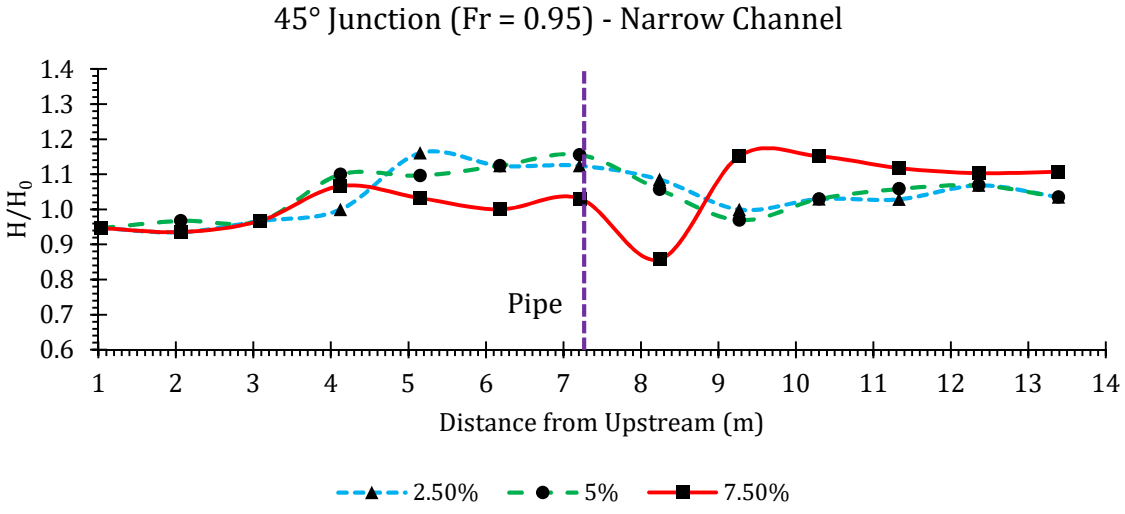

Figure A26. Water height ratios in a 45° junction for Fr = 0.95 in the narrow channel.

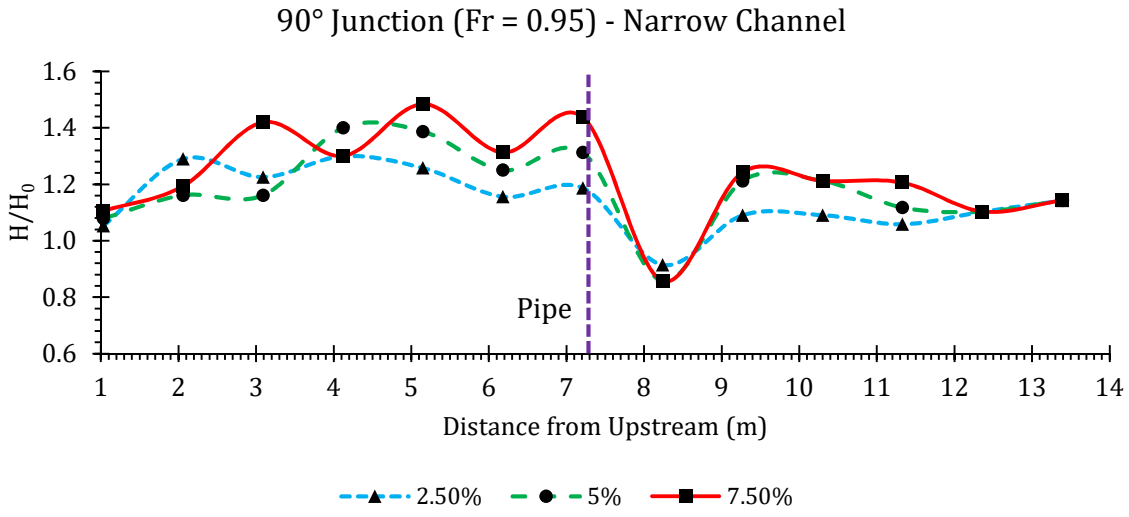

Figure A27. Water height ratios in a 90° junction for Fr = 0.95 in the narrow channel.

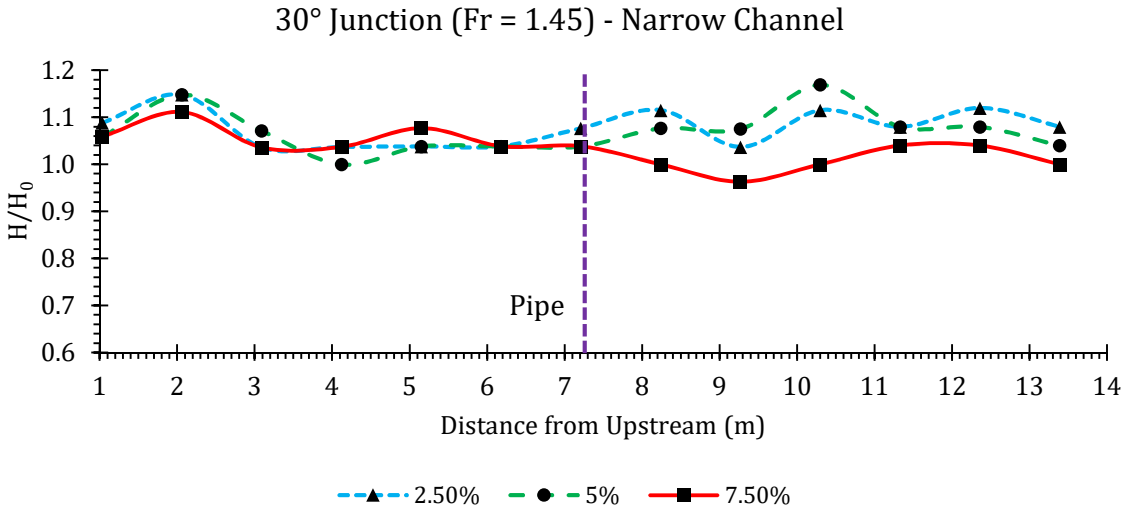

Figure A28. Water height ratios in a 30° junction for Fr = 1.45 in the narrow channel.

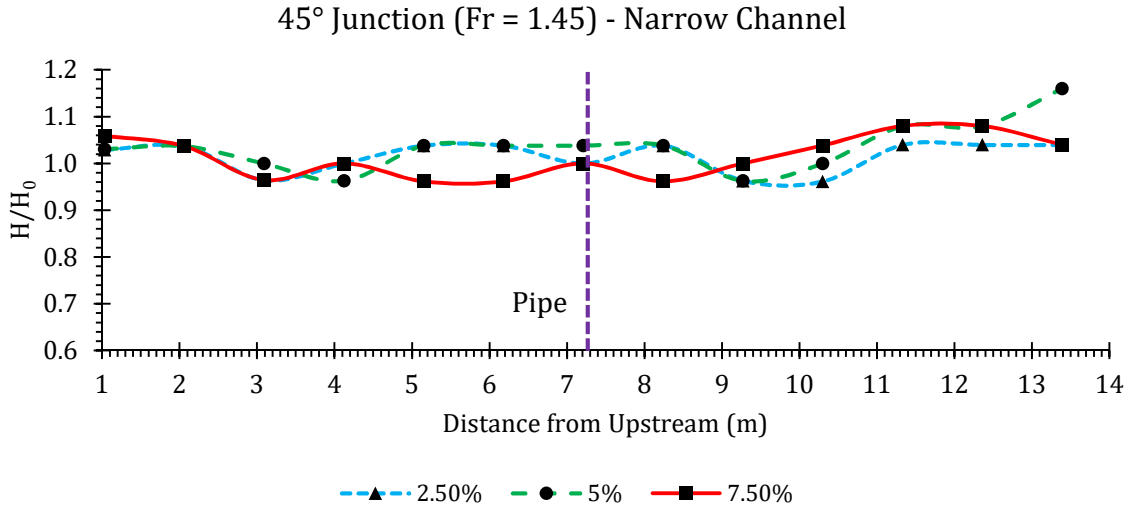

Figure A29. Water height ratios in a 45° junction for Fr = 1.45 in the narrow channel.

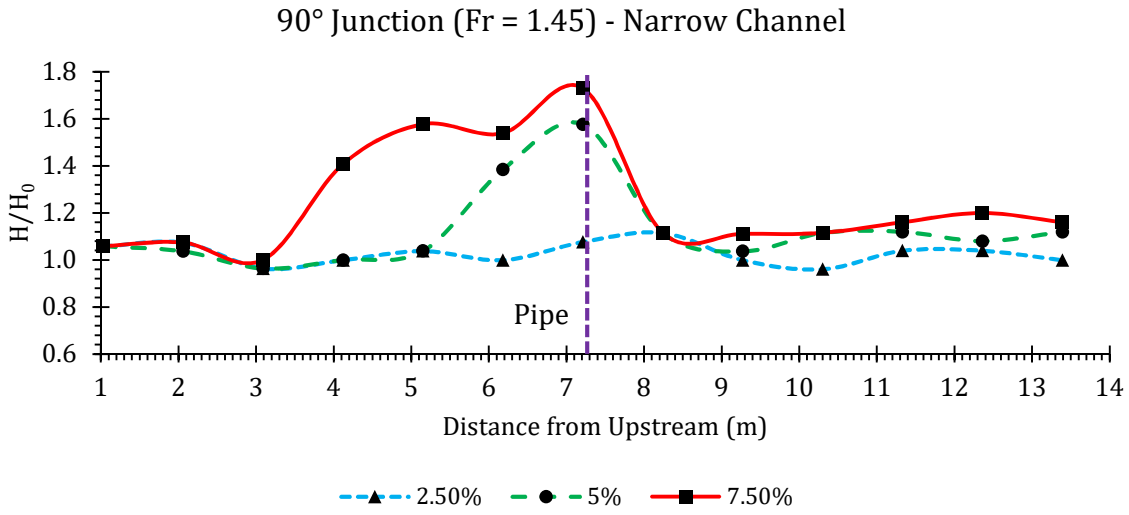

Figure A30. Water height ratios in a 90° junction for Fr = 1.45 in the narrow channel.

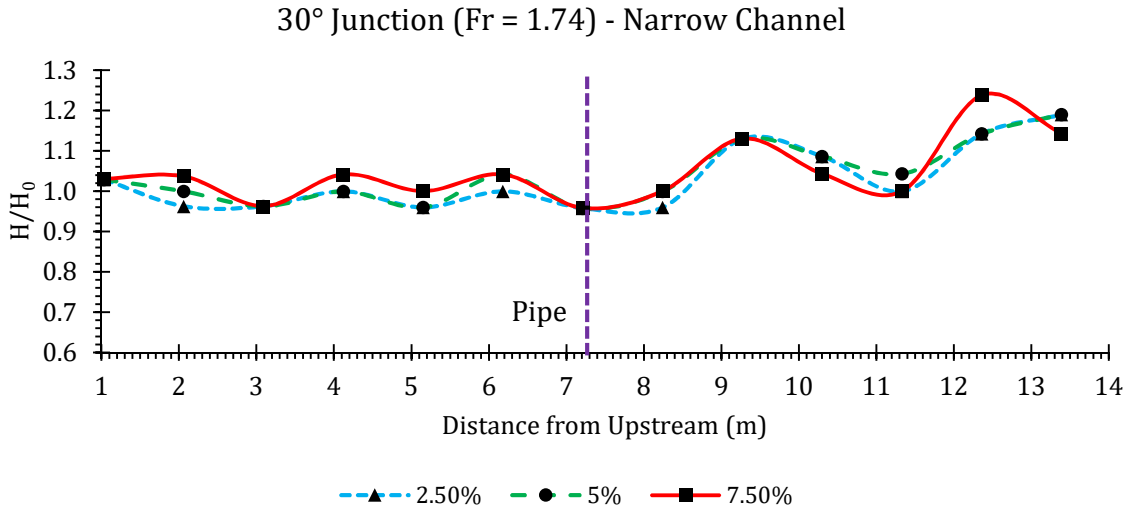

Figure A31. Water height ratios in a 30° junction for Fr = 1.74 in the narrow channel.

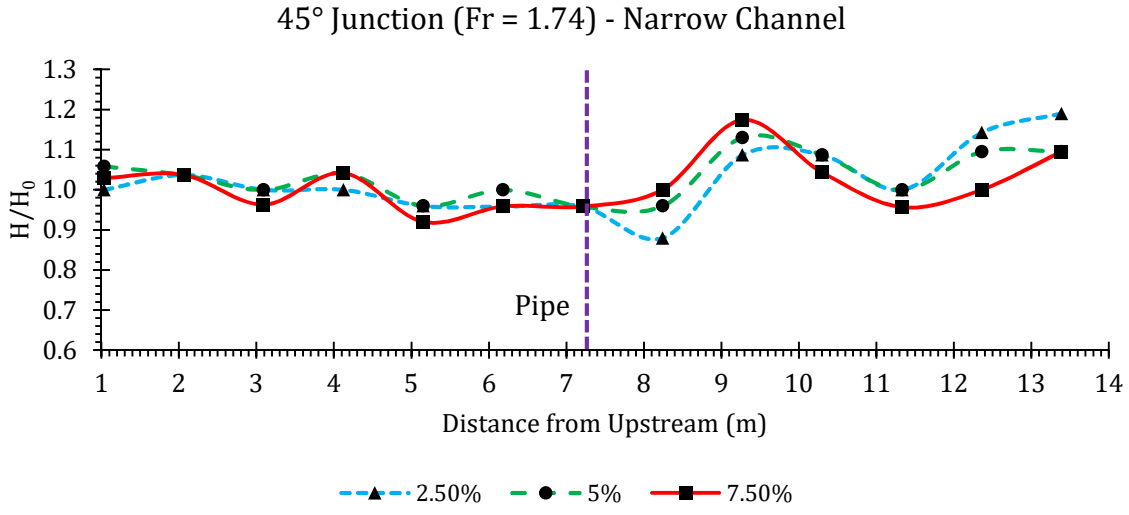

Figure A32. Water height ratios in a 45° junction for Fr = 1.74 in the narrow channel.

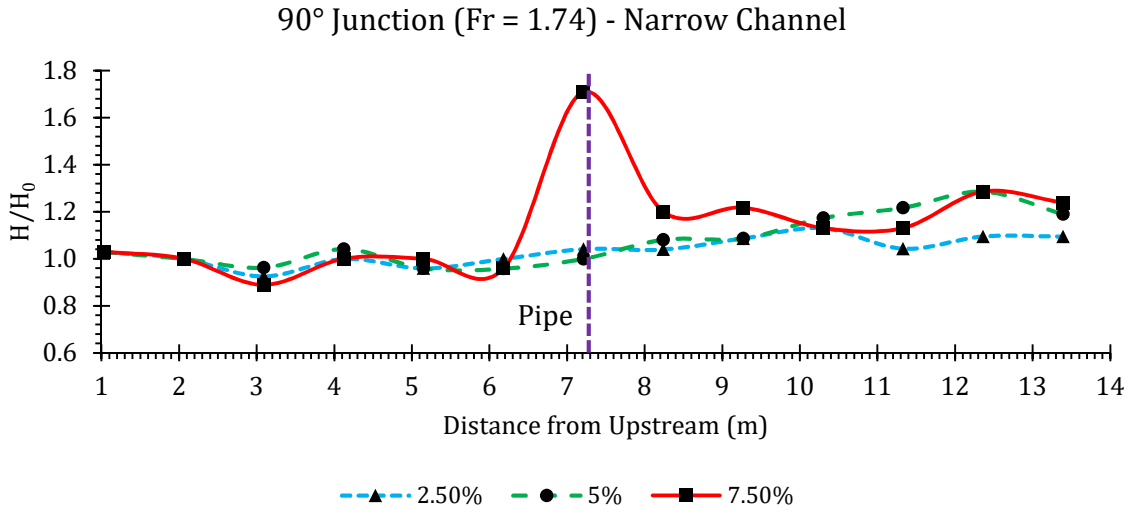

Figure A33. Water height ratios in a 90° junction for Fr = 1.74 in the narrow channel.

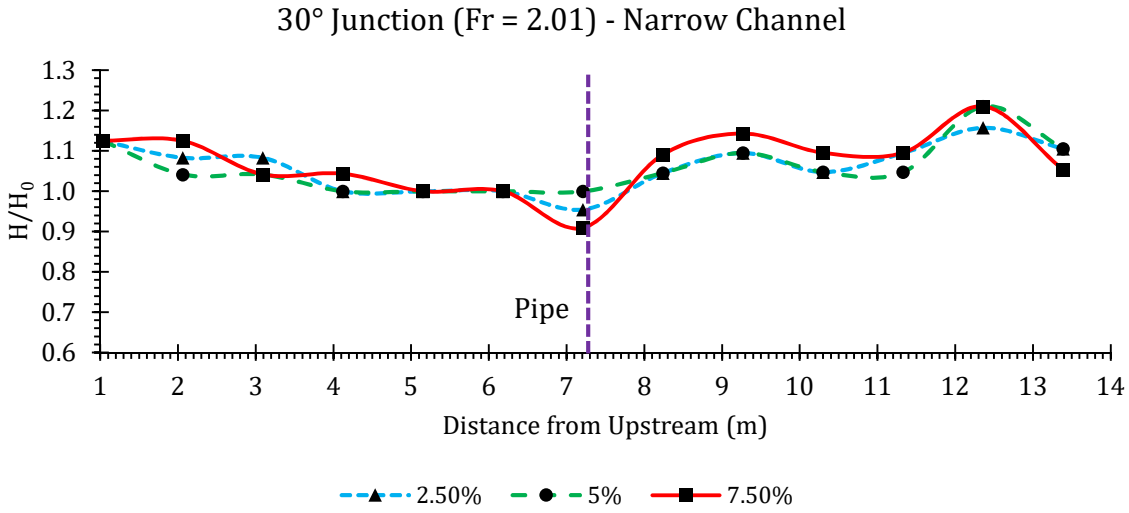

Figure A34. Water height ratios in a 30° junction for Fr = 2.01 in the narrow channel.

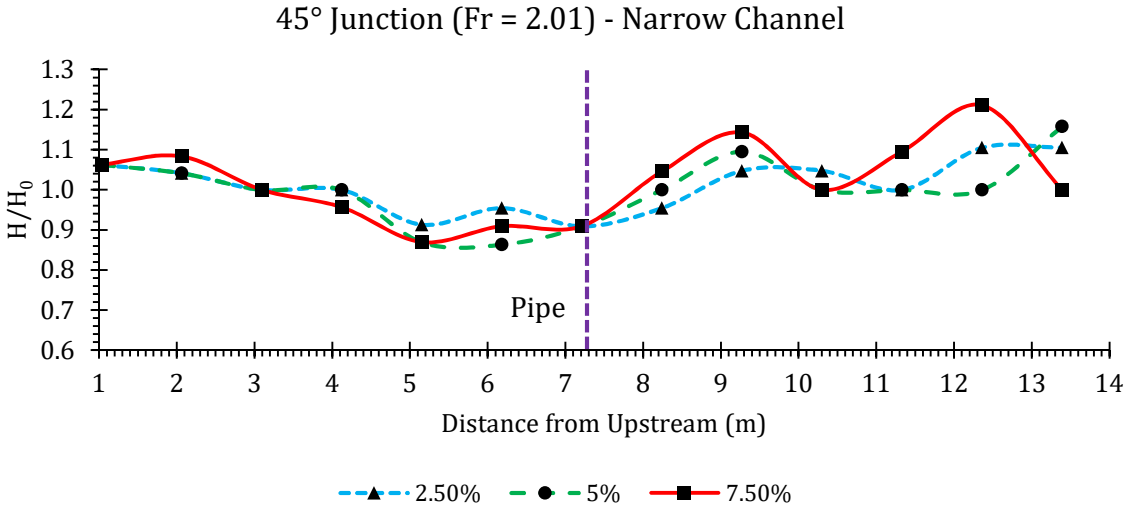

Figure A35. Water height ratios in a 45° junction for Fr = 2.01 in the narrow channel.

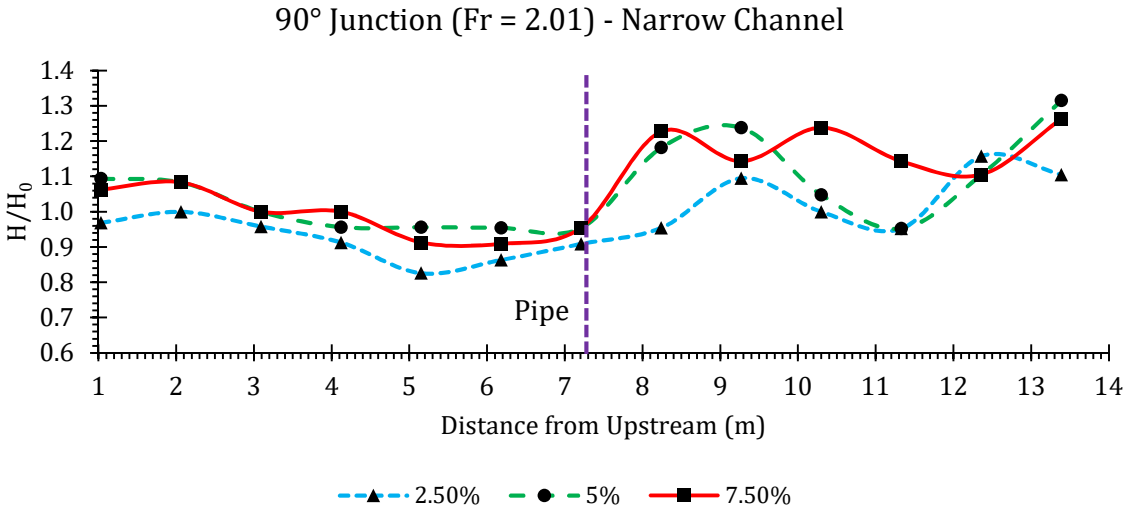

Figure A36. Water height ratios in a 90° junction for Fr = 2.01 in the narrow channel.

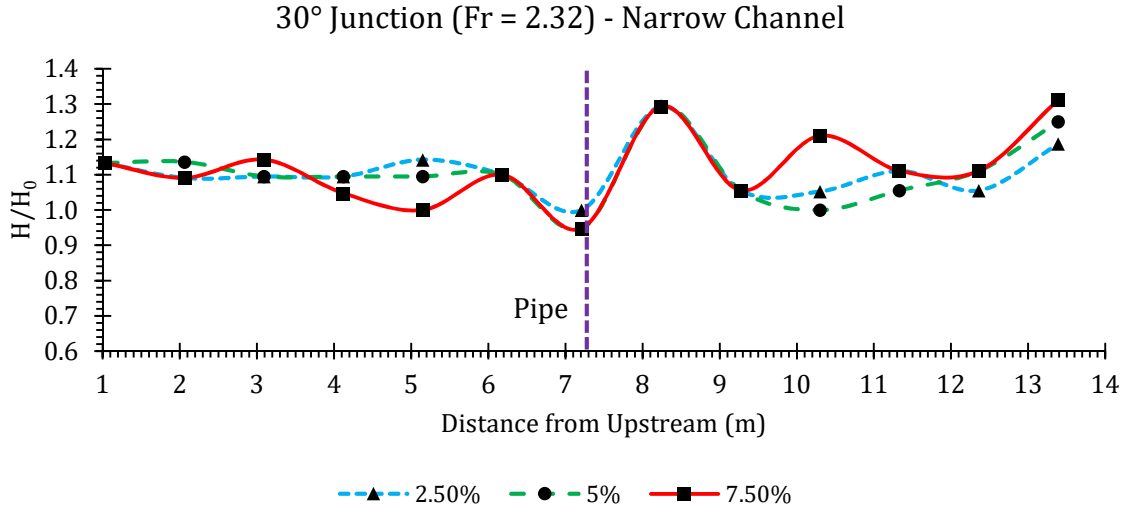

Figure A37. Water height ratios in a 30° junction for Fr = 2.32 in the narrow channel.

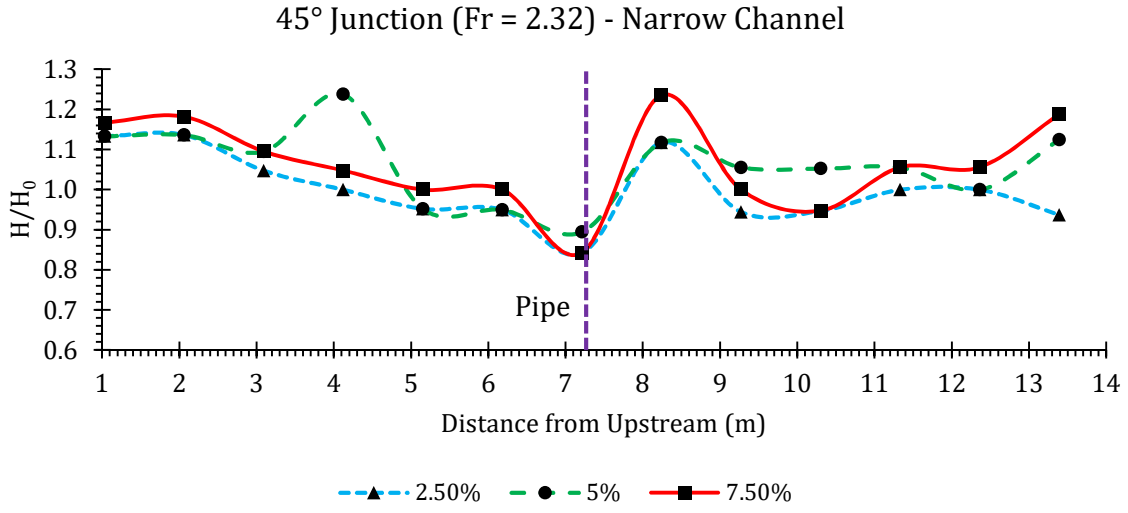

Figure A38. Water height ratios in a 45° junction for Fr = 2.32 in the narrow channel.

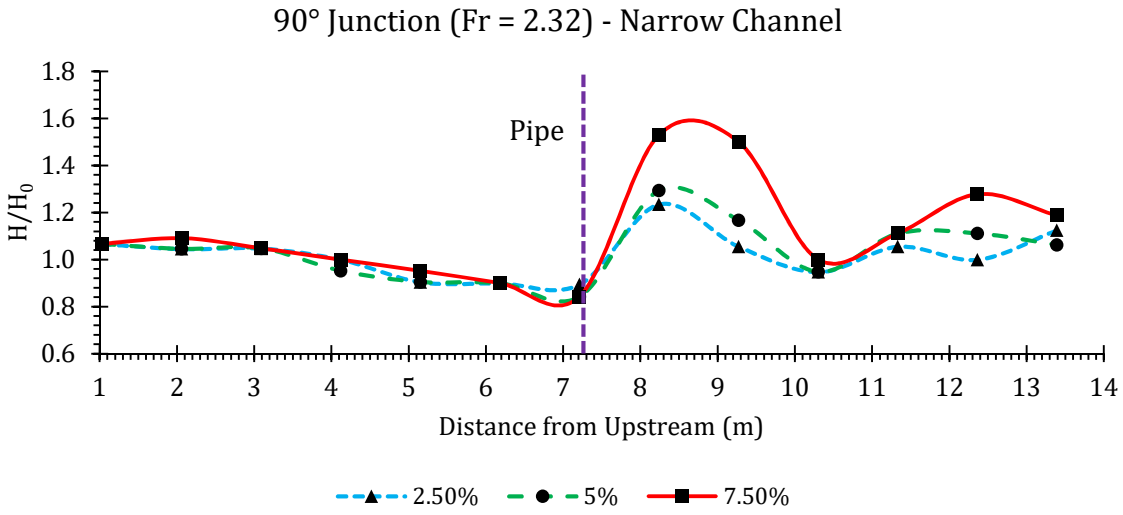

Figure A39. Water height ratios in a 90° junction for Fr = 2.32 in the narrow channel.

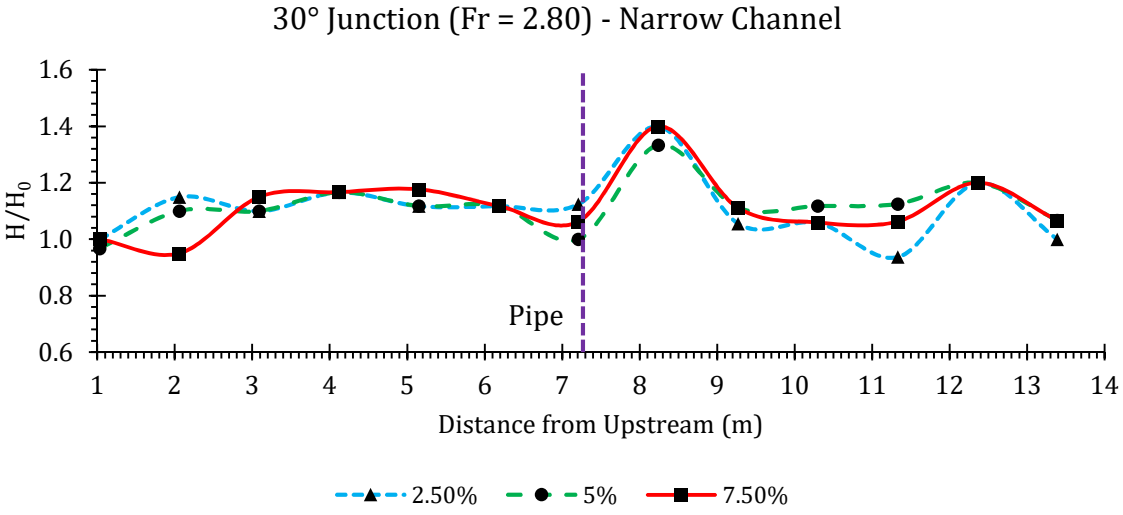

Figure A40. Water height ratios in a 30° junction for Fr = 2.80 in the narrow channel.

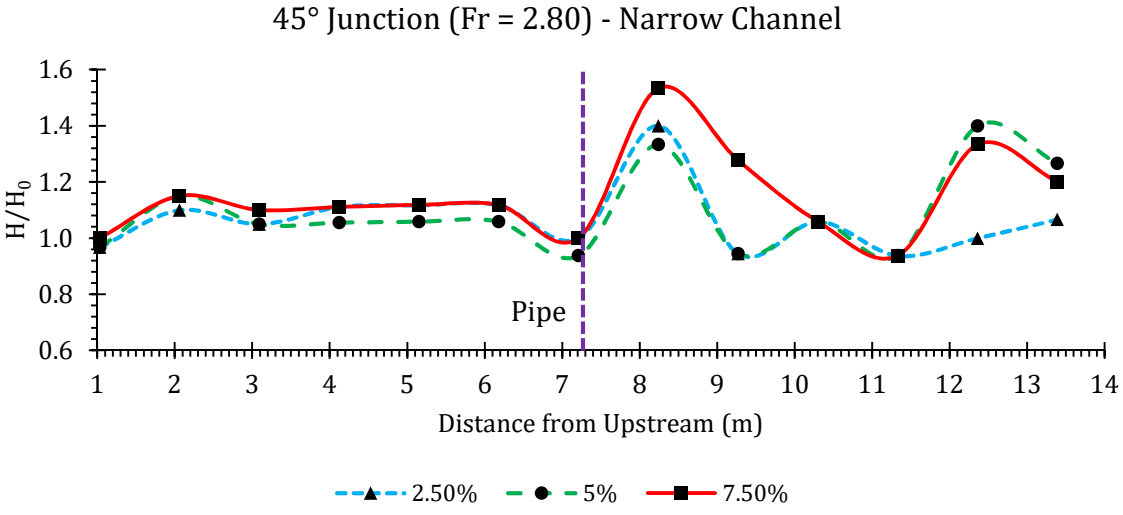

Figure A41. Water height ratios in a 45° junction for Fr = 2.80 in the narrow channel.

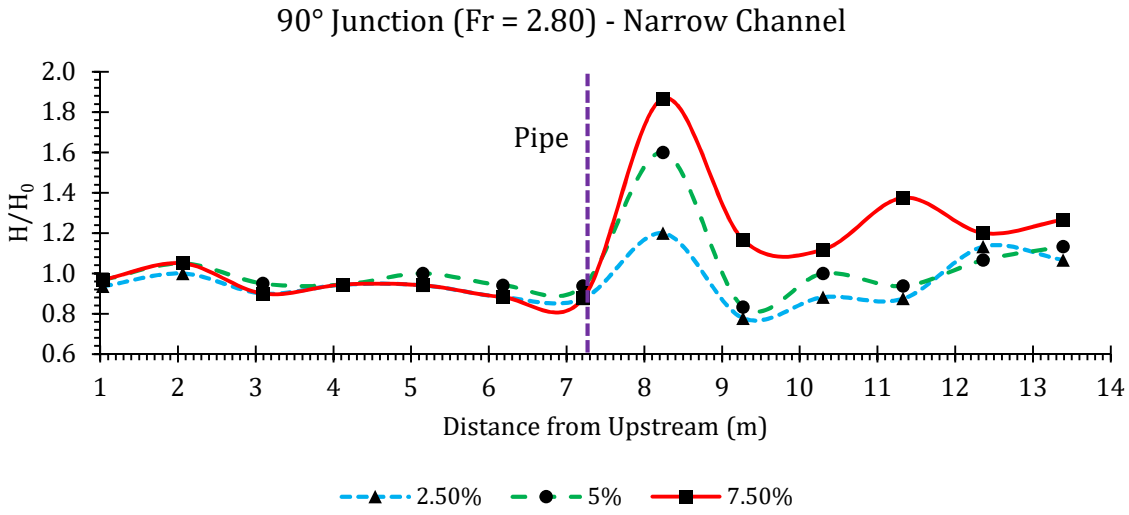

Figure A42. Water height ratios in a 90° junction for Fr = 2.80 in the narrow channel.

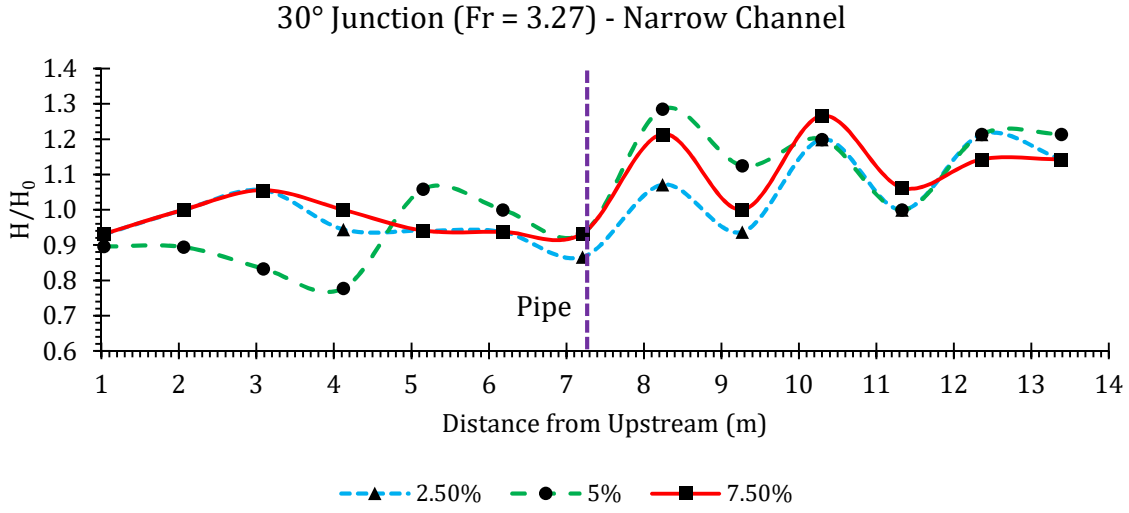

Figure A43. Water height ratios in a 30° junction for Fr = 3.27 in the narrow channel.

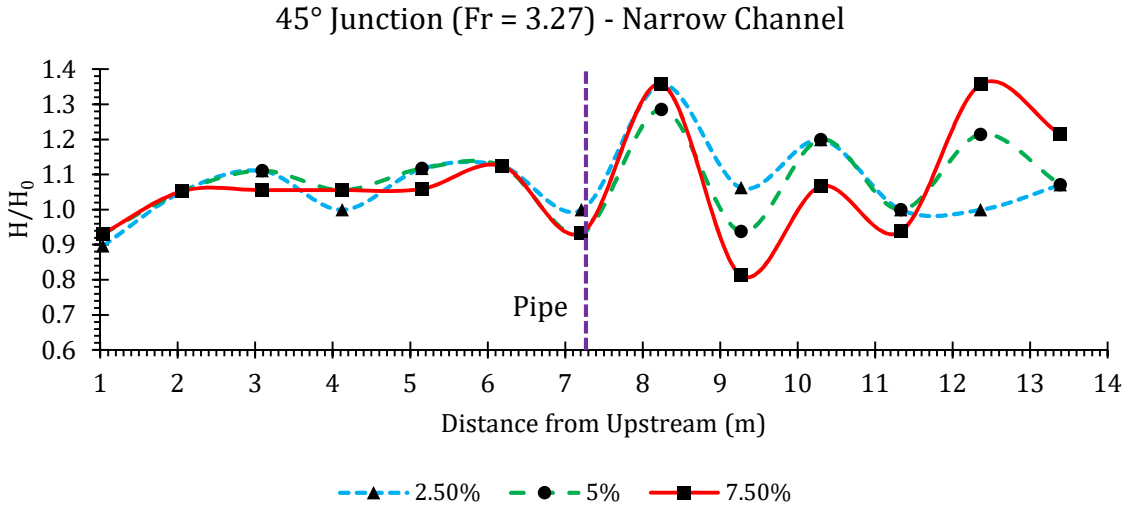

Figure A44. Water height ratios in a 45° junction for Fr = 3.27 in the narrow channel.

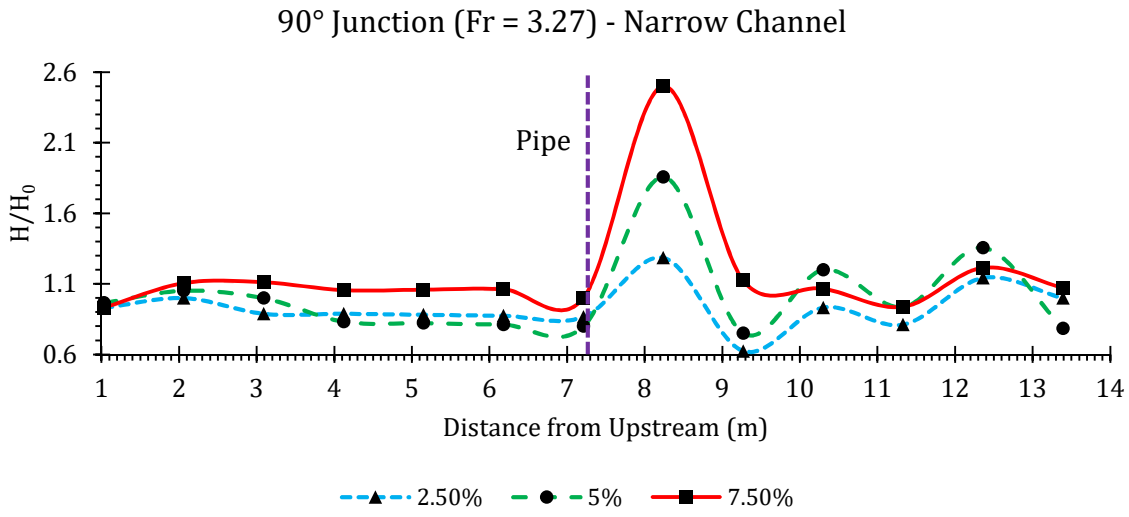

Figure A45. Water height ratios in a 90° junction for Fr = 3.27 in the narrow channel.

Appendix B

In Tables A1–A9, detailed FLOW-3D simulation results are presented. The last column in each table shows whether the impact of the lateral flow on the main channel flow was local (L), or it created waves (W) that propagated upstream (for sub-critical flow condition in the channel (Fr = 0.8)) or downstream (for super-critical flow conditions in the channel (Fr = 1.2, 2)).

Table A1. FLOW-3D simulation results for W = 3.05 m (10′) and Fr = 2.

W (m)	H_0 (m)	Fr (-)	Q Chan. (m^3/s)	V Chan. (m/s)	D Pipe (m)	q Pipe (m^3/s)	v Pipe (m/s)	θ Junc. (deg.)	$\frac{QV+qv(\cos\theta)}{qv(\sin\theta)}$	$\frac{H}{H_0}$	Impact
3.05	3.05	2	101.63	10.94	0.46	2.540	15.48	90	28.28	1.16	L
3.05	3.05	2	101.63	10.94	0.46	2.540	15.48	45	40.99	1.12	L
3.05	3.05	2	101.63	10.94	0.46	2.540	15.48	30	58.28	1.1	L
3.05	3.05	2	101.63	10.94	0.91	10.163	15.48	90	7.07	1.76	L
3.05	3.05	2	101.63	10.94	0.91	5.083	7.74	90	28.24	1.27	L
3.05	3.05	2	101.63	10.94	0.91	2.540	3.87	90	113.10	1.17	L
3.05	3.05	2	101.63	10.94	0.91	10.163	15.48	45	10.99	1.25	L
3.05	3.05	2	101.63	10.94	0.91	5.083	7.74	45	40.94	1.2	L
3.05	3.05	2	101.63	10.94	0.91	2.540	3.87	45	160.95	1.16	L
3.05	3.05	2	101.63	10.94	0.91	10.163	15.48	30	15.86	1.17	L
3.05	3.05	2	101.63	10.94	0.91	5.083	7.74	30	58.22	1.16	L
3.05	3.05	2	101.63	10.94	0.91	2.540	3.87	30	227.94	1.15	L
3.05	3.05	2	101.63	10.94	1.52	10.163	5.57	90	19.63	1.68	L
3.05	3.05	2	101.63	10.94	1.52	5.083	2.79	90	78.46	1.29	L
3.05	3.05	2	101.63	10.94	1.52	2.540	1.39	90	314.18	1.15	L
3.05	3.05	2	101.63	10.94	1.52	10.163	5.57	45	28.75	1.35	L
3.05	3.05	2	101.63	10.94	1.52	5.083	2.79	45	111.95	1.24	L
3.05	3.05	2	101.63	10.94	1.52	2.540	1.39	45	445.31	1.15	L
3.05	3.05	2	101.63	10.94	1.52	10.163	5.57	30	40.98	1.32	L
3.05	3.05	2	101.63	10.94	1.52	5.083	2.79	30	158.64	1.23	L
3.05	3.05	2	101.63	10.94	1.52	2.540	1.39	30	630.08	1.15	L
3.05	2.13	2	59.52	9.15	0.46	1.488	9.07	90	40.37	1.17	L
3.05	2.13	2	59.52	9.15	0.46	1.488	9.07	45	58.10	1.17	L
3.05	2.13	2	59.52	9.15	0.46	1.488	9.07	30	82.48	1.17	L
3.05	2.13	2	59.52	9.15	0.91	5.952	9.07	90	10.09	1.89	W
3.05	2.13	2	59.52	9.15	0.91	2.976	4.54	90	40.37	1.32	L
3.05	2.13	2	59.52	9.15	0.91	1.488	2.27	90	161.49	1.19	L

Table A1. *Cont.*

W (m)	H_0 (m)	Fr (-)	Q Chan. (m^3/s)	V Chan. (m/s)	D Pipe (m)	q Pipe (m^3/s)	v Pipe (m/s)	θ Junc. (deg.)	$\frac{QV+qv(\cos\theta)}{qv(\sin\theta)}$	$\frac{H}{H_0}$	Impact
3.05	2.13	2	59.52	9.15	0.91	5.952	9.07	45	15.27	1.26	L
3.05	2.13	2	59.52	9.15	0.91	2.976	4.54	45	58.10	1.18	L
3.05	2.13	2	59.52	9.15	0.91	1.488	2.27	45	229.39	1.18	L
3.05	2.13	2	59.52	9.15	0.91	5.952	9.07	30	21.92	1.18	L
3.05	2.13	2	59.52	9.15	0.91	2.976	4.54	30	82.48	1.18	L
3.05	2.13	2	59.52	9.15	0.91	1.488	2.27	30	324.72	1.18	L
3.05	2.13	2	59.52	9.15	1.52	5.952	3.26	90	28.04	1.84	W
3.05	2.13	2	59.52	9.15	1.52	2.976	1.63	90	112.15	1.33	L
3.05	2.13	2	59.52	9.15	1.52	1.488	0.82	90	448.59	1.2	L
3.05	2.13	2	59.52	9.15	1.52	5.952	3.26	45	40.65	1.49	L
3.05	2.13	2	59.52	9.15	1.52	2.976	1.63	45	159.60	1.28	L
3.05	2.13	2	59.52	9.15	1.52	1.488	0.82	45	635.41	1.19	L
3.05	2.13	2	59.52	9.15	1.52	5.952	3.26	30	57.81	1.43	L
3.05	2.13	2	59.52	9.15	1.52	2.976	1.63	30	226.03	1.3	L
3.05	2.13	2	59.52	9.15	1.52	1.488	0.82	30	898.92	1.17	L
3.05	1.22	2	25.71	6.92	0.46	1.286	7.83	90	17.66	1.38	W
3.05	1.22	2	25.71	6.92	0.46	0.643	3.92	90	70.65	1.23	L
3.05	1.22	2	25.71	6.92	0.46	1.286	7.83	45	25.98	1.26	L
3.05	1.22	2	25.71	6.92	0.46	0.643	3.92	45	100.91	1.2	L
3.05	1.22	2	25.71	6.92	0.46	1.286	7.83	30	37.06	1.2	L
3.05	1.22	2	25.71	6.92	0.46	0.643	3.92	30	143.03	1.2	L
3.05	1.22	2	25.71	6.92	0.91	2.571	3.92	90	17.66	1.93	W
3.05	1.22	2	25.71	6.92	0.91	1.286	1.96	90	70.65	1.39	W
3.05	1.22	2	25.71	6.92	0.91	0.643	0.98	90	282.60	1.17	L
3.05	1.22	2	25.71	6.92	0.91	2.571	3.92	45	25.98	1.53	W
3.05	1.22	2	25.71	6.92	0.91	1.286	1.96	45	100.91	1.36	L
3.05	1.22	2	25.71	6.92	0.91	0.643	0.98	45	400.66	1.25	L
3.05	1.22	2	25.71	6.92	0.91	2.571	3.92	30	37.06	1.5	L
3.05	1.22	2	25.71	6.92	0.91	1.286	1.96	30	143.03	1.36	L
3.05	1.22	2	25.71	6.92	0.91	0.643	0.98	30	566.93	1.25	L

Table A2. FLOW-3D simulation results for W = 7.62 m (25′) and Fr = 2.

W (m)	H_0 (m)	Fr (-)	Q Chan. (m^3/s)	V Chan. (m/s)	D Pipe (m)	q Pipe (m^3/s)	v Pipe (m/s)	θ Junc. (deg.)	$\frac{QV+qv(\cos\theta)}{qv(\sin\theta)}$	$\frac{H}{H_0}$	Impact
7.62	3.05	2	254.09	10.94	0.46	2.540	15.48	90	70.69	1.1	L
7.62	3.05	2	254.09	10.94	0.46	2.540	15.48	45	100.98	1.06	L
7.62	3.05	2	254.09	10.94	0.46	2.540	15.48	30	143.12	1.03	L
7.62	3.05	2	254.09	10.94	0.91	10.163	15.48	90	17.66	1.38	W
7.62	3.05	2	254.09	10.94	0.91	5.083	7.74	90	70.61	1.19	L
7.62	3.05	2	254.09	10.94	0.91	2.540	3.87	90	282.77	1.1	L
7.62	3.05	2	254.09	10.94	0.91	10.163	15.48	45	25.98	1.15	L
7.62	3.05	2	254.09	10.94	0.91	5.083	7.74	45	100.86	1.11	L
7.62	3.05	2	254.09	10.94	0.91	2.540	3.87	45	400.90	1.1	L
7.62	3.05	2	254.09	10.94	0.91	10.163	15.48	30	37.06	1.08	L
7.62	3.05	2	254.09	10.94	0.91	5.083	7.74	30	142.96	1.07	L
7.62	3.05	2	254.09	10.94	0.91	2.540	3.87	30	567.28	1.06	L
7.62	3.05	2	254.09	10.94	1.52	10.163	5.57	90	49.07	1.32	W
7.62	3.05	2	254.09	10.94	1.52	5.083	2.79	90	196.15	1.18	L
7.62	3.05	2	254.09	10.94	1.52	2.540	1.39	90	785.48	1.1	L
7.62	3.05	2	254.09	10.94	1.52	10.163	5.57	45	70.39	1.2	L
7.62	3.05	2	254.09	10.94	1.52	5.083	2.79	45	278.40	1.15	L
7.62	3.05	2	254.09	10.94	1.52	2.540	1.39	45	1111.84	1.1	L
7.62	3.05	2	254.09	10.94	1.52	10.163	5.57	30	99.86	1.17	L
7.62	3.05	2	254.09	10.94	1.52	5.083	2.79	30	394.04	1.15	L
7.62	3.05	2	254.09	10.94	1.52	2.540	1.39	30	1572.69	1.1	L
7.62	2.13	2	148.81	9.15	0.46	1.488	9.07	90	100.93	1.07	L
7.62	2.13	2	148.81	9.15	0.46	1.488	9.07	45	143.74	1.01	L
7.62	2.13	2	148.81	9.15	0.46	1.488	9.07	30	203.60	1.01	L
7.62	2.13	2	148.81	9.15	0.91	5.952	9.07	90	25.23	1.36	W
7.62	2.13	2	148.81	9.15	0.91	2.976	4.54	90	100.93	1.14	L
7.62	2.13	2	148.81	9.15	0.91	1.488	2.27	90	403.73	1.07	L
7.62	2.13	2	148.81	9.15	0.91	5.952	9.07	45	36.69	1.11	L
7.62	2.13	2	148.81	9.15	0.91	2.976	4.54	45	143.74	1.09	L
7.62	2.13	2	148.81	9.15	0.91	1.488	2.27	45	571.97	1.07	L
7.62	2.13	2	148.81	9.15	0.91	5.952	9.07	30	52.20	1.11	L
7.62	2.13	2	148.81	9.15	0.91	2.976	4.54	30	203.60	1.08	L
7.62	2.13	2	148.81	9.15	0.91	1.488	2.27	30	809.20	1.06	L
7.62	2.13	2	148.81	9.15	1.52	5.952	3.26	90	70.09	1.43	W
7.62	2.13	2	148.81	9.15	1.52	2.976	1.63	90	280.37	1.14	L
7.62	2.13	2	148.81	9.15	1.52	1.488	0.82	90	1121.48	1.07	L
7.62	2.13	2	148.81	9.15	1.52	5.952	3.26	45	100.13	1.22	L
7.62	2.13	2	148.81	9.15	1.52	2.976	1.63	45	397.50	1.12	L
7.62	2.13	2	148.81	9.15	1.52	1.488	0.82	45	1587.01	1.06	L
7.62	2.13	2	148.81	9.15	1.52	5.952	3.26	30	141.92	1.2	L
7.62	2.13	2	148.81	9.15	1.52	2.976	1.63	30	562.47	1.12	L
7.62	2.13	2	148.81	9.15	1.52	1.488	0.82	30	2244.70	1.06	L
7.62	1.22	2	64.28	6.92	0.46	1.286	7.83	90	44.16	1.17	L
7.62	1.22	2	64.28	6.92	0.46	0.643	3.92	90	176.63	1.07	L
7.62	1.22	2	64.28	6.92	0.46	1.286	7.83	45	63.45	1.08	L
7.62	1.22	2	64.28	6.92	0.46	0.643	3.92	45	250.79	1.02	L
7.62	1.22	2	64.28	6.92	0.46	1.286	7.83	30	90.04	1.01	L
7.62	1.22	2	64.28	6.92	0.46	0.643	3.92	30	354.98	1.01	L
7.62	1.22	2	64.28	6.92	0.91	2.571	3.92	90	44.16	1.39	W
7.62	1.22	2	64.28	6.92	0.91	1.286	1.96	90	176.63	1.17	L
7.62	1.22	2	64.28	6.92	0.91	0.643	0.98	90	706.50	1.08	L
7.62	1.22	2	64.28	6.92	0.91	2.571	3.92	45	63.45	1.27	L
7.62	1.22	2	64.28	6.92	0.91	1.286	1.96	45	250.79	1.15	L
7.62	1.22	2	64.28	6.92	0.91	0.643	0.98	45	1000.14	1.07	L
7.62	1.22	2	64.28	6.92	0.91	2.571	3.92	30	90.04	1.25	L
7.62	1.22	2	64.28	6.92	0.91	1.286	1.96	30	354.98	1.14	L
7.62	1.22	2	64.28	6.92	0.91	0.643	0.98	30	1414.73	1.06	L

Table A3. FLOW-3D simulation results for W = 15.24 m (50′) and Fr = 2.

W (m)	H_0 (m)	Fr (-)	Q Chan. (m^3/s)	V Chan. (m/s)	D Pipe (m)	q Pipe (m^3/s)	v Pipe (m/s)	θ Junc. (deg.)	$\frac{QV+qv(\cos\theta)}{qv(\sin\theta)}$	$\frac{H}{H_0}$	Impact
15.24	3.05	2	508.15	10.94	0.46	2.540	15.48	90	141.38	1.01	L
15.24	3.05	2	508.15	10.94	0.46	2.540	15.48	45	200.94	1.01	L
15.24	3.05	2	508.15	10.94	0.46	2.540	15.48	30	284.49	1.01	L
15.24	3.05	2	508.15	10.94	0.91	10.163	15.48	90	35.33	1.23	L
15.24	3.05	2	508.15	10.94	0.91	5.083	7.74	90	141.22	1.07	L
15.24	3.05	2	508.15	10.94	0.91	2.540	3.87	90	565.52	1.01	L
15.24	3.05	2	508.15	10.94	0.91	10.163	15.48	45	50.96	1.07	L
15.24	3.05	2	508.15	10.94	0.91	5.083	7.74	45	200.72	1.02	L
15.24	3.05	2	508.15	10.94	0.91	2.540	3.87	45	800.76	1.01	L
15.24	3.05	2	508.15	10.94	0.91	10.163	15.48	30	72.38	1.02	L
15.24	3.05	2	508.15	10.94	0.91	5.083	7.74	30	284.17	1.01	L
15.24	3.05	2	508.15	10.94	0.91	2.540	3.87	30	1132.76	1.01	L
15.24	3.05	2	508.15	10.94	1.52	10.163	5.57	90	98.13	1.24	L
15.24	3.05	2	508.15	10.94	1.52	5.083	2.79	90	392.28	1.08	L
15.24	3.05	2	508.15	10.94	1.52	2.540	1.39	90	1570.88	1.03	L
15.24	3.05	2	508.15	10.94	1.52	10.163	5.57	45	139.77	1.14	L
15.24	3.05	2	508.15	10.94	1.52	5.083	2.79	45	555.77	1.08	L
15.24	3.05	2	508.15	10.94	1.52	2.540	1.39	45	2222.55	1.05	L
15.24	3.05	2	508.15	10.94	1.52	10.163	5.57	30	197.98	1.12	L
15.24	3.05	2	508.15	10.94	1.52	5.083	2.79	30	786.29	1.06	L
15.24	3.05	2	508.15	10.94	1.52	2.540	1.39	30	3143.48	1.01	L
15.24	2.13	2	297.61	9.15	0.46	1.488	9.07	90	201.87	1.05	L
15.24	2.13	2	297.61	9.15	0.46	1.488	9.07	45	286.48	1.01	L
15.24	2.13	2	297.61	9.15	0.46	1.488	9.07	30	405.47	1.01	L
15.24	2.13	2	297.61	9.15	0.91	5.952	9.07	90	50.47	1.25	L
15.24	2.13	2	297.61	9.15	0.91	2.976	4.54	90	201.87	1.11	L
15.24	2.13	2	297.61	9.15	0.91	1.488	2.27	90	807.47	1.09	L
15.24	2.13	2	297.61	9.15	0.91	5.952	9.07	45	72.37	1.09	L
15.24	2.13	2	297.61	9.15	0.91	2.976	4.54	45	286.48	1.06	L
15.24	2.13	2	297.61	9.15	0.91	1.488	2.27	45	1142.93	1.02	L
15.24	2.13	2	297.61	9.15	0.91	5.952	9.07	30	102.67	1.07	L
15.24	2.13	2	297.61	9.15	0.91	2.976	4.54	30	405.47	1.04	L
15.24	2.13	2	297.61	9.15	0.91	1.488	2.27	30	1616.67	1.01	L
15.24	2.13	2	297.61	9.15	1.52	5.952	3.26	90	140.19	1.3	L
15.24	2.13	2	297.61	9.15	1.52	2.976	1.63	90	560.74	1.11	L
15.24	2.13	2	297.61	9.15	1.52	1.488	0.82	90	2242.96	1.07	L
15.24	2.13	2	297.61	9.15	1.52	5.952	3.26	45	199.25	1.17	L
15.24	2.13	2	297.61	9.15	1.52	2.976	1.63	45	794.01	1.07	L
15.24	2.13	2	297.61	9.15	1.52	1.488	0.82	45	3173.03	1.02	L
15.24	2.13	2	297.61	9.15	1.52	5.952	3.26	30	282.10	1.17	L
15.24	2.13	2	297.61	9.15	1.52	2.976	1.63	30	1123.21	1.08	L
15.24	2.13	2	297.61	9.15	1.52	1.488	0.82	30	4487.66	1.02	L
15.24	1.22	2	128.56	6.92	0.46	1.286	7.83	90	88.31	1.08	L
15.24	1.22	2	128.56	6.92	0.46	0.643	3.92	90	353.25	1.06	L
15.24	1.22	2	128.56	6.92	0.46	1.286	7.83	45	125.89	1.03	L
15.24	1.22	2	128.56	6.92	0.46	0.643	3.92	45	500.57	1.01	L
15.24	1.22	2	128.56	6.92	0.46	1.286	7.83	30	178.36	1.01	L
15.24	1.22	2	128.56	6.92	0.46	0.643	3.92	30	708.23	1.01	L
15.24	1.22	2	128.56	6.92	0.91	2.571	3.92	90	88.31	1.23	L
15.24	1.22	2	128.56	6.92	0.91	1.286	1.96	90	353.25	1.06	L
15.24	1.22	2	128.56	6.92	0.91	0.643	0.98	90	1413.00	1.03	L
15.24	1.22	2	128.56	6.92	0.91	2.571	3.92	45	125.89	1.15	L
15.24	1.22	2	128.56	6.92	0.91	1.286	1.96	45	500.57	1.04	L
15.24	1.22	2	128.56	6.92	0.91	0.643	0.98	45	1999.28	1.02	L
15.24	1.22	2	128.56	6.92	0.91	2.571	3.92	30	178.36	1.14	L
15.24	1.22	2	128.56	6.92	0.91	1.286	1.96	30	708.23	1.03	L
15.24	1.22	2	128.56	6.92	0.91	0.643	0.98	30	2827.73	1.01	L

Table A4. FLOW-3D simulation results for W = 3.05 m (10′) and Fr = 1.2.

W (m)	H_0 (m)	Fr (-)	Q Chan. (m^3/s)	V Chan. (m/s)	D Pipe (m)	q Pipe (m^3/s)	v Pipe (m/s)	θ Junc. (deg.)	$\frac{QV+qv(\cos\theta)}{qv(\sin\theta)}$	$\frac{H}{H_0}$	Impact
3.05	3.05	1.2	60.97	6.56	0.46	1.524	9.29	90	28.26	1.2	L
3.05	3.05	1.2	60.97	6.56	0.46	1.524	9.29	45	40.97	1.2	L
3.05	3.05	1.2	60.97	6.56	0.46	1.524	9.29	30	58.25	1.2	L
3.05	3.05	1.2	60.97	6.56	0.91	6.097	9.29	90	7.07	1.78	L
3.05	3.05	1.2	60.97	6.56	0.91	3.048	4.64	90	28.26	1.43	L
3.05	3.05	1.2	60.97	6.56	0.91	1.524	2.32	90	113.04	1.18	L
3.05	3.05	1.2	60.97	6.56	0.91	6.097	9.29	45	10.99	1.26	L
3.05	3.05	1.2	60.97	6.56	0.91	3.048	4.64	45	40.97	1.23	L
3.05	3.05	1.2	60.97	6.56	0.91	1.524	2.32	45	160.86	1.15	L
3.05	3.05	1.2	60.97	6.56	0.91	6.097	9.29	30	15.86	1.22	L
3.05	3.05	1.2	60.97	6.56	0.91	3.048	4.64	30	58.25	1.2	L
3.05	3.05	1.2	60.97	6.56	0.91	1.524	2.32	30	227.81	1.15	L
3.05	3.05	1.2	60.97	6.56	1.52	6.097	3.34	90	19.63	1.84	L
3.05	3.05	1.2	60.97	6.56	1.52	3.048	1.67	90	78.50	1.43	L
3.05	3.05	1.2	60.97	6.56	1.52	1.524	0.84	90	314.00	1.19	L
3.05	3.05	1.2	60.97	6.56	1.52	6.097	3.34	45	28.75	1.57	L
3.05	3.05	1.2	60.97	6.56	1.52	3.048	1.67	45	112.02	1.33	L
3.05	3.05	1.2	60.97	6.56	1.52	1.524	0.84	45	445.06	1.17	L
3.05	3.05	1.2	60.97	6.56	1.52	6.097	3.34	30	40.98	1.54	L
3.05	3.05	1.2	60.97	6.56	1.52	3.048	1.67	30	158.73	1.32	L
3.05	3.05	1.2	60.97	6.56	1.52	1.524	0.84	30	629.73	1.17	L
3.05	2.13	1.2	35.71	5.49	0.46	1.785	10.88	90	10.10	1.28	L
3.05	2.13	1.2	35.71	5.49	0.46	0.893	5.44	90	40.38	1.2	L
3.05	2.13	1.2	35.71	5.49	0.46	1.785	10.88	45	15.28	1.2	L
3.05	2.13	1.2	35.71	5.49	0.46	0.893	5.44	45	58.11	1.2	L
3.05	2.13	1.2	35.71	5.49	0.46	1.785	10.88	30	21.92	1.2	L
3.05	2.13	1.2	35.71	5.49	0.46	0.893	5.44	30	82.50	1.2	L
3.05	2.13	1.2	35.71	5.49	0.91	3.571	5.44	90	10.10	1.85	L
3.05	2.13	1.2	35.71	5.49	0.91	1.785	2.72	90	40.38	1.36	L
3.05	2.13	1.2	35.71	5.49	0.91	0.893	1.36	90	161.54	1.15	L
3.05	2.13	1.2	35.71	5.49	0.91	3.571	5.44	45	15.28	1.33	L
3.05	2.13	1.2	35.71	5.49	0.91	1.785	2.72	45	58.11	1.23	L
3.05	2.13	1.2	35.71	5.49	0.91	0.893	1.36	45	229.45	1.12	L
3.05	2.13	1.2	35.71	5.49	0.91	3.571	5.44	30	21.92	1.27	L
3.05	2.13	1.2	35.71	5.49	0.91	1.785	2.72	30	82.50	1.22	L
3.05	2.13	1.2	35.71	5.49	0.91	0.893	1.36	30	324.81	1.11	L
3.05	2.13	1.2	35.71	5.49	1.52	3.571	1.96	90	28.04	1.87	L
3.05	2.13	1.2	35.71	5.49	1.52	1.785	0.98	90	112.18	1.35	L
3.05	2.13	1.2	35.71	5.49	1.52	0.893	0.49	90	448.71	1.15	L
3.05	2.13	1.2	35.71	5.49	1.52	3.571	1.96	45	40.66	1.66	L
3.05	2.13	1.2	35.71	5.49	1.52	1.785	0.98	45	159.64	1.31	L
3.05	2.13	1.2	35.71	5.49	1.52	0.893	0.49	45	635.58	1.13	L
3.05	2.13	1.2	35.71	5.49	1.52	3.571	1.96	30	57.82	1.63	L
3.05	2.13	1.2	35.71	5.49	1.52	1.785	0.98	30	226.09	1.31	L
3.05	2.13	1.2	35.71	5.49	1.52	0.893	0.49	30	899.16	1.13	L
3.05	1.22	1.2	15.43	4.15	0.46	1.543	9.41	90	4.41	1.65	L
3.05	1.22	1.2	15.43	4.15	0.46	0.772	4.70	90	17.66	1.2	L
3.05	1.22	1.2	15.43	4.15	0.46	0.386	2.35	90	70.62	1.08	L
3.05	1.22	1.2	15.43	4.15	0.46	1.543	9.41	45	7.24	1.1	L
3.05	1.22	1.2	15.43	4.15	0.46	0.772	4.70	45	25.97	1.07	L
3.05	1.22	1.2	15.43	4.15	0.46	0.386	2.35	45	100.88	1.03	L
3.05	1.22	1.2	15.43	4.15	0.46	1.543	9.41	30	10.56	1.03	L
3.05	1.22	1.2	15.43	4.15	0.46	0.772	4.70	30	37.04	1.03	L
3.05	1.22	1.2	15.43	4.15	0.46	0.386	2.35	30	142.98	1.03	L
3.05	1.22	1.2	15.43	4.15	0.91	1.543	2.35	90	17.66	1.78	L
3.05	1.22	1.2	15.43	4.15	0.91	0.772	1.18	90	70.62	1.28	L
3.05	1.22	1.2	15.43	4.15	0.91	0.386	0.59	90	282.50	1.09	L
3.05	1.22	1.2	15.43	4.15	0.91	1.543	2.35	45	25.97	1.52	L
3.05	1.22	1.2	15.43	4.15	0.91	0.772	1.18	45	100.88	1.25	L
3.05	1.22	1.2	15.43	4.15	0.91	0.386	0.59	45	400.51	1.08	L
3.05	1.22	1.2	15.43	4.15	0.91	1.543	2.35	30	37.04	1.48	L
3.05	1.22	1.2	15.43	4.15	0.91	0.772	1.18	30	142.98	1.25	L
3.05	1.22	1.2	15.43	4.15	0.91	0.386	0.59	30	566.72	1.07	L

Table A5. FLOW-3D simulation results for W = 7.62 m (25′) and Fr = 1.2.

W (m)	H_0 (m)	Fr (-)	Q Chan. (m^3/s)	V Chan. (m/s)	D Pipe (m)	q Pipe (m^3/s)	v Pipe (m/s)	θ Junc. (deg.)	$\frac{QV+qv(\cos\theta)}{qv(\sin\theta)}$	$\frac{H}{H_0}$	Impact
7.62	3.05	1.2	152.43	6.56	0.46	1.524	9.29	90	70.66	1.01	L
7.62	3.05	1.2	152.43	6.56	0.46	1.524	9.29	45	100.92	1.01	L
7.62	3.05	1.2	152.43	6.56	0.46	1.524	9.29	30	143.05	1.01	L
7.62	3.05	1.2	152.43	6.56	0.91	6.097	9.29	90	17.66	1.27	W
7.62	3.05	1.2	152.43	6.56	0.91	3.048	4.64	90	70.66	1.07	L
7.62	3.05	1.2	152.43	6.56	0.91	1.524	2.32	90	282.63	1.01	L
7.62	3.05	1.2	152.43	6.56	0.91	6.097	9.29	45	25.98	1.06	L
7.62	3.05	1.2	152.43	6.56	0.91	3.048	4.64	45	100.92	1.01	L
7.62	3.05	1.2	152.43	6.56	0.91	1.524	2.32	45	400.69	1.01	L
7.62	3.05	1.2	152.43	6.56	0.91	6.097	9.29	30	37.06	1.01	L
7.62	3.05	1.2	152.43	6.56	0.91	3.048	4.64	30	143.05	1.01	L
7.62	3.05	1.2	152.43	6.56	0.91	1.524	2.32	30	566.98	1.01	L
7.62	3.05	1.2	152.43	6.56	1.52	6.097	3.34	90	49.07	1.26	L
7.62	3.05	1.2	152.43	6.56	1.52	3.048	1.67	90	196.27	1.17	L
7.62	3.05	1.2	152.43	6.56	1.52	1.524	0.84	90	785.07	1.01	L
7.62	3.05	1.2	152.43	6.56	1.52	6.097	3.34	45	70.39	1.14	L
7.62	3.05	1.2	152.43	6.56	1.52	3.048	1.67	45	278.57	1.06	L
7.62	3.05	1.2	152.43	6.56	1.52	1.524	0.84	45	1111.26	1.01	L
7.62	3.05	1.2	152.43	6.56	1.52	6.097	3.34	30	99.87	1.13	L
7.62	3.05	1.2	152.43	6.56	1.52	3.048	1.67	30	394.27	1.05	L
7.62	3.05	1.2	152.43	6.56	1.52	1.524	0.84	30	1571.88	1.01	L
7.62	2.13	1.2	89.28	5.49	0.46	1.785	10.88	90	25.24	1.04	L
7.62	2.13	1.2	89.28	5.49	0.46	0.893	5.44	90	100.98	1.01	L
7.62	2.13	1.2	89.28	5.49	0.46	1.785	10.88	45	36.70	1.01	L
7.62	2.13	1.2	89.28	5.49	0.46	0.893	5.44	45	143.80	1.01	L
7.62	2.13	1.2	89.28	5.49	0.46	1.785	10.88	30	52.22	1.01	L
7.62	2.13	1.2	89.28	5.49	0.46	0.893	5.44	30	203.69	1.01	L
7.62	2.13	1.2	89.28	5.49	0.91	3.571	5.44	90	25.24	1.21	W
7.62	2.13	1.2	89.28	5.49	0.91	1.785	2.72	90	100.98	1.06	L
7.62	2.13	1.2	89.28	5.49	0.91	0.893	1.36	90	403.91	1.01	L
7.62	2.13	1.2	89.28	5.49	0.91	3.571	5.44	45	36.70	1.04	L
7.62	2.13	1.2	89.28	5.49	0.91	1.785	2.72	45	143.80	1.02	L
7.62	2.13	1.2	89.28	5.49	0.91	0.893	1.36	45	572.21	1.01	L
7.62	2.13	1.2	89.28	5.49	0.91	3.571	5.44	30	52.22	1.01	L
7.62	2.13	1.2	89.28	5.49	0.91	1.785	2.72	30	203.69	1.01	L
7.62	2.13	1.2	89.28	5.49	0.91	0.893	1.36	30	809.54	1.01	L
7.62	2.13	1.2	89.28	5.49	1.52	3.571	1.96	90	70.12	1.21	W
7.62	2.13	1.2	89.28	5.49	1.52	1.785	0.98	90	280.49	1.05	L
7.62	2.13	1.2	89.28	5.49	1.52	0.893	0.49	90	1121.96	1.01	L
7.62	2.13	1.2	89.28	5.49	1.52	3.571	1.96	45	100.17	1.15	L
7.62	2.13	1.2	89.28	5.49	1.52	1.785	0.98	45	397.67	1.04	L
7.62	2.13	1.2	89.28	5.49	1.52	0.893	0.49	45	1587.69	1.01	L
7.62	2.13	1.2	89.28	5.49	1.52	3.571	1.96	30	141.98	1.13	L
7.62	2.13	1.2	89.28	5.49	1.52	1.785	0.98	30	562.71	1.04	L
7.62	2.13	1.2	89.28	5.49	1.52	0.893	0.49	30	2245.66	1.01	L
7.62	1.22	1.2	38.60	4.15	0.46	1.543	9.41	90	11.04	1.25	W
7.62	1.22	1.2	38.60	4.15	0.46	0.772	4.70	90	44.16	1.09	L
7.62	1.22	1.2	38.60	4.15	0.46	0.386	2.35	90	176.62	1.01	L
7.62	1.22	1.2	38.60	4.15	0.46	1.543	9.41	45	16.61	1.18	L
7.62	1.22	1.2	38.60	4.15	0.46	0.772	4.70	45	63.45	1.05	L
7.62	1.22	1.2	38.60	4.15	0.46	0.386	2.35	45	250.79	1.01	L
7.62	1.22	1.2	38.60	4.15	0.46	1.543	9.41	30	23.81	1.01	L
7.62	1.22	1.2	38.60	4.15	0.46	0.772	4.70	30	90.04	1.01	L
7.62	1.22	1.2	38.60	4.15	0.46	0.386	2.35	30	354.98	1.01	L
7.62	1.22	1.2	38.60	4.15	0.91	1.543	2.35	90	44.16	1.27	L
7.62	1.22	1.2	38.60	4.15	0.91	0.772	1.18	90	176.62	1.12	L
7.62	1.22	1.2	38.60	4.15	0.91	0.386	0.59	90	706.50	1.04	L
7.62	1.22	1.2	38.60	4.15	0.91	1.543	2.35	45	63.45	1.2	L
7.62	1.22	1.2	38.60	4.15	0.91	0.772	1.18	45	250.79	1.09	L
7.62	1.22	1.2	38.60	4.15	0.91	0.386	0.59	45	1000.14	1.02	L
7.62	1.22	1.2	38.60	4.15	0.91	1.543	2.35	30	90.04	1.17	L
7.62	1.22	1.2	38.60	4.15	0.91	0.772	1.18	30	354.98	1.08	L
7.62	1.22	1.2	38.60	4.15	0.91	0.386	0.59	30	1414.73	1.01	L

Table A6. FLOW-3D simulation results for W = 15.24 m (50′) and Fr = 1.2.

W (m)	H_0 (m)	Fr (-)	Q Chan. (m^3/s)	V Chan. (m/s)	D Pipe (m)	q Pipe (m^3/s)	v Pipe (m/s)	θ Junc. (deg.)	$\frac{QV+qv(\cos\theta)}{qv(\sin\theta)}$	$\frac{H}{H_0}$	Impact
15.24	3.05	1.2	304.83	6.56	0.46	1.524	9.29	90	141.30	1.01	L
15.24	3.05	1.2	304.83	6.56	0.46	1.524	9.29	45	200.83	1.01	L
15.24	3.05	1.2	304.83	6.56	0.46	1.524	9.29	30	284.33	1.01	L
15.24	3.05	1.2	304.83	6.56	0.91	6.097	9.29	90	35.33	1.1	L
15.24	3.05	1.2	304.83	6.56	0.91	3.048	4.64	90	141.30	1.02	L
15.24	3.05	1.2	304.83	6.56	0.91	1.524	2.32	90	565.20	1.01	L
15.24	3.05	1.2	304.83	6.56	0.91	6.097	9.29	45	50.96	1.03	L
15.24	3.05	1.2	304.83	6.56	0.91	3.048	4.64	45	200.83	1.01	L
15.24	3.05	1.2	304.83	6.56	0.91	1.524	2.32	45	800.31	1.01	L
15.24	3.05	1.2	304.83	6.56	0.91	6.097	9.29	30	72.38	1.01	L
15.24	3.05	1.2	304.83	6.56	0.91	3.048	4.64	30	284.33	1.01	L
15.24	3.05	1.2	304.83	6.56	0.91	1.524	2.32	30	1132.13	1.01	L
15.24	3.05	1.2	304.83	6.56	1.52	6.097	3.34	90	98.13	1.1	L
15.24	3.05	1.2	304.83	6.56	1.52	3.048	1.67	90	392.50	1.02	L
15.24	3.05	1.2	304.83	6.56	1.52	1.524	0.84	90	1570.00	1.01	L
15.24	3.05	1.2	304.83	6.56	1.52	6.097	3.34	45	139.77	1.03	L
15.24	3.05	1.2	304.83	6.56	1.52	3.048	1.67	45	556.08	1.02	L
15.24	3.05	1.2	304.83	6.56	1.52	1.524	0.84	45	2221.32	1.01	L
15.24	3.05	1.2	304.83	6.56	1.52	6.097	3.34	30	197.98	1.05	L
15.24	3.05	1.2	304.83	6.56	1.52	3.048	1.67	30	786.73	1.02	L
15.24	3.05	1.2	304.83	6.56	1.52	1.524	0.84	30	3141.73	1.01	L
15.24	2.13	1.2	178.54	5.49	0.46	1.785	10.88	90	50.48	1.02	L
15.24	2.13	1.2	178.54	5.49	0.46	0.893	5.44	90	201.92	1.01	L
15.24	2.13	1.2	178.54	5.49	0.46	1.785	10.88	45	72.39	1.01	L
15.24	2.13	1.2	178.54	5.49	0.46	0.893	5.44	45	286.56	1.01	L
15.24	2.13	1.2	178.54	5.49	0.46	1.785	10.88	30	102.69	1.01	L
15.24	2.13	1.2	178.54	5.49	0.46	0.893	5.44	30	405.57	1.01	L
15.24	2.13	1.2	178.54	5.49	0.91	3.571	5.44	90	50.48	1.11	L
15.24	2.13	1.2	178.54	5.49	0.91	1.785	2.72	90	201.92	1.03	L
15.24	2.13	1.2	178.54	5.49	0.91	0.893	1.36	90	807.68	1.01	L
15.24	2.13	1.2	178.54	5.49	0.91	3.571	5.44	45	72.39	1.02	L
15.24	2.13	1.2	178.54	5.49	0.91	1.785	2.72	45	286.56	1.01	L
15.24	2.13	1.2	178.54	5.49	0.91	0.893	1.36	45	1143.24	1.01	L
15.24	2.13	1.2	178.54	5.49	0.91	3.571	5.44	30	102.69	1.01	L
15.24	2.13	1.2	178.54	5.49	0.91	1.785	2.72	30	405.57	1.01	L
15.24	2.13	1.2	178.54	5.49	0.91	0.893	1.36	30	1617.10	1.01	L
15.24	2.13	1.2	178.54	5.49	1.52	3.571	1.96	90	140.22	1.12	L
15.24	2.13	1.2	178.54	5.49	1.52	1.785	0.98	90	560.89	1.04	L
15.24	2.13	1.2	178.54	5.49	1.52	0.893	0.49	90	2243.57	1.01	L
15.24	2.13	1.2	178.54	5.49	1.52	3.571	1.96	45	199.31	1.06	L
15.24	2.13	1.2	178.54	5.49	1.52	1.785	0.98	45	794.22	1.02	L
15.24	2.13	1.2	178.54	5.49	1.52	0.893	0.49	45	3173.89	1.01	L
15.24	2.13	1.2	178.54	5.49	1.52	3.571	1.96	30	282.18	1.06	L
15.24	2.13	1.2	178.54	5.49	1.52	1.785	0.98	30	1123.52	1.02	L
15.24	2.13	1.2	178.54	5.49	1.52	0.893	0.49	30	4488.87	1.01	L
15.24	1.22	1.2	77.16	4.15	0.46	1.543	9.41	90	22.07	1.19	L
15.24	1.22	1.2	77.16	4.15	0.46	0.772	4.70	90	88.28	1.04	L
15.24	1.22	1.2	77.16	4.15	0.46	0.386	2.35	90	353.12	1.01	L
15.24	1.22	1.2	77.16	4.15	0.46	1.543	9.41	45	32.21	1.01	L
15.24	1.22	1.2	77.16	4.15	0.46	0.772	4.70	45	125.85	1.01	L
15.24	1.22	1.2	77.16	4.15	0.46	0.386	2.35	45	500.39	1.01	L
15.24	1.22	1.2	77.16	4.15	0.46	1.543	9.41	30	45.87	1.01	L
15.24	1.22	1.2	77.16	4.15	0.46	0.772	4.70	30	178.29	1.01	L
15.24	1.22	1.2	77.16	4.15	0.46	0.386	2.35	30	707.97	1.01	L
15.24	1.22	1.2	77.16	4.15	0.91	1.543	2.35	90	88.28	1.14	L
15.24	1.22	1.2	77.16	4.15	0.91	0.772	1.18	90	353.12	1.05	L
15.24	1.22	1.2	77.16	4.15	0.91	0.386	0.59	90	1412.48	1.02	L
15.24	1.22	1.2	77.16	4.15	0.91	1.543	2.35	45	125.85	1.05	L
15.24	1.22	1.2	77.16	4.15	0.91	0.772	1.18	45	500.39	1.02	L
15.24	1.22	1.2	77.16	4.15	0.91	0.386	0.59	45	1998.55	1.01	L
15.24	1.22	1.2	77.16	4.15	0.91	1.543	2.35	30	178.29	1.02	L
15.24	1.22	1.2	77.16	4.15	0.91	0.772	1.18	30	707.97	1.01	L
15.24	1.22	1.2	77.16	4.15	0.91	0.386	0.59	30	2826.69	1.01	L

Table A7. FLOW-3D simulation results for W = 3.05 m (10′) and Fr = 0.8.

W (m)	H_0 (m)	Fr (-)	Q Chan. (m^3/s)	V Chan. (m/s)	D Pipe (m)	q Pipe (m^3/s)	v Pipe (m/s)	θ Junc. (deg.)	$\frac{QV+qv(\cos\theta)}{qv(\sin\theta)}$	$\frac{H}{H_0}$	Impact
3.05	3.05	0.8	40.66	4.38	0.46	2.033	12.39	90	7.07	1.33	W
3.05	3.05	0.8	40.66	4.38	0.46	1.017	6.20	90	28.26	1.17	L
3.05	3.05	0.8	40.66	4.38	0.46	2.033	12.39	45	10.99	1.1	L
3.05	3.05	0.8	40.66	4.38	0.46	1.017	6.20	45	40.97	1.1	L
3.05	3.05	0.8	40.66	4.38	0.46	2.033	12.39	30	15.86	1.1	L
3.05	3.05	0.8	40.66	4.38	0.46	1.017	6.20	30	58.25	1.1	L
3.05	3.05	0.8	40.66	4.38	0.91	4.066	6.20	90	7.07	1.71	W
3.05	3.05	0.8	40.66	4.38	0.91	2.033	3.10	90	28.26	1.39	W
3.05	3.05	0.8	40.66	4.38	0.91	1.017	1.55	90	113.04	1.19	L
3.05	3.05	0.8	40.66	4.38	0.91	4.066	6.20	45	10.99	1.36	L
3.05	3.05	0.8	40.66	4.38	0.91	2.033	3.10	45	40.97	1.31	L
3.05	3.05	0.8	40.66	4.38	0.91	1.017	1.55	45	160.86	1.18	L
3.05	3.05	0.8	40.66	4.38	0.91	4.066	6.20	30	15.86	1.32	L
3.05	3.05	0.8	40.66	4.38	0.91	2.033	3.10	30	58.25	1.29	L
3.05	3.05	0.8	40.66	4.38	0.91	1.017	1.55	30	227.81	1.18	L
3.05	3.05	0.8	40.66	4.38	1.52	4.066	2.23	90	19.63	1.7	W
3.05	3.05	0.8	40.66	4.38	1.52	2.033	1.12	90	78.50	1.4	W
3.05	3.05	0.8	40.66	4.38	1.52	1.017	0.56	90	314.00	1.2	L
3.05	3.05	0.8	40.66	4.38	1.52	4.066	2.23	45	28.75	1.58	W
3.05	3.05	0.8	40.66	4.38	1.52	2.033	1.12	45	112.02	1.35	W
3.05	3.05	0.8	40.66	4.38	1.52	1.017	0.56	45	445.06	1.2	L
3.05	3.05	0.8	40.66	4.38	1.52	4.066	2.23	30	40.98	1.54	W
3.05	3.05	0.8	40.66	4.38	1.52	2.033	1.12	30	158.73	1.35	W
3.05	3.05	0.8	40.66	4.38	1.52	1.017	0.56	30	629.73	1.2	L
3.05	2.13	0.8	23.81	3.66	0.46	2.381	14.51	90	2.52	1.72	W
3.05	2.13	0.8	23.81	3.66	0.46	1.191	7.26	90	10.09	1.36	W
3.05	2.13	0.8	23.81	3.66	0.46	0.595	3.63	90	40.36	1.14	L
3.05	2.13	0.8	23.81	3.66	0.46	2.381	14.51	45	4.57	1.08	L
3.05	2.13	0.8	23.81	3.66	0.46	1.191	7.26	45	15.27	1.08	L
3.05	2.13	0.8	23.81	3.66	0.46	0.595	3.63	45	58.07	1.08	L
3.05	2.13	0.8	23.81	3.66	0.46	2.381	14.51	30	6.78	1.05	L
3.05	2.13	0.8	23.81	3.66	0.46	1.191	7.26	30	21.91	1.05	L
3.05	2.13	0.8	23.81	3.66	0.46	0.595	3.63	30	82.45	1.05	L
3.05	2.13	0.8	23.81	3.66	0.91	2.381	3.63	90	10.09	1.76	W
3.05	2.13	0.8	23.81	3.66	0.91	1.191	1.81	90	40.36	1.41	W
3.05	2.13	0.8	23.81	3.66	0.91	0.595	0.91	90	161.43	1.16	L
3.05	2.13	0.8	23.81	3.66	0.91	2.381	3.63	45	15.27	1.47	W
3.05	2.13	0.8	23.81	3.66	0.91	1.191	1.81	45	58.07	1.32	L
3.05	2.13	0.8	23.81	3.66	0.91	0.595	0.91	45	229.29	1.16	L
3.05	2.13	0.8	23.81	3.66	0.91	2.381	3.63	30	21.91	1.42	W
3.05	2.13	0.8	23.81	3.66	0.91	1.191	1.81	30	82.45	1.31	L
3.05	2.13	0.8	23.81	3.66	0.91	0.595	0.91	30	324.59	1.15	L
3.05	2.13	0.8	23.81	3.66	1.52	2.381	1.31	90	28.03	1.73	W
3.05	2.13	0.8	23.81	3.66	1.52	1.191	0.65	90	112.10	1.4	W
3.05	2.13	0.8	23.81	3.66	1.52	0.595	0.33	90	448.41	1.17	L
3.05	2.13	0.8	23.81	3.66	1.52	2.381	1.31	45	40.63	1.7	W
3.05	2.13	0.8	23.81	3.66	1.52	1.191	0.65	45	159.54	1.35	W
3.05	2.13	0.8	23.81	3.66	1.52	0.595	0.33	45	635.15	1.17	L
3.05	2.13	0.8	23.81	3.66	1.52	2.381	1.31	30	57.78	1.64	W
3.05	2.13	0.8	23.81	3.66	1.52	1.191	0.65	30	225.94	1.35	W
3.05	2.13	0.8	23.81	3.66	1.52	0.595	0.33	30	898.55	1.17	L
3.05	1.22	0.8	10.28	2.77	0.46	1.028	6.26	90	4.42	1.72	W
3.05	1.22	0.8	10.28	2.77	0.46	0.514	3.13	90	17.67	1.34	L
3.05	1.22	0.8	10.28	2.77	0.46	0.257	1.57	90	70.69	1.15	L
3.05	1.22	0.8	10.28	2.77	0.46	1.028	6.26	45	7.25	1.18	L
3.05	1.22	0.8	10.28	2.77	0.46	0.514	3.13	45	25.99	1.18	L
3.05	1.22	0.8	10.28	2.77	0.46	0.257	1.57	45	100.97	1.09	L
3.05	1.22	0.8	10.28	2.77	0.46	1.028	6.26	30	10.57	1.18	L
3.05	1.22	0.8	10.28	2.77	0.46	0.514	3.13	30	37.08	1.18	L
3.05	1.22	0.8	10.28	2.77	0.46	0.257	1.57	30	143.11	1.09	L
3.05	1.22	0.8	10.28	2.77	0.91	1.028	1.57	90	17.67	1.65	W
3.05	1.22	0.8	10.28	2.77	0.91	0.514	0.78	90	70.69	1.38	W
3.05	1.22	0.8	10.28	2.77	0.91	0.257	0.39	90	282.76	1.17	L
3.05	1.22	0.8	10.28	2.77	0.91	1.028	1.57	45	25.99	1.63	W
3.05	1.22	0.8	10.28	2.77	0.91	0.514	0.78	45	100.97	1.34	W
3.05	1.22	0.8	10.28	2.77	0.91	0.257	0.39	45	400.88	1.17	L
3.05	1.22	0.8	10.28	2.77	0.91	1.028	1.57	30	37.08	1.55	W
3.05	1.22	0.8	10.28	2.77	0.91	0.514	0.78	30	143.11	1.31	W
3.05	1.22	0.8	10.28	2.77	0.91	0.257	0.39	30	567.24	1.17	L

Table A8. FLOW-3D simulation results for W = 7.62 m (25′) and Fr = 0.8.

W (m)	H_0 (m)	Fr (-)	Q Chan. (m^3/s)	V Chan. (m/s)	D Pipe (m)	q Pipe (m^3/s)	v Pipe (m/s)	θ Junc. (deg.)	$\frac{QV+qv(\cos\theta)}{qv(\sin\theta)}$	$\frac{H}{H_0}$	Impact
7.62	3.05	0.8	101.66	4.38	0.46	2.033	12.39	90	17.66	1.14	L
7.62	3.05	0.8	101.66	4.38	0.46	1.017	6.20	90	70.65	1.01	L
7.62	3.05	0.8	101.66	4.38	0.46	2.033	12.39	45	25.98	1.01	L
7.62	3.05	0.8	101.66	4.38	0.46	1.017	6.20	45	100.91	1.01	L
7.62	3.05	0.8	101.66	4.38	0.46	2.033	12.39	30	37.06	1.01	L
7.62	3.05	0.8	101.66	4.38	0.46	1.017	6.20	30	143.03	1.01	L
7.62	3.05	0.8	101.66	4.38	0.91	4.066	6.20	90	17.66	1.4	L
7.62	3.05	0.8	101.66	4.38	0.91	2.033	3.10	90	70.65	1.16	L
7.62	3.05	0.8	101.66	4.38	0.91	1.017	1.55	90	282.60	1.04	L
7.62	3.05	0.8	101.66	4.38	0.91	4.066	6.20	45	25.98	1.14	L
7.62	3.05	0.8	101.66	4.38	0.91	2.033	3.10	45	100.91	1.08	L
7.62	3.05	0.8	101.66	4.38	0.91	1.017	1.55	45	400.66	1.01	L
7.62	3.05	0.8	101.66	4.38	0.91	4.066	6.20	30	37.06	1.09	L
7.62	3.05	0.8	101.66	4.38	0.91	2.033	3.10	30	143.03	1.07	L
7.62	3.05	0.8	101.66	4.38	0.91	1.017	1.55	30	566.93	1.01	L
7.62	3.05	0.8	101.66	4.38	1.52	4.066	2.23	90	49.06	1.41	L
7.62	3.05	0.8	101.66	4.38	1.52	2.033	1.12	90	196.25	1.17	L
7.62	3.05	0.8	101.66	4.38	1.52	1.017	0.56	90	785.00	1.04	L
7.62	3.05	0.8	101.66	4.38	1.52	4.066	2.23	45	70.38	1.28	L
7.62	3.05	0.8	101.66	4.38	1.52	2.033	1.12	45	278.54	1.15	L
7.62	3.05	0.8	101.66	4.38	1.52	1.017	0.56	45	1111.16	1.04	L
7.62	3.05	0.8	101.66	4.38	1.52	4.066	2.23	30	99.86	1.26	L
7.62	3.05	0.8	101.66	4.38	1.52	2.033	1.12	30	394.23	1.13	L
7.62	3.05	0.8	101.66	4.38	1.52	1.017	0.56	30	1571.73	1.04	L
7.62	2.13	0.8	59.55	3.66	0.46	2.381	14.51	90	6.31	1.25	L
7.62	2.13	0.8	59.55	3.66	0.46	1.191	7.26	90	25.23	1.11	L
7.62	2.13	0.8	59.55	3.66	0.46	0.595	3.63	90	100.92	1.01	L
7.62	2.13	0.8	59.55	3.66	0.46	2.381	14.51	45	9.92	1.01	L
7.62	2.13	0.8	59.55	3.66	0.46	1.191	7.26	45	36.68	1.01	L
7.62	2.13	0.8	59.55	3.66	0.46	0.595	3.63	45	143.72	1.01	L
7.62	2.13	0.8	59.55	3.66	0.46	2.381	14.51	30	14.35	1.01	L
7.62	2.13	0.8	59.55	3.66	0.46	1.191	7.26	30	52.19	1.01	L
7.62	2.13	0.8	59.55	3.66	0.46	0.595	3.63	30	203.57	1.01	L
7.62	2.13	0.8	59.55	3.66	0.91	2.381	3.63	90	25.23	1.38	L
7.62	2.13	0.8	59.55	3.66	0.91	1.191	1.81	90	100.92	1.13	L
7.62	2.13	0.8	59.55	3.66	0.91	0.595	0.91	90	403.67	1.03	L
7.62	2.13	0.8	59.55	3.66	0.91	2.381	3.63	45	36.68	1.18	L
7.62	2.13	0.8	59.55	3.66	0.91	1.191	1.81	45	143.72	1.09	L
7.62	2.13	0.8	59.55	3.66	0.91	0.595	0.91	45	571.87	1.01	L
7.62	2.13	0.8	59.55	3.66	0.91	2.381	3.63	30	52.19	1.17	L
7.62	2.13	0.8	59.55	3.66	0.91	1.191	1.81	30	203.57	1.08	L
7.62	2.13	0.8	59.55	3.66	0.91	0.595	0.91	30	809.06	1.01	L
7.62	2.13	0.8	59.55	3.66	1.52	2.381	1.31	90	70.08	1.38	L
7.62	2.13	0.8	59.55	3.66	1.52	1.191	0.65	90	280.32	1.14	L
7.62	2.13	0.8	59.55	3.66	1.52	0.595	0.33	90	1121.30	1.04	L
7.62	2.13	0.8	59.55	3.66	1.52	2.381	1.31	45	100.11	1.3	L
7.62	2.13	0.8	59.55	3.66	1.52	1.191	0.65	45	397.44	1.13	L
7.62	2.13	0.8	59.55	3.66	1.52	0.595	0.33	45	1586.75	1.03	L
7.62	2.13	0.8	59.55	3.66	1.52	2.381	1.31	30	141.89	1.29	L
7.62	2.13	0.8	59.55	3.66	1.52	1.191	0.65	30	562.38	1.13	L
7.62	2.13	0.8	59.55	3.66	1.52	0.595	0.33	30	2244.32	1.02	L
7.62	1.22	0.8	25.71	2.77	0.46	1.028	6.26	90	11.05	1.3	L
7.62	1.22	0.8	25.71	2.77	0.46	0.514	3.13	90	44.20	1.16	L
7.62	1.22	0.8	25.71	2.77	0.46	0.257	1.57	90	176.82	1.04	L
7.62	1.22	0.8	25.71	2.77	0.46	1.028	6.26	45	16.63	1.11	L
7.62	1.22	0.8	25.71	2.77	0.46	0.514	3.13	45	63.52	1.06	L
7.62	1.22	0.8	25.71	2.77	0.46	0.257	1.57	45	251.06	1.02	L
7.62	1.22	0.8	25.71	2.77	0.46	1.028	6.26	30	23.83	1.04	L
7.62	1.22	0.8	25.71	2.77	0.46	0.514	3.13	30	90.14	1.03	L
7.62	1.22	0.8	25.71	2.77	0.46	0.257	1.57	30	355.37	1.01	L
7.62	1.22	0.8	25.71	2.77	0.91	1.028	1.57	90	44.20	1.35	L
7.62	1.22	0.8	25.71	2.77	0.91	0.514	0.78	90	176.82	1.15	L
7.62	1.22	0.8	25.71	2.77	0.91	0.257	0.39	90	707.28	1.05	L
7.62	1.22	0.8	25.71	2.77	0.91	1.028	1.57	45	63.52	1.28	L
7.62	1.22	0.8	25.71	2.77	0.91	0.514	0.78	45	251.06	1.12	L
7.62	1.22	0.8	25.71	2.77	0.91	0.257	0.39	45	1001.24	1.03	L
7.62	1.22	0.8	25.71	2.77	0.91	1.028	1.57	30	90.14	1.27	L
7.62	1.22	0.8	25.71	2.77	0.91	0.514	0.78	30	355.37	1.13	L
7.62	1.22	0.8	25.71	2.77	0.91	0.257	0.39	30	1416.29	1.01	L

Table A9. FLOW-3D simulation results for W = 15.24 m (50′) and Fr = 0.8.

W (m)	H_0 (m)	Fr (-)	Q Chan. (m^3/s)	V Chan. (m/s)	D Pipe (m)	q Pipe (m^3/s)	v Pipe (m/s)	θ Junc. (deg.)	$\frac{QV+qv(\cos\theta)}{qv(\sin\theta)}$	$\frac{H}{H_0}$	Impact
15.24	3.05	0.8	203.32	4.38	0.46	2.033	12.39	90	35.33	1.03	L
15.24	3.05	0.8	203.32	4.38	0.46	1.017	6.20	90	141.30	1.01	L
15.24	3.05	0.8	203.32	4.38	0.46	2.033	12.39	45	50.96	1.01	L
15.24	3.05	0.8	203.32	4.38	0.46	1.017	6.20	45	200.83	1.01	L
15.24	3.05	0.8	203.32	4.38	0.46	2.033	12.39	30	72.38	1.01	L
15.24	3.05	0.8	203.32	4.38	0.46	1.017	6.20	30	284.33	1.01	L
15.24	3.05	0.8	203.32	4.38	0.91	4.066	6.20	90	35.33	1.18	L
15.24	3.05	0.8	203.32	4.38	0.91	2.033	3.10	90	141.30	1.05	L
15.24	3.05	0.8	203.32	4.38	0.91	1.017	1.55	90	565.20	1.01	L
15.24	3.05	0.8	203.32	4.38	0.91	4.066	6.20	45	50.96	1.04	L
15.24	3.05	0.8	203.32	4.38	0.91	2.033	3.10	45	200.83	1.01	L
15.24	3.05	0.8	203.32	4.38	0.91	1.017	1.55	45	800.31	1.01	L
15.24	3.05	0.8	203.32	4.38	0.91	4.066	6.20	30	72.38	1.01	L
15.24	3.05	0.8	203.32	4.38	0.91	2.033	3.10	30	284.33	1.01	L
15.24	3.05	0.8	203.32	4.38	0.91	1.017	1.55	30	1132.13	1.01	L
15.24	3.05	0.8	203.32	4.38	1.52	4.066	2.23	90	98.13	1.17	L
15.24	3.05	0.8	203.32	4.38	1.52	2.033	1.12	90	392.50	1.04	L
15.24	3.05	0.8	203.32	4.38	1.52	1.017	0.56	90	1570.00	1.01	L
15.24	3.05	0.8	203.32	4.38	1.52	4.066	2.23	45	139.77	1.1	L
15.24	3.05	0.8	203.32	4.38	1.52	2.033	1.12	45	556.08	1.03	L
15.24	3.05	0.8	203.32	4.38	1.52	1.017	0.56	45	2221.32	1.01	L
15.24	3.05	0.8	203.32	4.38	1.52	4.066	2.23	30	197.98	1.09	L
15.24	3.05	0.8	203.32	4.38	1.52	2.033	1.12	30	786.73	1.01	L
15.24	3.05	0.8	203.32	4.38	1.52	1.017	0.56	30	3141.73	1.01	L
15.24	2.13	0.8	119.07	3.66	0.46	2.381	14.51	90	12.61	1.16	L
15.24	2.13	0.8	119.07	3.66	0.46	1.191	7.26	90	50.45	1.03	L
15.24	2.13	0.8	119.07	3.66	0.46	0.595	3.63	90	201.79	1.01	L
15.24	2.13	0.8	119.07	3.66	0.46	2.381	14.51	45	18.84	1.01	L
15.24	2.13	0.8	119.07	3.66	0.46	1.191	7.26	45	72.34	1.01	L
15.24	2.13	0.8	119.07	3.66	0.46	0.595	3.63	45	286.37	1.01	L
15.24	2.13	0.8	119.07	3.66	0.46	2.381	14.51	30	26.96	1.01	L
15.24	2.13	0.8	119.07	3.66	0.46	1.191	7.26	30	102.62	1.01	L
15.24	2.13	0.8	119.07	3.66	0.46	0.595	3.63	30	405.30	1.01	L
15.24	2.13	0.8	119.07	3.66	0.91	2.381	3.63	90	50.45	1.18	L
15.24	2.13	0.8	119.07	3.66	0.91	1.191	1.81	90	201.79	1.07	L
15.24	2.13	0.8	119.07	3.66	0.91	0.595	0.91	90	807.14	1.01	L
15.24	2.13	0.8	119.07	3.66	0.91	2.381	3.63	45	72.34	1.08	L
15.24	2.13	0.8	119.07	3.66	0.91	1.191	1.81	45	286.37	1.03	L
15.24	2.13	0.8	119.07	3.66	0.91	0.595	0.91	45	1142.47	1.01	L
15.24	2.13	0.8	119.07	3.66	0.91	2.381	3.63	30	102.62	1.08	L
15.24	2.13	0.8	119.07	3.66	0.91	1.191	1.81	30	405.30	1.02	L
15.24	2.13	0.8	119.07	3.66	0.91	0.595	0.91	30	1616.01	1.01	L
15.24	2.13	0.8	119.07	3.66	1.52	2.381	1.31	90	140.13	1.17	L
15.24	2.13	0.8	119.07	3.66	1.52	1.191	0.65	90	560.51	1.06	L
15.24	2.13	0.8	119.07	3.66	1.52	0.595	0.33	90	2242.06	1.02	L
15.24	2.13	0.8	119.07	3.66	1.52	2.381	1.31	45	199.17	1.12	L
15.24	2.13	0.8	119.07	3.66	1.52	1.191	0.65	45	793.69	1.04	L
15.24	2.13	0.8	119.07	3.66	1.52	0.595	0.33	45	3171.75	1.01	L
15.24	2.13	0.8	119.07	3.66	1.52	2.381	1.31	30	281.99	1.12	L
15.24	2.13	0.8	119.07	3.66	1.52	1.191	0.65	30	1122.76	1.05	L
15.24	2.13	0.8	119.07	3.66	1.52	0.595	0.33	30	4485.85	1.01	L
15.24	1.22	0.8	51.40	2.77	0.46	1.028	6.26	90	22.09	1.2	L
15.24	1.22	0.8	51.40	2.77	0.46	0.514	3.13	90	88.36	1.09	L
15.24	1.22	0.8	51.40	2.77	0.46	0.257	1.57	90	353.44	1.02	L
15.24	1.22	0.8	51.40	2.77	0.46	1.028	6.26	45	32.24	1.07	L
15.24	1.22	0.8	51.40	2.77	0.46	0.514	3.13	45	125.96	1.04	L
15.24	1.22	0.8	51.40	2.77	0.46	0.257	1.57	45	500.85	1.01	L
15.24	1.22	0.8	51.40	2.77	0.46	1.028	6.26	30	45.91	1.02	L
15.24	1.22	0.8	51.40	2.77	0.46	0.514	3.13	30	178.45	1.01	L
15.24	1.22	0.8	51.40	2.77	0.46	0.257	1.57	30	708.62	1.01	L
15.24	1.22	0.8	51.40	2.77	0.91	1.028	1.57	90	88.36	1.24	L
15.24	1.22	0.8	51.40	2.77	0.91	0.514	0.78	90	353.44	1.08	L
15.24	1.22	0.8	51.40	2.77	0.91	0.257	0.39	90	1413.78	1.02	L
15.24	1.22	0.8	51.40	2.77	0.91	1.028	1.57	45	125.96	1.19	L
15.24	1.22	0.8	51.40	2.77	0.91	0.514	0.78	45	500.85	1.07	L
15.24	1.22	0.8	51.40	2.77	0.91	0.257	0.39	45	2000.38	1.01	L
15.24	1.22	0.8	51.40	2.77	0.91	1.028	1.57	30	178.45	1.16	L
15.24	1.22	0.8	51.40	2.77	0.91	0.514	0.78	30	708.62	1.01	L
15.24	1.22	0.8	51.40	2.77	0.91	0.257	0.39	30	2829.29	1.01	L

References

1. Gurram, S.K.; Karki, K.S.; Hager, W.H. Subcritical junction flow. *J. Hydraul. Eng.* **1997**, *123*, 447–455. [CrossRef]
2. Best, J.L. Flow Dynamics and Sediment Transport at River Channel Confluences. Ph.D. Thesis, University of London, London, UK, 1985.
3. U.S. Army Engineer District. *Supercritical Flow at Open Channel Junction*; Report No. 2-100; U.S. Army Engineer District: Los Angeles, CA, USA, 1975.
4. Taylor, E.H. Flow characteristics at rectangular open-channel junctions. *Trans. ASCE* **1944**, *109*, 893–902.
5. Mignot, E.; Bonakdari, H.; Knothe, P.; Liperne Kouyi, G.; Bessette, A.; Riviere, N.; Bertrand-Krajewski, J.L. Experiments and 3D simulations of flow structures in junctions and their influence on location of flowmeters. *Water Sci. Technol.* **2012**, *66*, 1325–1332. [CrossRef] [PubMed]
6. Constantinescu, G.; Miyawaki, S.; Rhoads, B.; Sukhodolov, A. Numerical evaluation of the effects of planform geometry and inflow conditions on flow, turbulence structure, and bed shear velocity at a stream confluence with a concordant bed. *J. Geophys. Res.* **2014**, *119*, 2079–2097. [CrossRef]
7. Webber, N.B.; Greated, C.A. An investigation of flow behaviour at the junction of rectangular channels. *ICE Proc.* **1966**, *34*, 321–334. [CrossRef]
8. Hsu, C.; Wu, F.; Lee, W. Flow at 90° equal-width open-channel junction. *J. Hydraul. Eng.* **1998**, *124*, 186–191. [CrossRef]
9. Nedelec, Y.; Gay, B. Experimental study of a right-angled end junction between a pipe and an open channel. *J. Hydraul. Eng.* **2008**, *134*. [CrossRef]
10. GREYLINE AVFM 5.0 User's Manual (2017) [Online]. Available online: http://www.greyline.com/pdf/AVFM%205.0%20Manual.pdf (accessed on 15 February 2018).
11. Lin, J.; Soong, H. Junction losses in open channel flows. *Water Resour. Res.* **1979**, *15*, 414–418. [CrossRef]
12. Garcia-Navarro, M.; Saviron, J. Numerical simulation of unsteady flow at open channel junctions. *J. Hydraul. Res.* **1992**, *30*, 595–609. [CrossRef]
13. Mays, L.W. *Stormwater Collection Systems Design Book*; McGraw-Hill: New York, NY, USA, 2011.
14. Yen, B.C. Hydraulics of sewers. *Adv. Hydrosci.* **1986**, *14*, 1122.
15. Nazari-Sharabian, M.; Nazari-Sharabian, A.; Karakouzian, M.; Karami, M. Sacrificial Piles as Scour Countermeasures in River Bridges—A Numerical Study using FLOW-3D. *Civ. Eng. J.* **2020**, *6*. [CrossRef]
16. Karami, M.; Kabiri-Samani, A.; Nazari-Sharabian, M.; Karakouzian, M. Investigating the Effects of Transient Flow in Concrete-Lined Pressure Tunnels and Developing a New Analytical Formula for Pressure Wave Velocity. *Tunn. Undergr. Space Technol.* **2019**, *91*, 102992. [CrossRef]
17. Flow Science, Inc. Santa Fe, NM, USA. FLOW-3D® Version 12.0 User's Manual (2018) [Online]. Available online: https://www.flow3d.com (accessed on 3 February 2019).
18. Hydrologic Criteria and Drainage Design Manual (HCDDM) of the Clark County Regional Flood Control District (CCRFCD). Available online: http://www.ccrfcd.org/hcddm.htm (accessed on 3 February 2019).
19. Nash, J.E.; Sutcliffe, J.V. River flow forecasting through conceptual models. Part 1: A discussion of principles. *J. Hydrol.* **1970**, *103*, 282–290. [CrossRef]
20. Kenworthy, S.; Rhoads, B. Hydrologic control of spatial patterns of suspended sediment concentration at a stream confluence. *J. Hydrol.* **1995**, *168*, 251–263. [CrossRef]